Left-invariant evolutions of wavelet transforms on the similitude group

EINDHOVEN UNIVERSITY OF TECHNOLOGY
Department of Mathematics and Computer Science

CASA-Report 13-17
June 2013

Left-invariant evolutions of wavelet transforms on the similitude group

by

U. Sharma, R. Duits

Centre for Analysis, Scientific computing and Applications
Department of Mathematics and Computer Science
Eindhoven University of Technology
P.O. Box 513
5600 MB Eindhoven, The Netherlands
ISSN: 0926-4507

Left-invariant evolutions of wavelet transforms on the Similitude Group

Upanshu Sharma and Remco Duits

June 7, 2013

Abstract

Enhancement of multiple-scale elongated structures in noisy image data is relevant for many biomedical applications but commonly used PDE-based enhancement techniques often fail at crossings in an image. To get an overview of how an image is composed of local multiple-scale elongated structures we construct a multiple scale orientation score, which is a continuous wavelet transform on the similitude group, $SIM(2)$. Our unitary transform maps the space of images onto a reproducing kernel space defined on $SIM(2)$, allowing us to robustly relate Euclidean (and scaling) invariant operators on images to left-invariant operators on multiple-scale orientation scores. Rather than often used wavelet (soft-)thresholding techniques, we employ the group structure in the wavelet domain to arrive at left-invariant evolutions and flows (diffusion), for contextual crossing preserving enhancement of multiple scale elongated structures in noisy images. We present experiments that display benefits of our work compared to recent PDE techniques acting directly on the images and to our previous work on left-invariant diffusions on orientation scores defined on Euclidean motion group.

Keywords: Continuous wavelet transform, Left-invariant vector fields, Similitude group, Orientation scores, Evolution equations, Diffusions on Lie groups, Medical imaging

1 Introduction

Elongated structures in the human body such as fibres and blood vessels often require analysis for diagnostic purposes. A wide variety of medical imaging techniques such as magnetic resonance imaging (MRI), microscopy, X-ray flouroscopy, fundus imaging etc. exist to achieve this. Many (bio)medical questions related to such images require detection and tracking of the elongated structures present therein. Due to the desire to reduce acquisition time and radiation dosage the acquired medical images are often noisy, of low contrast and suffer from occlusions and incomplete data. Furthermore multiple-scale elongated structures exhibit crossings and bifurcations which is a notorious problem in (medical) imaging. Hence crossing-preserving enhancement of these structures is an important preprocessing step for subsequent detection.

In recent years PDE based techniques have gained popularity in the field of image processing. Due to well posed mathematical results these techniques lend themselves to stable algorithms and also allow mathematical and geometrical interpretation of classical methods such as Gaussian filtering, dilation or erosion etc. on $\mathbb{R}^d$.

These techniques typically regard the original image, $f \in \mathbb{R}^2 \to \mathbb{R}$, as an initial state of a parabolic (diffusion like) evolution process yielding filtered versions, $u_f : \mathbb{R}^2 \times \mathbb{R}^+ \to \mathbb{R}$. Here u_f is called the scale space representation of image f. The domain of u_f is scale space $\mathbb{R}^2 \times \mathbb{R}^+$. A typical scale space evolution is of the form

$$\begin{cases} \partial_s u_f(\mathbf{x}, s) & = \nabla_{\mathbf{x}} \cdot (C(u_f(\cdot, s))(\mathbf{x}) \nabla_{\mathbf{x}} u_f)(\mathbf{x}, s) \\ u_f(\mathbf{x}, 0) & = f(\mathbf{x}), \end{cases} \tag{1}$$

where $C(u_f(\cdot,s))(\mathbf{x})$ models the diffusivity depending on the differential structure at $(\mathbf{x}, s, u_f(\mathbf{x},s))$. For $C = 1$, (1) is the usual heat equation. The corresponding evolution is known in image processing as a Gaussian Scale Space [1, 2]. In their seminal paper [3], Perona and Malik proposed nonlinear filters to bridge scale space and restoration ideas. Based on the observation that diffusion should not occur when the (local) gradient value is large (to avoid blurring the edges), they pointed out that nonlinear adaptive isotropic diffusion is achieved by replacing $C = 1$ by $C(u_f(\cdot,s))(\mathbf{x}) = c(\|\nabla_{\mathbf{x}} u_f(\mathbf{x},s)\|)$, where $c : \mathbb{R}^+ \to \mathbb{R}^+$ is some smooth strictly decaying positive function vanishing at infinity. An improvement of the Perona-Malik scheme is the "coherence-enhancing diffusion" (CED) introduced by Weickert [4] which additionally uses the direction of the gradient $\nabla_{\mathbf{x}} u_f$ leading to diffusion constant c being replaced by a diffusion matrix.
However these methods often fail in image analysis applications with crossing or bifurcating curves as the direction of gradient at these structures is ill-defined, see [5] for more details. In [6] the authors present techniques which effectively deal with the particular case of X-junctions by relying on the 2-nd order jet of Gaussian derivatives in the image domain. Passing through higher order jets of Gaussian derivatives and induced Euclidean invariant differential operators does not allow one to generically deal with complex crossings and/or bifurcating structures. Instead we need differential frames in higher dimensional affine Lie groups such as done for $G = SE(d)$ where $d = 2, 3$, see [5, 7]. This framework known as Orientation Scores (OS) for the case of $G = SE(2)$ will be explained later in this section.

1.1 Why incorporate Scale?

In this paper we wish to extend the aforementioned orientation score framework to the case of the Similitude group (group of planar translations, rotations and scaling), for the following reasons:

- Adapting the diffusivity via local frames based on Gaussian derivatives is effective [6, 8] to enhance images without crossings. However these gauge frames are aligned for instance with a *single* Gaussian gradient direction, which is unstable in the vicinity of complex structures such as generic crossings and/or bifurcations. At these complex structures one needs multiple spatial frames per position. Therefore following the general idea of Scale spaces on affine Lie groups [9, 10, 11, 12], a natural next step would be to extend the domain of images to the affine Lie group $SIM(2) = \mathbb{R}^2 \rtimes (\mathbb{R}^+ \times SO(2))$ in order to have well posed gauge frames at crossing structures (adapted to multiple orientations and scales that are locally present).

- In the primary visual cortex both multiple scales and orientations are encoded per position. It is generally believed that receptive field profiles in neurophysiological experiments can be modelled by Gaussian derivatives [13, 14, 15, 16] and this provides a biological motivation to incorporate scales.

- Elongated (possibly crossing) structures often exhibit multiple scales. Earlier work by one of the authors [5, 7] proposes generic crossing preserving flows via invertible orientation scores (employing differential gauge frames within the scores). However, this approach treats all scales in the same way. As a result these flows do not adequately deal with images containing elongated structures with strongly varying widths (scales). Therefore we must encode and process multiple scales in the scores.

1.2 Our main results

There are two main motivating questions (see Figure 1) for the work presented in this article.

1. Can we design a *well-posed invertible score*, which is a complex-valued function on a Lie group $SIM(2)$, combining the strengths of directional wavelets [17, 18, 19], curvelets [20, 21, 22] and also allow for accurate and efficient implementation of subsequent contextual-enhancement operators?

2. Can we construct contextual flows in the wavelet domain, in order to ensure that only the wavelet coefficients that are coherent (from both probabilistic and group theoretical perspective, [23]) with the surrounding coefficients become dominant?

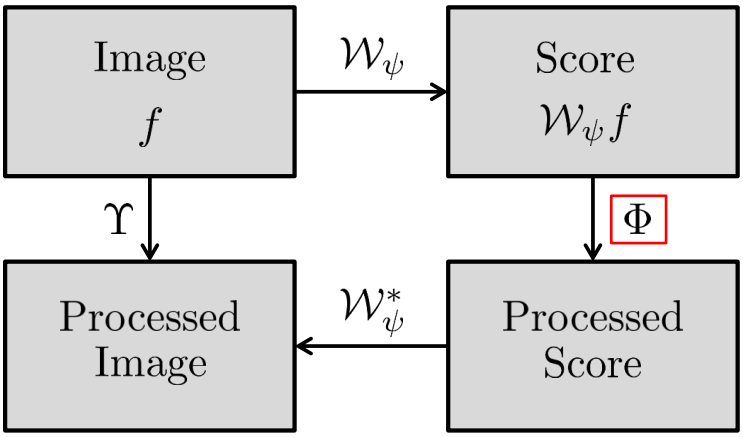

Figure 1: A schematic view on processing images $f : \mathbb{R}^2 \to \mathbb{R}$ via invertible scores $\mathcal{W}_\psi f : G \to \mathbb{C}$ defined on Lie group $G = \mathbb{R}^2 \rtimes T$. Design of well posed transform $\mathcal{W}_\psi$ and of appropriate operators Φ is the main objective of this article. Note that $\Upsilon = \mathcal{W}_\psi^* \circ \Phi \circ \mathcal{W}_\psi$, i.e. spatial processes are realized via invertible scores akin to cortical columns in the visual brain [24].

Our answer to both these questions is indeed affirmative. The first question is answered in two parts. In Theorem 7 a unitarity result for scores on algebraic affine Lie groups, $G = \mathbb{R}^d \rtimes T$, is presented wherein we provide an explicit description for the range of the wavelet transform. This result is then applied to the particular case of $G = SE(2)$ and $G = SIM(2)$ in Corollary 10. In practice there are upper/lower bounds on scaling and so in Theorem 13 we provide stability analysis and condition number of a modified continuous wavelet transform on $SIM(2)$ which can be used for practical applications. Figure 2 depicts the use of this wavelet transform in practice.
The second half of this article is dedicated to answering the second question. Theorem 17 proves that only left-invariant operators in the score domain correspond to Euclidean (and scaling) invariant operators on images. Therefore in this article we restrict ourselves to left-invariant PDEs on $SIM(2)$. Theorem 19 provides a stochastic connection to our left-invariant flows in the wavelet domain, as these PDEs are forward Kolmogorov equations corresponding to stochastic processes for multiple-scale contour enhancement on $SIM(2)$. Using the general theory of coercive operators on Lie groups, in Eq.(69) Gaussian estimates for the Green's function of linear diffusion on $SIM(2)$ are derived. Finally in Eq.(72) we present a nonlinear left-invariant adaptive diffusion on multiple scale orientation scores and provide experiments to validate it's practical advantages.

1.3 Invertible Orientation Scores

Based on the early work by Kalitzin [25], Duits et al. [7, 12] introduced the framework of invertible orientation score (OS) to effectively handle the problem of generic crossing curves in the context of bio-medical applications. In this subsection we briefly explain the concept of invertible OS developed in [7, 12] since our work builds on this theory.
The Euclidean motion group (i.e. the group of planar rotations and translations) $SE(2)$ is defined as $SE(2) = \mathbb{R}^2 \rtimes SO(2)$ where $SO(2)$ is the group of planar rotations. An OS, $U_f : SE(2) \to \mathbb{C}$ of an image $f : \mathbb{R}^2 \to \mathbb{R}$ is obtained by means of an anisotropic convolution kernel $\check{\psi} : \mathbb{R}^2 \to \mathbb{C}$ via

$$U_f(g) = \int_{\mathbb{R}^2} \overline{\check{\psi}(\mathbf{R}_\theta^{-1}(\mathbf{y} - \mathbf{x}))} f(\mathbf{y}) d\mathbf{y}, \;\; g = (\mathbf{x}, \theta) \in SE(2),$$

where $\psi(-\mathbf{x}) = \check{\psi}(\mathbf{x})$ and $\mathbf{R}_\theta \in SO(2)$ is the 2D counter-clockwise rotation matrix. Assume $\psi \in \mathbb{L}_2(\mathbb{R}^2)$, then the transform $\mathcal{W}_\psi$ which maps images $f \in \mathbb{L}_2(\mathbb{R}^2)$ can be rewritten as

$$U_f(g) = (\mathcal{W}_\psi f)(g) = (\mathcal{U}_g \psi, f)_{\mathbb{L}_2(\mathbb{R}^2)},$$

where $g \mapsto \mathcal{U}_g$ is a unitary (group-)representation of the Euclidean motion group $SE(2)$ into $\mathbb{L}_2(\mathbb{R}^2)$ given by $\mathcal{U}_g f(\mathbf{y}) = f(\mathbf{R}_\theta^{-1}(\mathbf{y} - \mathbf{x}))$ for all $g = (\mathbf{x}, \mathbf{R}_\theta) \in SE(2)$ and for all $f \in \mathbb{L}_2(\mathbb{R}^2)$. With this wavelet transform the OS, $U_f : SE(2) \to \mathbb{C}$ is constructed by means of an admissible vector $\psi \in \mathbb{L}(\mathbb{R}^2)$ such that the transform $\mathcal{W}_\psi$

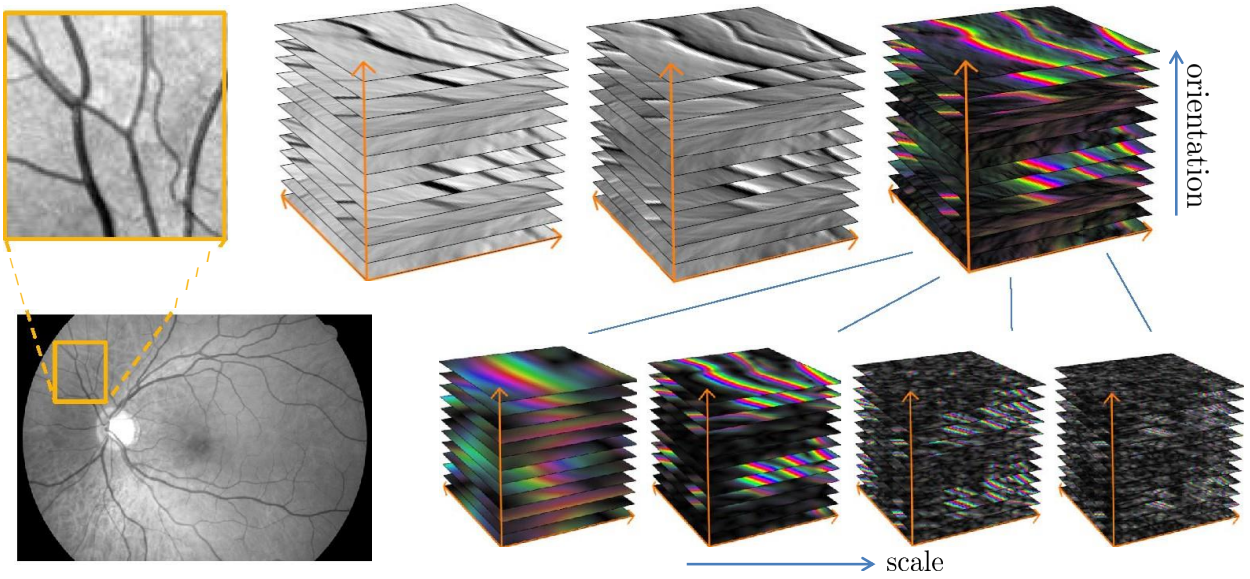

Figure 2: Top row: original image, the real-part of the orientation score reflects the centerlines, the imaginary part of the orientation reflects the edges of the bloodvessels, the orientation score (color represents phase direction and intensity represents the absolute value). Bottom row: visualizations of multiple scale orientation scores that allow us to include scale adaptation in our enhancement and detection.

is unitary onto the unique reproducing kernel Hilbert space $\mathbb{C}_K^{SE(2)}$ of functions on $SE(2)$ with reproducing kernel $K(g,h) = (\mathcal{U}_g\psi, \mathcal{U}_h\psi)$, which is a closed vector subspace of $\mathbb{L}_2(SE(2))$. Note that,

$$(\mathcal{W}_\psi f)(\mathbf{x},\theta) = (\mathcal{U}_{\mathbf{x},\theta}\psi, f)_{\mathbb{L}_2(\mathbb{R}^2)} = (\mathcal{F}\mathcal{T}_{\mathbf{x}}\mathcal{R}_\theta\psi, \mathcal{F}f)_{\mathbb{L}_2(\mathbb{R}^2)} = \mathcal{F}^{-1}(\overline{\mathcal{R}_\theta\mathcal{F}\psi}\cdot\mathcal{F}f)$$

where $\mathcal{F}$ denotes the Fourier transform and the rotation and translation operators on $\mathbb{L}_2(\mathbb{R}^2)$ are defined by $\mathcal{R}_\theta f(\mathbf{y}) = f(\mathcal{R}_\theta^{-1}\mathbf{y})$ and $\mathcal{T}_{\mathbf{x}} f(\mathbf{y}) = f(\mathbf{y}-\mathbf{x})$. This leads to the essential Plancherel formula,

$$\begin{aligned}
\|\mathcal{W}_\psi f\|^2_{\mathbb{C}_K^{SE(2)}} &= \int_{\mathbb{R}^2}\int_0^{2\pi} |(\mathcal{F}\mathcal{W}_\psi f)(\boldsymbol{\omega},\theta)|^2 \frac{1}{M_\psi(\boldsymbol{\omega})} d\boldsymbol{\omega} d\theta \\
&= \int_{\mathbb{R}^2}\int_0^{2\pi} |(\mathcal{F}f)(\boldsymbol{\omega})|^2 |\mathcal{F}\psi(\mathbf{R}_\theta^T\boldsymbol{\omega})|^2 \frac{1}{M_\psi(\boldsymbol{\omega})} d\boldsymbol{\omega} d\theta \\
&= \int_{\mathbb{R}^2} |(\mathcal{F}f)(\boldsymbol{\omega})|^2 d\boldsymbol{\omega} = \|f\|_{\mathbb{L}_2(\mathbb{R}^2)},
\end{aligned}$$

where $M_\psi \in C(\mathbb{R}^2,\mathbb{R})$ is given by $M_\psi(\boldsymbol{\omega}) = \int_0^{2\pi} |\mathcal{F}\psi(\mathbf{R}_\theta^T\boldsymbol{\omega})|^2 d\theta$. If ψ is chosen such that $M_\psi = 1$ then we gain $\mathbb{L}_2$ norm preservation. But this is not possible as $\psi \in \mathbb{L}_2(\mathbb{R}^2)\cap\mathbb{L}_1(\mathbb{R}^2)$ implies that M_ψ is a continuous function vanishing at infinity. In practice, however, because of finite grid sampling, $\mathcal{U}$ is restricted to the space of disc limited images,

$$\mathbb{L}_2^o(\mathbb{R}^2) = \{f \in \mathbb{L}_2(\mathbb{R}^2) |\ \mathrm{supp}(\mathcal{F}f) \subset B_{0,o}\}.$$

Since the wavelet transform $\mathcal{W}_\psi$ maps the space of images $\mathbb{L}_2(\mathbb{R}^2)$ unitarily onto the space of orientation

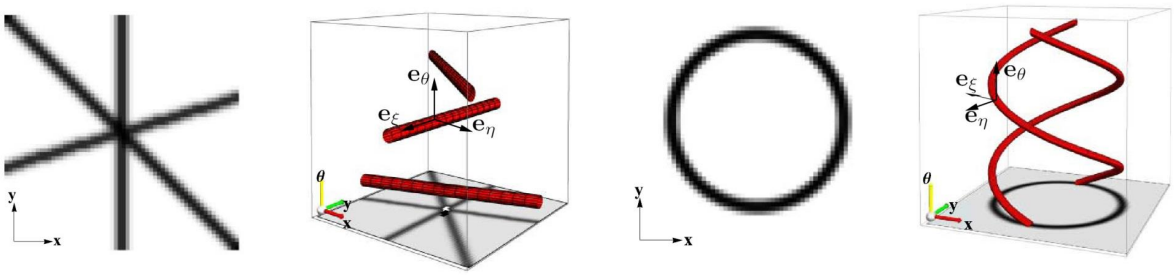

Figure 3: Illustration of the orientation score construction for a crossing and a circle. This framework unwraps a crossing in the orientation score domain. In the case of the circle, the resulting response in a 3D orientation score is a spiral as the orientation changes linearly as one traverses the circle. Note that the orientation dimension (displayed vertically) is 2π periodic.

scores $\mathbb{C}_K^{SE(2)}$ (provided $M_\psi > 0$) the original image $f : \mathbb{R}^2 \to \mathbb{R}$ can be reconstructed from it's orientation score $U_f : SE(2) \to \mathbb{C}$ by using the adjoint of the wavelet transform,

$$f = \mathcal{W}_\psi^* \mathcal{W}_\psi[f] = \mathcal{F}^{-1}\left[\boldsymbol{\omega} \mapsto \int_0^{2\pi} \mathcal{F}[U_f(\cdot,\theta)](\boldsymbol{\omega}) M_\psi^{-1}(\boldsymbol{\omega}) d\theta\right].$$

The ideas presented here are a special case of the general results shown in Section 2. For examples of wavelets ψ for which $M_\psi = 1|_{B_{0,\varrho}}$ and details on fast approximative reconstruction by integration over angles only, see [12]. For details on image processing (particularly enhancement and completion of crossing elongated structures) via orientation scores, see [5, 26, 27, 28]. An intuitive illustration of the relation between an elongated structure in a 2D image and the corresponding elongated structure in an orientation score is given in Figure 3. In *top row* of Figure 2 we also depict a practical example of an invertible orientation score.

1.4 Structure of the article

This article is structured as follows.

- **(Section 2) Unitary operators between images and scores:** An abstract unitarity result is presented and used to arrive at a wavelet transform on the Similitude group, $SIM(2)$. Stability of this transform is then discussed followed by an explicit construction of so called proper wavelets that allow a stable (re)construction of the transformed image.
- **(Section 3) Operators on scores:** Employing the group structure in the wavelet domain a general framework for operators on the scores, which involves left-invariant evolutions is discussed. These operators are interpreted in a differential geometric (and probabilistic) setting to provides a strong intuitive rationale for their choice.
- **(Section 4) Left-invariant diffusions:** Gaussian estimates for the Green's function of linear diffusion on $SIM(2)$ are derived followed by a discussion of non-linear adaptive diffusion.
- **(Section 5) Practical results:** In this section experiments that show the advantages of adaptive non-linear diffusion on multi-scale orientation scores in comparison to PDE techniques and previous work on orientation scores are presented.

1.5 Preliminaries and Notations

Let T and S be locally compact groups and let $\tau : T \to Aut(S)$ be a group homomorphism. The **semi-direct product** $S^d \rtimes_\tau T$ is defined to be the group (which is again locally compact) with underlying group

$\{(s,t)|s \in S, t \in T\}$ and group operation

$$(s,t)(s',t') = (s\tau(t)s', tt'). \tag{2}$$

In this work we mainly consider the the $2D$-Similitude group (group of rotations, translations and dilations) $SIM(2) = \mathbb{R}^2 \rtimes (\mathbb{R}^+ \times SO(2))$, where $SO(2)$ is the group of planar rotations. The group product given by

$$gg' = (\mathbf{b}, a, \theta)(\mathbf{b}', a', \theta') = (\mathbf{b} + aR_\theta \mathbf{b}', aa', \theta + \theta'), \quad g = (\mathbf{b}, a, \theta), g' = (\mathbf{b}', a', \theta') \in \mathbb{R}^2 \rtimes (\mathbb{R}^+ \times SO(2)).$$

A representation $\mathcal{R}$ of a group G into a Hilbert space H is a homomorphism $\mathcal{R}$ between G and $B(H)$, the space of bounded linear operators on H, i.e. $\mathcal{R}_{gh} = \mathcal{R}_g \mathcal{R}_h$ for all $g, h \in G$ and $\mathcal{R}_e = I$. A representation $\mathcal{R}$ is irreducible if the only invariant closed subspaces of H are $\{\mathbf{0}\}$ and H, else reducible. We consider unitary representations, i.e, $\mathcal{U}_g^* = \mathcal{U}_g^{-1} = \mathcal{U}_{g^{-1}}$ for all $g \in G$ and $\psi \in H$), which will be denoted by $\mathcal{U}$ rather than $\mathcal{R}$. Within the class of unitary representations we consider the representations of $\mathbb{R}^d \rtimes T$ in $\mathbb{L}_2(\mathbb{R}^d)$ which are given by

$$(\mathcal{U}_g \psi)(x) = \frac{1}{\sqrt{det(\tau(t))}} \psi((\tau^{-1}(t))(\mathbf{x} - \mathbf{b})), \text{ with } g = (\mathbf{b}, \tau(t)) \in \mathbb{R}^d \rtimes T. \tag{3}$$

These representations are called **left-regular actions** of $G = \mathbb{R}^d \rtimes T$ in $\mathbb{L}_2(\mathbb{R}^d)$.
Let $\mathbf{b} \in \mathbb{R}^d$, $a > 0$ and $g \in G$ with corresponding $\tau(g) \in Aut(\mathbb{R}^d)$. Then the unitary operators $f \mapsto \check{f}, \mathcal{T}_b, \mathcal{D}_a$ and $\mathcal{R}_g$ on $\mathbb{L}_2(\mathbb{R}^d)$ are defined by

$$\begin{aligned} \check{f}(\mathbf{x}) &= f(-\mathbf{x}) & \mathcal{T}_b \psi(\mathbf{x}) &= \psi(\mathbf{x} - \mathbf{b}) \\ \mathcal{D}_a \psi(\mathbf{x}) &= \frac{1}{a^{\frac{d}{2}}} \psi\left(\frac{\mathbf{x}}{a}\right) & \mathcal{R}_g \psi(\mathbf{x}) &= \frac{1}{\sqrt{det\tau(g)}} \psi((\tau(g))^{-1}\mathbf{x}). \end{aligned} \tag{4}$$

The mappings $\mathbf{b} \mapsto \mathcal{T}_b$, $g \mapsto \mathcal{R}_g$, $a \mapsto \mathcal{D}_a$ are respectively left regular actions of $\mathbb{R}^d$, $D(d)$, G into $\mathbb{L}_2\mathbb{R}^d$.
A functional Hilbert space[1] is a Hilbert space consisting of complex valued functions on an index set $\mathbb{I}$ on which the point evaluation δ_a, is a continuous/bounded linear functional for all $\mathbf{a} \in \mathbb{I}$. Consequently, it has a Riesz representant $K_\mathbf{a} \in H$

$$f(\mathbf{a}) = \langle \delta_\mathbf{a}, f \rangle = (K_\mathbf{a}, f)_H.$$

The function $K : \mathbb{I} \times \mathbb{I} \to \mathbb{C}$ given by $K(\mathbf{a}, \mathbf{b})_H = (K_\mathbf{a}, K_\mathbf{b})_H = K_\mathbf{b}(\mathbf{a})$ is called reproducing kernel.

2 Unitary operators between images and scores

In this section we present an abstract wavelet transform from a Hilbert space to a functional Hilbert space and use it to arrive at a wavelet transform on the Similitude group, $SIM(2)$. Stability of this transform is then discussed followed by an explicit construction of so called proper wavelets. The continuous wavelet transform constructed by unitary irreducible representations of locally compact groups was first formulated by Grossman et al. [29]. Given a Hilbert space H and a unitary irreducible representation $g \mapsto \mathcal{U}_g$ of any locally compact group G in H, a nonzero vector $\psi \in H$ is called admissible if

$$C_\psi := \int_G \frac{|\mathcal{U}_g \psi, \psi|^2}{(\psi, \psi)_H} d\mu_G(g) < \infty, \tag{5}$$

where μ_G denotes the left invariant Haar measure on G. Given an admissible vector $\underset{\sim}{\psi}$ and a unitary representation of a a locally compact group G in a Hilbert space H, the wavelet transform $\widetilde{\mathcal{W}}_\psi : H \to \mathbb{L}_2(G)$ is defined by

$$(\widetilde{\mathcal{W}}[f])(g) = (\mathcal{U}_g \psi, f)_H.$$

The next result is well known in mathematical physics [23].

[1] Also known as reproducing kernel Hilbert space.

Theorem 1. *The wavelet transform ($\mathcal{W}_\psi$) is a linear isometry (up to a constant) from the Hilbert space H onto a closed subspace $\mathbb{C}^G_{K_\psi}$ of $\mathbb{L}_2(G, d\mu)$:*

$$\|\mathcal{W}_\psi[f]\|^2_{\mathbb{L}_2(G)} = C_\psi \|f\|^2_H,$$

where the space $\mathbb{C}^G_{K_\psi}$ is the unique functional Hilbert space with reproducing kernel

$$K_\psi(g, g') = \frac{1}{C_\psi}(\mathcal{U}_g\psi, \mathcal{U}_{g'}\psi)_H.$$

We are interested in the $2D$-Similitude group, $SIM(2) = \mathbb{R}^2 \rtimes (\mathbb{R}^+ \times SO(2))$ which is the group of planar translations, rotations and scaling, and the left regular action $\mathcal{U}$ of $SIM(2)$ in $\mathbb{L}_2(\mathbb{R}^2)$ given by

$$(\mathcal{U}_{b,e^{i\theta},a}\psi)(\mathbf{x}) = \frac{1}{a}\psi\left(\frac{R_\theta^{-1}(\mathbf{x}-\mathbf{b})}{a}\right),\ a>0,\ \theta\in[0,2\pi],\ b\in\mathbb{R}^2. \tag{6}$$

which is an irreducible unitary representation, for proof see [30, P.51]. Though the results in [29] are applicable to our context, we now present a more general theory for wavelets which avoids the condition of irreducible representations and allows for construction of (admissible wavelets) suited to our application area of image processing. First we construct unitary maps from a Hilbert space H into a functional Hilbert space $\mathbb{C}^{\mathbb{I}}_K$, which is a vector subspace of $C^{\mathbb{I}}$, the vector space of complex valued functions on a set $\mathbb{I}$ (not necessarily a group). Following which we consider the special case of affine groups and obtain a unitary operator $\mathcal{W}_\psi : H \to \mathbb{C}^G_K$.
Subsequently we apply these results to the case $SE(2)$ and $SIM(2)$. This produces invertible orientation scores and invertible multiple scale orientation scores respectively. However if we insist on (ψ-independent) $\mathbb{L}_2$-norm preservation as presented in [29] problems arise at the origin and/or at infinity in the frequency domain[2].

2.1 Construction of a Unitary Map from a H to a $\mathbb{C}^{\mathbb{I}}_K$

A functional Hilbert space is a Hilbert space such that point evaluation is continuous, so that by Reisz representation theorem there exists a set $\{K_m | m \in \mathbb{I}\}$ with

$$(K_m, f)_H = f(m),\ \text{for all } m \in \mathbb{I} \text{ and } f \in H. \tag{7}$$

Define $K(m, m') = K_{m'}(m) = (K_m, K_{m'})_H$ for $m, m' \in \mathbb{I}$. K is called reproducing kernel and it is a function of positive type on $\mathbb{I}$ i.e.

$$\sum_{i=1}^n \sum_{j=1}^n K(m_i, m_j)\bar{c_i}c_j \geq 0,\ \textit{for all } n \in \mathbb{N},\ c_1, \ldots, c_n \in \mathbb{C},\ m_1, \ldots, m_n \in \mathbb{I}.$$

Therefore to every functional Hilbert space there belongs a reproducing kernel, which is a function of positive type. Conversely as mentioned by Aronszajn [31], a function K of positive type on set $\mathbb{I}$, induces a unique functional Hilbert space consisting of functions on $\mathbb{I}$ with reproducing kernel K.
The span of the set $\{K_m | m \in \mathbb{I}\}$ is dense in the functional Hilbert space. Indeed if $f \in H$ is orthogonal to all K_m then $f = 0$ on $\mathbb{I}$. Let $V = \{\phi_m | m \in \mathbb{I}\}$ be a subset of H. Define function $K : \mathbb{I} \times \mathbb{I} \to \mathbb{C}$ by $K(m, m') = (\phi_m, \phi_{m'})$. Given such a function, we define $K_m : \mathbb{I} \to \mathbb{C}$ as $K_m(m') = K(m, m')$. Then since $WV := \text{span}\{K_m(\cdot) | m \in \mathbb{I}\}$ is dense in H and since $\|\phi\|_{\mathbb{C}^{\mathbb{I}}_K} = \|\hat{\phi}\|_{(\mathbb{C}^{\mathbb{I}}_K)^*} = \sup_{g \in WV} \frac{|\hat{\phi}(g)|}{\|g\|}$ with dual $\hat{\phi} \in (\mathbb{C}^{\mathbb{I}}_K)^*$ determined by $\hat{\phi}(K_m) = (K_m, \phi)_{\mathbb{C}^{\mathbb{I}}_K} = \phi(m)$, we obtain the following fundamental result:

[2] In case of $SE(2)$ it is or and in case of $SIM(2)$ it is and.

Theorem 2. *If the span of $V = \{\phi_m | m \in \mathbb{I}\}$ is dense in H, then the transform $\mathcal{W} : H \to \mathbb{C}_K^{\mathbb{I}}$ defined by*

$$(\mathcal{W}[f])(m) = (\phi_m, f)_H \tag{8}$$

is a unitary mapping, i.e. $\|\mathcal{W}[f]\|_{\mathbb{C}_K^{\mathbb{I}}} = \|f\|_H$.

Proof. See [12, Ch:7.2] and [32] for details. □

When $\mathbb{I} = G$, for some locally compact group G, the norm on $\mathbb{C}_K^{\mathbb{G}}$ has a simpler explicit form compared to description given in [12, Ch:7.2] and [33, Lemma 1.7]. In what follows, we give an explicit characterization of $\mathbb{C}_K^{\mathbb{G}}$, in the case $G = \mathbb{R}^d \rtimes T$, with T a linear algebraic Lie-group, $\mathcal{U}$ the left-regular action of G onto $H = \mathbb{L}_2(\mathbb{R}^2)$ and thereby formulate a wavelet reconstruction theorem for affine groups.
Define the set $\Omega = \{\omega \in \mathbb{R}^d |$ Stab(ω) is compact$\}$, where Stab$(\omega) = \{t \in T |\ \tau(t)^T\omega = \omega\}$. This set is measurable [34, Ch 5.1]. We define,

$$H = \{f \in \mathbb{L}_2(\mathbb{R}^d) \cap \mathbb{L}_1(\mathbb{R}^d) |\ \text{supp}(\mathcal{F}f) \subset \overline{\Omega}\}. \tag{9}$$

Remark 3. *For matrix groups other than ones considered in this article Ω can be an empty set. For e.g. $\mathbb{R}^4 \rtimes SO(2,2)$, for all $\omega \in \mathbb{R}^4,\ \omega \neq 0$, Stab$(\omega) \equiv SO(2,1)$ or $SO(1,2)$ and these groups are not compact. Hence in this case $\Omega = \phi$.*

We call $\psi \in \mathbb{L}_2(\mathbb{R}^d)$ an admissible wavelet if

$$0 < M_\psi(\omega) := (2\pi) \int_T \left| \frac{\mathcal{F}[\mathcal{R}_t\psi(\omega)]}{\sqrt{det\tau(t)}} \right|^2 d\mu_T(t) < \infty \text{ for almost every } \omega \in \Omega, \tag{10}$$

where we recall that $\mathcal{R}_t$ is given by (4).

Remark 4. *In (10) we do not assume uniform bounds as for the unitarity result of $\mathcal{W}_\psi$ we do not need uniform bounds. However when quantifying stability w.r.t. $\mathbb{L}_2$-norms on input and output uniform bounds will become crucial.*

We define $\tilde{\psi}$ almost everywhere on $\mathbb{R}^d$ by

$$\tilde{\psi}(\mathbf{x}) = \int_T \frac{1}{det\tau(t)} (\overline{\mathcal{R}_t\check{\psi}} * \mathcal{R}_t\psi)(\mathbf{x}) d\mu_T(t), \tag{11}$$

where $\check{\psi}$ is defined in (4). Note that $\tilde{\psi}$ is the inverse Fourier transform of M_ψ.

Lemma 5. *Let $\psi \in H$ be an admissible wavelet. Then the span of $V_\psi = \{\mathcal{U}_g\psi | g \in G\}$, is dense in H, i.e. $\overline{\langle V_\psi \rangle} = H$.*

Proof. This follows from the general results in [34]. For details see Appendix. □

Corollary 6. *Set $G = \mathbb{R}^d \rtimes T$. If the wavelet ψ is admissible, then the corresponding wavelet transform $\mathcal{W}_\psi : H \to \mathbb{C}_K^G$ is unitary.*

Proof. Follows from Theorem 2 and Lemma 5. □

Theorem 7. *Let $G = \mathbb{R}^d \rtimes T$ and ψ be an admissible wavelet. Then $\mathcal{T}_{M_\psi}\Phi \in \mathbb{L}_2(G, d\mu_G(g))$ for all $\Phi \in \mathbb{C}_K^G$, where*

$$[\mathcal{T}_{M_\psi}[\phi]](\mathbf{b}, t) = \mathcal{F}^{-1}\left[\boldsymbol{\omega} \mapsto (2\pi)^{-d/4} M_\psi^{-1/2}(\boldsymbol{\omega}) \mathcal{F}[\phi(\cdot, t)](\boldsymbol{\omega})\right](\mathbf{b}).$$

Therefore $(\cdot,\cdot)_{\mathcal{T}_{M_\psi}} : \mathbb{C}_K^G \times \mathbb{C}_K^G \to \mathbb{C}$ *defined by*

$$(\Phi, \Psi)_{M_\psi} = (\mathcal{T}_{M_\psi}[\Phi], \mathcal{T}_{M_\psi}[\Psi])_{\mathbb{L}_2(G)}, \tag{12}$$

is an explicit characterization of the inner product on $\mathbb{C}_K^G$*, which is the unique functional Hilbert space with reproducing kernel* $K : G \times G \to \mathbb{C}$ *given by*

$$K(g,h) = (\mathcal{U}_g\psi, \mathcal{U}_h\psi)_{\mathbb{L}_2(\mathbb{R}^d)} = (\mathcal{U}_{h^{-1}g}\psi, \psi)_{\mathbb{L}_2(\mathbb{R}^d)},\ g,h \in G. \tag{13}$$

The wavelet transformation $\mathcal{W}_\psi : H \to \mathbb{C}_K^G$ *given by*

$$\mathcal{W}_\psi[f](\mathbf{b},t) = (\mathcal{U}_g\psi, f)_{\mathbb{L}_2(\mathbb{R}^d)},\ f \in \mathbb{L}_2(\mathbb{R}^d),\ g = (\mathbf{b},t) \in \mathbb{R}^d \rtimes T, \tag{14}$$

is a unitary mapping from H *to* $\mathbb{C}_K^G$*. The space* $\mathbb{C}_K^G$ *is a closed subspace of the Hilbert space* $\mathbb{H}_\psi \otimes \mathbb{L}_2(T; \frac{d\mu_T(t)}{det(\tau(t))})$*, where*

$$\mathbb{H}_\psi = \{f \in H |\ M_\psi^{-\frac{1}{2}}\mathcal{F}[f] \in \mathbb{L}_2(\mathbb{R}^d)\}$$

is equipped with the inner product

$$(f_1, f_2) = (M_\psi^{-\frac{1}{2}}\mathcal{F}[f_1], M_\psi^{-\frac{1}{2}}\mathcal{F}[f_2])_{\mathbb{L}_2(\mathbb{R}^d;(2\pi)^{-d/2}d\mathbf{x})},\ \textit{for all } f_1,\ f_2 \in H.$$

The orthogonal projection $\mathbb{P}_\psi$ *of* $\mathbb{H}_\psi \otimes \mathbb{L}_2(T; \frac{d\mu_T(t)}{det(\tau(t))})$ *onto* $\mathbb{C}_K^G$ *is given by* $(\mathbb{P}_\psi[\Phi])(g) = (K(\cdot,g), \Phi))_{M_\phi}$.

Proof. See B for proof. □

Remark 8. *Since* $\mathcal{W}_\psi : H \to \mathbb{C}_K^G$ *is unitary, the inverse equals the adjoint and thus the image* f *can be reconstructed from it's orientation score* $\mathcal{W}_\psi[f]$ *by*

$$f = \mathcal{W}_\psi^*[\mathcal{W}_\psi[f]] = \mathcal{F}^{-1}\left[\boldsymbol{\omega} \mapsto \frac{1}{(2\pi)^{d/2}} \int_T \mathcal{F}[\mathcal{W}_\psi[f](\cdot,t)](\omega)\mathcal{F}[\mathcal{R}_t\psi](\boldsymbol{\omega})\frac{d\mu_T}{|det(\tau(t))|}M_\psi^{-1}(\boldsymbol{\omega})\right].$$

Definition 9. *The inner product on* $\mathbb{H}_\psi \otimes \mathbb{L}_2(T; \frac{d\mu_T(t)}{det(\tau(t))})$ *induces a norm* $\|.\|_{M_\psi} : \mathbb{H}_\psi \otimes \mathbb{L}_2\left(T; \frac{d\mu_T(t)}{det(\tau(t))}\right) \to \mathbb{R}^+$*, which is given by*

$$\|\Phi\|_{M_\psi} = \sqrt{(\Phi,\Phi)_{M_\psi}} = \int_{\mathbb{R}^2}\int_T |\mathcal{F}[\Phi(\cdot,t)](\boldsymbol{\omega})|^2(2\pi)^{-d/2}M_\psi^{-1}(\boldsymbol{\omega})\frac{d\mu_T(t)}{det(\tau(t))}d\boldsymbol{\omega},$$

which is called the M_ψ*-norm.*

2.2 Orientation Scores

In this case $G = SE(2)$, $(\mathcal{U}_{g=(\mathbf{b},\theta)}\psi)(\mathbf{x}) = \psi\left(\mathbf{R}_\theta^{-1}(\mathbf{x}-\mathbf{b})\right)$, $\Omega = \mathbb{R}^2$ and $H = \mathbb{L}_2(\mathbb{R}^2) \cap \mathbb{L}_1(\mathbb{R}^2)$ leading to [7, Thm 1]. For more details on construction as well operators on Orientation Scores see [27, 28]. For $\psi \in \mathbb{L}_2(\mathbb{R}^2) \cap \mathbb{L}_1(\mathbb{R}^2)$, M_ψ is a continuous function vanishing at infinity. Quadratic norm preservation i.e. $M_\psi = 1$ and a unitary operator $\mathcal{W}_\psi : \mathbb{L}_2(\mathbb{R}^2) \to \mathbb{L}_2(SE(2))$ cannot be obtained and one can rely on either distributions $\psi \in \mathbb{H}^{-s}(\mathbb{R}^2)$ with $s > 1$ and distributional wavelet transforms or restrict to disc-limited images, which is appropriate for imaging applications.

2.3 Multiple Scale Orientation Scores

Consider the case $T := SO(2) \times \mathbb{R}^+$, $G := SIM(2) = \mathbb{R}^2 \rtimes_\tau (SO(2) \times \mathbb{R}^+)$ where[3] the semi-direct product is defined to be the group with underlying set $\mathbb{R}^2 \times (SO(2) \times \mathbb{R}^+)$ equipped with the group product

$$(\mathbf{x}, a, \theta)(\mathbf{x}', a', \theta') = (\mathbf{x} + \tau(a, \theta)\mathbf{x}', aa', \theta + \theta'), \quad \forall (\mathbf{x}, a, \theta), (\mathbf{x}', a', \theta') \in SIM(2), \tag{15}$$

where[4] $\tau(a, \theta) = a\mathbf{R}_\theta$.
Since both $\mathbb{R}^2$ and $SO(2) \times \mathbb{R}^+$ are locally compact groups, $SIM(2)$ is a locally compact group as well and thus has a left-invariant Haar measure defined on it. Consider the unitary representation of $SIM(2)$ in $\mathbb{L}_2(\mathbb{R}^2)$ given by,

$$\mathcal{U}_{g=(\mathbf{b},a,\theta)}\psi(\mathbf{x}) = \frac{1}{a}\psi\left(\frac{\mathbf{R}_\theta^{-1}(\mathbf{x} - \mathbf{b})}{a}\right), \ a > 0, \ \theta \in [0, 2\pi], \ \mathbf{b} \in \mathbb{R}^2, \tag{16}$$

We denote $\mathcal{U} : (\mathbf{x}, t) = (\mathbf{x}, a, \theta) \mapsto \mathcal{U}_{(\mathbf{x},t)}$ as

$$\mathcal{U}_{\mathbf{x},t} f = \mathcal{T}_\mathbf{x}\mathcal{R}_t f, \quad t = (a, \theta) \in \mathbb{R}^+ \times SO(2) \tag{17}$$

where $(\mathcal{T}_\mathbf{x} f)(\mathbf{x}') = f(\mathbf{x}' - \mathbf{x})$ and $(\mathcal{R}_t f)(\mathbf{x}') = \frac{1}{a} f(\frac{1}{a}\mathbf{R}_\theta \mathbf{x}')$ for all $x, x' \in \mathbb{R}^2$.
Theorem 7 has the following important consequence for our application of (multiple-scale) orientation scores in image analysis.

Corollary 10. *The space of multiple scale orientation scores is a reproducing kernel Hilbert space $\mathbb{C}_K^{SIM(2)}$ which is a closed subspace of $\mathbb{H}_\psi \otimes \mathbb{L}_2(SO(2) \times \mathbb{R}^+; \frac{d\mu_T(t)}{det(\tau(t))})$ which is a vector subspace[5] of $\mathbb{L}_2(G)$. The inner product on $\mathbb{C}_K^{\mathbb{R}^2 \rtimes (SO(2)\times\mathbb{R}^+)}$ is given by* (12) *and is explicitly characterized by means of the function M_ψ given by,*

$$M_\psi(\boldsymbol{\omega}) = (2\pi) \int\limits_{T=SO(2)\times\mathbb{R}^+} \left| \frac{(\mathcal{F}[\mathcal{R}_t\psi])(\boldsymbol{\omega})}{\sqrt{det\tau(t)}} \right|^2 d\mu_T(t). \tag{18}$$

The wavelet transform which maps an image $f \in \mathbb{L}_2(\mathbb{R}^2) \cap \mathbb{L}_1(\mathbb{R}^2)$ onto its orientation score $U_f \in \mathbb{C}_K^{SIM(2)}$ is a unitary mapping: $\|f\|^2_{\mathbb{L}_2(\mathbb{R}^2)} = \|\mathcal{W}_\psi[f]\|^2_{M_\psi}$. Thus the image f can be reconstructed from its orientation score $U_f := \mathcal{W}_\psi[f]$ by means of the adjoint wavelet transformation $\mathcal{W}_\psi^*$:

$$f = \mathcal{W}_\psi^*[\mathcal{W}_\psi[f]] = \mathcal{F}^{-1}\left[\boldsymbol{\omega} \mapsto \frac{1}{(2\pi)} \int\limits_{\mathbb{R}^+} \int\limits_0^{2\pi} \mathcal{F}[U_f(\cdot, a, e^{i\theta})](\boldsymbol{\omega})\mathcal{F}[\mathcal{R}_{a,e^{i\theta}}\psi](\boldsymbol{\omega}) d\theta \frac{da}{a} M_\psi^{-1}(\boldsymbol{\omega})\right]. \tag{19}$$

Proof. Follows by Theorem 7 and $\Omega = \mathbb{R}^2 \backslash \{0\}$ such that $\overline{\Omega} = \mathbb{R}^2$ and $H = \mathbb{L}_2(\mathbb{R}^2) \cap \mathbb{L}_1(\mathbb{R}^2)$. □

Explicitly M_ψ as defined in (18) can be written as,

$$M_\psi(\boldsymbol{\omega}) = (2\pi) \int\limits_T \left| \frac{\mathcal{F}[\mathcal{R}_t\psi](\omega)}{\sqrt{det\tau(t)}} \right|^2 d\mu_T(t) = (2\pi) \int\limits_0^{2\pi} \int\limits_{\mathbb{R}^+} \left| \frac{\mathcal{F}[\mathcal{R}_{(a,\theta)}\psi](\boldsymbol{\omega})}{a} \right|^2 \frac{da}{a} d\theta = 2\pi \int\limits_0^{2\pi} \int\limits_{\mathbb{R}} |\hat{\psi}(e^\tau \mathbf{R}_\theta^{-1}\boldsymbol{\omega})|^2 d\tau d\theta \tag{20}$$

for all $t = (a, \theta) \in SO(2) \times \mathbb{R}^+$. Note that in the last equality we have made use of the substitution $\tau = \log_e(a)$.

[3] We drop the subscript τ from the semi-direct product hereon for the ease of notation.
[4] $\mathbf{R}_\theta$ is the standard counter-clockwise rotation matrix.
[5] i.e. is a subspace as a vector space, but is equipped with a different norm

2.4 The Discrete Analogue

Hereon in this section we deal with the practical aspects of the implementation of the continuous wavelet transform discussed in the previous sections.
Recall that $SIM(2) = \mathbb{R}^2 \rtimes (SO(2) \times \mathbb{R}^+)$ where $T = (SO(2) \times \mathbb{R}^+)$ is a locally compact group, but not a compact group. We can choose $SO(2)$ to be finite rotation group, denoted by $\mathbb{T}_N$ (equipped with discrete topology) which is locally compact [6] i.e.

$$\mathbb{T}_N = \{e^{ik\Delta_{\mathbb{T}}} | k \in \{0, 1, \ldots, N-1\}, \Delta_{\mathbb{T}} = \frac{2\pi}{N}\}, \text{ for } N \in \mathbb{N}. \tag{21}$$

On the other hand the scaling group $\mathbb{R}^+$ cannot be written in terms of a finite scaling group due to the following well known result from group theory that

Lemma 11. *Every finite subgroup of the multiplicative group of a field is a cyclic subgroup.*

See [35] for proof. The only finite subgroups of the group $\mathbb{R}^* = (\mathbb{R}/\{0\}, *)$ are $\{1\}$ and $\mathbb{Z}_2 = \{-1, 1\}$. The scaling group $\mathbb{R}^+$ is a subgroup of $\mathbb{R}^*$ and therefore it does not have any finite subgroups other than the trivial subgroup. So it is important to note that, we loose the inherent group structure in the discrete version, unlike in the case of orientation score over the Euclidean motion group $SE(2)$, see [12, Sec 4.4].
Consider the scaling group $\mathbb{R}^+$; this group consists of all positive reals greater than zero. In the discrete case we need to have a lower and an upper bound on the choice of the scales. We assume that $a \in [a^-, a^+]$ where $0 < a^- < a^+$. We have the following discretization for scales,

$$\mathbb{D}_M = \left\{ e^{(\tau^- + k\Delta_{\mathbb{D}})} | k \in \{0, 1, \ldots M-1\}, \Delta_{\mathbb{D}} = \frac{e^{\tau^+} - e^{\tau^-}}{M} \right\}, \text{ for } M \in \mathbb{N}, \tag{22}$$

where $\tau^- = \log(a^-)$ and $\tau^+ = \log(a^+)$.
Using the notation, $t_{kl} = (a_l, \theta_k),\ k \in \{0, 1, \ldots, N-1\},\ l \in \{0, 1, \ldots, M-1\}$ where $a_l = \tau^- + k\Delta_{\mathbb{D}}$ and $\theta_k = k\Delta_{\mathbb{T}}$, we write the discrete version of (17)

$$U_f^{N,M}(\mathbf{b}, a_l, \theta_k) = (\mathcal{T}_{\mathbf{b}} \mathcal{R}_{(a_l, \theta_k)} \psi, f)_{\mathbb{L}_2(\mathbb{R}^2)}, \tag{23}$$

which is the discrete orientation score of an image $f \in \mathbb{L}_2(\mathbb{R}^2)$. We emphasize that we do not consider a wavelet transform on a discrete subgroup of $SIM(2)$ group (due to Lemma 11) but rather a discretized version of the continuous wavelet transform. The discrete version of M_ψ is,

$$M_\psi^D(\boldsymbol{\omega}) = \frac{1}{N} \frac{1}{M} \sum_{k=0}^{N-1} \sum_{l=0}^{M-1} \left| \frac{\mathcal{F}(\mathcal{R}_{(a_l, \theta_k)} \psi)(\boldsymbol{\omega})}{a_l} \right|^2. \tag{24}$$

2.5 Stable reconstruction of an image from OS

In Corollary 10 we have a unitarity result where $\mathbb{C}_K^{SIM(2)} \subset \mathbb{H}_\psi \otimes \mathbb{L}_2(SO(2) \times \mathbb{R}^+; \frac{d\mu_T(t)}{det(\tau(t))})$ depends on the wavelet ψ. For stability estimates one requires $\mathbb{L}^2$-norms on both the domain and the range. This means we must impose uniform lower and upper bounds in (10), which is possible only when we restrict the space of images to functions in $\mathbb{L}_2(\mathbb{R}^2) \cap \mathbb{L}_1(\mathbb{R}^2)$ whose Fourier transform is contained in an annulus. The space of these images is a Hilbert space given by,

$$\mathbb{L}_2^{\varrho^-, \varrho^+}(\mathbb{R}^2) = \{f \in \mathbb{L}_2(\mathbb{R}^2) | \text{ supp}(\mathcal{F}[f]) \subset B_{0,\varrho^+} \backslash B_{0,\varrho^-}\}, \quad \varrho^+ > \varrho^- > 0. \tag{25}$$

A practical motivation for the assumption of an upper bound (ϱ^+) on the support of the Fourier transform of the images is the Nyquist theorem, which states that *every band-limited function is determined by its values*

[6] Topological spaces with a discrete topology are locally compact.

on a discrete grid. E.g. if $u_B : \mathbb{R}^2 \to \mathbb{C}$ is band-limited on a square: $\text{supp}(\mathcal{F}[u_B]) \subset [-l/2, l/2] \times [-l/2, l/2]$, then

$$u_B(x,y) = \sum_{(k_1,k_1)\in\mathbb{Z}^2} u_B\left(\frac{2\pi k_1}{l}, \frac{2\pi k_2}{l}\right) sinc\left(\frac{lx}{2} - k_1\pi\right) sinc\left(\frac{ly}{2} - k_2\pi\right),$$

where the cutoff frequency $\varrho = l/2$ is called the Nyquist frequency.
The value for ϱ^- directly relates to the coarsest scale we wish to detect in the spatial domain. Therefore the removal of extremely low frequencies from the image essentially corresponds to background removal in the image which is often an essential pre-processing step in medical image processing, see [36, 37].
We wish to construct a wavelet transform

$$\mathcal{W}_\psi^{\varrho^-,\varrho^+} : \mathbb{L}_2^{\varrho^-,\varrho^+}(\mathbb{R}^2) \to \mathbb{L}_2(SIM(2)) \tag{26}$$

which requires that (recall Eq.25),

$$\mathcal{U}_{\mathbf{x},a,\theta}\psi \in \mathbb{L}_2^{\varrho^-,\varrho^+}(\mathbb{R}^2), \text{ where } a \in [a^-, a^+] \text{ and } \theta \in [0, 2\pi], \text{ with } a^+ > 1 > a^- \text{ such that } \frac{\rho^-}{a^-} < \frac{\rho^+}{a^+}.$$

Therefore we choose

$$\psi \in \mathbb{L}_1(\mathbb{R}^2) \cap \mathbb{L}_2(\mathbb{R}^2) \text{ with } \text{supp}(\mathcal{F}[\psi]) \subset B_{0,\varrho^+/a^+} \backslash B_{0,\varrho^-/a^-} \tag{27}$$

and therefore we satisfy $\text{supp}(\mathcal{F}[\mathcal{U}_{\mathbf{x},a,\theta}\psi]) \subset B_{0,\varrho^+} \backslash B_{0,\varrho^-}$, where $a \in [a^-, a^+]$ and $\theta \in [0, 2\pi]$.
Note that in our current context, $\psi \in \mathbb{L}_2^{\varrho^-,\varrho^+}(\mathbb{R}^2)$ is called an *admissible wavelet* if

$$0 < M_\psi = (2\pi) \int_0^{2\pi} \int_{a^-}^{a^+} \left| \frac{\mathcal{F}[\mathcal{R}_{a,\theta}\psi]}{\sqrt{det\tau(t)}} \right|^2 \frac{da}{a} d\theta < \infty \text{ on } B_{0,\varrho^+} \backslash B_{0,\varrho^-}, \tag{28}$$

where $\mathcal{R}_t$ is given by (4). Corresponding to (11) we can define $\tilde{\psi}$ as,

$$\tilde{\psi}(\mathbf{x}) = \int_0^{2\pi} \int_{a^-}^{a^+} (\overline{\mathcal{R}_{a,\theta}\tilde{\psi}} * \mathcal{R}_{a,\theta}\psi)(\mathbf{x}) \frac{da}{a} d\theta. \tag{29}$$

By the compactness of the set $[-\pi, \pi] \times [a^-, a^+]$ and since the convolution of two $\mathbb{L}_1(\mathbb{R}^2)$ functions is again in $\mathbb{L}_1(\mathbb{R}^2)$, we have that $\tilde{\psi} \in \mathbb{L}_1(\mathbb{R}^2)$, and so its Fourier transform $M_\psi = \mathcal{F}\tilde{\psi}$ is a bounded continuous function on $B_{0,\varrho^+} \backslash B_{0,\varrho^-}$. We define, $SIM_+^- := \mathbb{R}^2 \times [-\pi, \pi] \times [a^-, a^+]$.

Definition 12. *Let ψ be an admissible wavelet in the sense of* (28)*. Then the wavelet transform $\mathcal{W}_\psi^{\varrho^-,\varrho^+} : \mathbb{L}_2^{\varrho^-,\varrho^+}(\mathbb{R}^2) \to \mathbb{L}^2(SIM_+^-)$ is given by*

$$(\mathcal{W}_\psi^{\varrho^-,\varrho^+}[f])(g) = \frac{1}{a} \int_{\mathbb{R}^2} \overline{\psi\left(R_\theta^{-1}\left(\frac{\mathbf{y}-\mathbf{x}}{a}\right)\right)} f(\mathbf{y}) d\mathbf{y}, \ f \in \mathbb{L}_2^{\varrho^-,\varrho^+}(\mathbb{R}^2),$$

for almost every $g = (\mathbf{x}, a, \theta) \in SIM_+^-$.

Quantification of Stability The usual way to quantify well-posedness/stability of an invertible linear transformation $A : V \to W$ from a Banach space $(V, \|\cdot\|_V)$ to a Banach space $(W, \|\cdot\|_W)$ is by means of the condition number

$$cond(A) = \|A^{-1}\|\|A\| = \left(\sup_{x\in V} \frac{\|\mathbf{x}\|_V}{\|A\mathbf{x}\|_W}\right)\left(\sup_{x\in V} \frac{\|A\mathbf{x}\|_W}{\|\mathbf{x}\|_V}\right) \geq 1. \tag{30}$$

The closer it approximates 1, the more stable the operator and its inverse is. The condition number depends on the norms imposed on V and W. We wish to apply this general concept to the wavelet transformation which maps image f to its scale orientation score U_f. Recall from Corollary 10 that the wavelet transform is a unitary mapping from the space $\mathbb{L}_2(\mathbb{R}^2)$ to the space $\mathbb{C}_K^{SIM(2)}$ respectively equipped with the $\mathbb{L}_2$-norm and the M_ψ-norm. Thus choosing these norms the condition number becomes 1. However from a practical point of view it is more appropriate to impose the $\mathbb{L}_2(SIM(2))$-norm on the score since it does not depend on the choice of the wavelet ψ and we also use a $\mathbb{L}_2$-norm on the space of images.

Theorem 13. *Let ψ be an admissible wavelet, with $M_\psi(\boldsymbol{\omega}) > 0$ for all $\boldsymbol{\omega} \in B_{0,\varrho^+} \backslash B_{0,\varrho^-}$. Then the condition number $cond(\mathcal{W}_\psi^{\varrho^-,\varrho^+})$ of the wavelet transformation $\mathcal{W}_\psi^{\varrho^-,\varrho^+} : \mathbb{L}_2^{\varrho^-,\varrho^+}(\mathbb{R}^2) \to \mathbb{L}_2(G)$, $(G = SIM_+^-)$ is[7] defined by*

$$cond(\mathcal{W}_\psi^{\varrho^-,\varrho^+}) = \|(\mathcal{W}_\psi^{\varrho^-,\varrho^+})^{-1}\|\|(\mathcal{W}_\psi^{\varrho^-,\varrho^+})\| = \left(\sup_{f\in\mathbb{L}_2^{\varrho^-,\varrho^+}(\mathbb{R}^2)} \frac{\|f\|_{\mathbb{L}_2(\mathbb{R}^2)}}{\|U_f\|_{\mathbb{L}_2(G)}}\right)\left(\sup_{f\in\mathbb{L}_2^{\varrho^-,\varrho^+}(\mathbb{R}^2)} \frac{\|U_f\|_{\mathbb{L}_2(G)}}{\|f\|_{\mathbb{L}_2(\mathbb{R}^2)}}\right)$$

and satisfies

$$1 \leq (cond(\mathcal{W}_\psi^{\varrho^-,\varrho^+}))^2 \leq \left(\sup_{\varrho^-\leq\|\boldsymbol{\omega}\|\leq\varrho^+} M_\psi^{-1}(\boldsymbol{\omega})\right)\left(\sup_{\varrho^-\leq\|\boldsymbol{\omega}\|\leq\varrho^+} M_\psi(\boldsymbol{\omega})\right).$$

Proof. Since $M_\psi > 0$ and is continuous on the compact set $B_{0,\varrho^+}\backslash B_{0,\varrho^-} = \{\boldsymbol{\omega} \in \mathbb{R}^2 | \varrho^- < \|\boldsymbol{\omega}\| < \varrho^+\}$, $\sup_{\varrho^-<\|\boldsymbol{\omega}\|<\varrho^+} M_\psi(\boldsymbol{\omega}) = \max_{\varrho^-<\|\boldsymbol{\omega}\|<\varrho^+} M_\psi(\boldsymbol{\omega})$ do exist. The same holds for M_ψ^{-1}. Furthermore for all $f \in \mathbb{L}_2^{\varrho^-,\varrho^+}(\mathbb{R}^2)$, the restriction of the corresponding orientation scores, to fixed orientations and scales also belong to the same space, i.e. $U_f(\cdot, a, e^{i\theta}) \in \mathbb{L}_2^{\varrho^-,\varrho^+}(\mathbb{R}^2)$, where $\theta \in [0, 2\pi]$, $a \in [a^-, a^+]$. This follows from

$$(\mathcal{W}_\psi f)(\mathbf{x}, t) = \int_{\mathbb{R}^2} \overline{\mathcal{R}_t\check{\psi}(\mathbf{x}-\mathbf{x}')} f(\mathbf{x}')d\mathbf{x}' = (\overline{\mathcal{R}_t\check{\psi}} *_{\mathbb{R}^2} f)(\mathbf{x}) = \left(\mathcal{F}^{-1}(\overline{\mathcal{F}\mathcal{R}_t\psi}\mathcal{F}f)\right)(\mathbf{x}), \tag{31}$$

which gives, $\mathcal{F}[U_f](\boldsymbol{\omega}) = \mathcal{F}[\overline{\mathcal{R}_t\check{\psi}}](\boldsymbol{\omega})\mathcal{F}[f](\boldsymbol{\omega})$. By Corollary 10 we have $\|f\|^2_{\mathbb{L}_2(\mathbb{R}^2)} = \|U_f\|^2_{M_\psi}$ and

$$\begin{aligned}(\mathrm{cond}(\mathcal{W}_\psi^{\varrho^-,\varrho^+}))^2 &= \left(\sup_{f\in\mathbb{L}_2^{\varrho^-,\varrho^+}(\mathbb{R}^2)} \frac{\|U_f\|_{M_\psi}}{\|U_f\|_{\mathbb{L}_2(G)}}\right)\left(\sup_{f\in\mathbb{L}_2^{\varrho^-,\varrho^+}(\mathbb{R}^2)} \frac{\|U_f\|_{\mathbb{L}_2(G)}}{\|U_f\|_{M_\psi}}\right)\\ &\leq \left(\sup_{\varrho^-\leq\|\boldsymbol{\omega}\|\leq\varrho^+} M_\psi^{-1}(\boldsymbol{\omega})\right)\left(\sup_{\varrho^-\leq\|\boldsymbol{\omega}\|\leq\varrho^+} M_\psi(\boldsymbol{\omega})\right).\end{aligned}$$

Further we have, $1 = \|(\mathcal{W}_\psi^{\varrho^-,\varrho^+})^{-1}(\mathcal{W}_\psi^{\varrho^-,\varrho^+})\| \leq \|(\mathcal{W}_\psi^{\varrho^-,\varrho^+})^{-1}\|\|(\mathcal{W}_\psi^{\varrho^-,\varrho^+})\|$. □ □

Corollary 14. *The stability of the (inverse) wavelet transformation $\mathcal{W}_\psi^{\varrho^-,\varrho^+} : \mathbb{L}_2^{\varrho^-,\varrho^+}(\mathbb{R}^2) \to \mathbb{L}^2(SIM_+^-)$ is optimal if $M_\psi^\varrho(\boldsymbol{\omega}) =$ constant for all $\boldsymbol{\omega} \in \mathbb{R}$, with $\varrho^- \leq \|\boldsymbol{\omega}\| \leq \varrho^+$.*

Thus, in general, the closer the function M_ψ approximates the constant function, say $1_{B_{0,\varrho^+}\backslash B_{0,\varrho^-}}$, the better the M_ψ norm on $\mathbb{C}_K^{SIM(2)}$ approximates the $\mathbb{L}_2(SIM_+^-)$ norm, the better the stability of reconstruction. In case of a good approximation, i.e. $M_\psi \approx 1_{B_{0,\varrho^+}\backslash B_{0,\varrho^-}}$, the reconstruction formula in Corollary 10 can be simplified to,

$$f \approx \mathcal{F}^{-1}\left[\boldsymbol{\omega} \mapsto \frac{1}{(2\pi)} \int_{a^-}^{a^+}\int_0^{2\pi} \mathcal{F}[U_f(\cdot, a, e^{i\theta})](\boldsymbol{\omega})\mathcal{F}[\mathcal{R}_{a,e^{i\theta}}\psi](\boldsymbol{\omega})d\theta\frac{da}{a}\right]. \tag{32}$$

[7]Note that while the norm is $\mathbb{L}_2(SIM(2))$-norm we only consider an interval in the scaling group.

2.6 Design of Proper Wavelets

In this sequel a wavelet $\psi \in \mathbb{L}_2(\mathbb{R}^2) \cap \mathbb{L}_1(\mathbb{R}^2)$ with M_ψ smoothly approximating $1_{B_{0,\varrho^+} \setminus B_{0,\varrho^-}}$, is called a **proper wavelet**. The entire class of proper wavelets allows for a lot of freedom in the choice of ψ. In practice it is mostly sufficient to consider wavelets that are similar to the long elongated patch one would like to detect and orthogonal to structures of local patches which should not be detected, in other words employing the basic principle of template matching. We restrict the possible choices by listing below certain practical requirements to be fulfilled by our transform.

1. The wavelet transform should yield a finite number of orientations (N_0) and scales (M_0).
2. The wavelet should be strongly directional, in order to obtain sharp responses on oriented structures.
3. The transformation should handle lines, contours and oriented patters. Thus the wavelet should pick up edge, ridge and periodic profiles.
4. In order to pick up local structures, the wavelet should be localized in spatial domain.

To ensure that the wavelet is strongly directional and minimize uncertainty in $SIM(2)$, we require that the support of the wavelet be contained in a convex cone in the Fourier domain, [17].
The following lemma gives a simple but practical approach to obtain proper wavelets ψ, with $M_\psi = 1_{B_{0,\varrho^+} \setminus B_{0,\varrho^-}}$. Note that we make use of polar coordinates (ρ, φ), $\rho = \|\boldsymbol{\omega}\|$, $\boldsymbol{\omega} = (\rho\cos\varphi, \rho\cos\varphi)$.

Lemma 15. *Let τ^-, τ^+ be chosen such that $\tau^- = \log(a^-)$ and $\tau^+ = \log(a^+)$, where $0 < a \in [a^-, a^+]$ is the finite interval of scaling. Let $A : SO(2) \to \mathbb{C}\backslash\mathbb{R}^-$ and $B : [\tau^-, \tau^+] \to \mathbb{C}\backslash\mathbb{R}^-$ such that*

$$2\pi \int_0^{2\pi} |A(\varphi)| d\varphi = 1, \ \int_{\tau^-}^{\tau^+} |B(\rho)| d\rho = 1, \tag{33}$$

then the wavelet $\psi = \mathcal{F}^{-1}[\boldsymbol{\omega} \to \sqrt{A(\varphi)B(\rho)}]$ with $\boldsymbol{\omega} = (\rho\cos\varphi, \rho\cos\varphi)$ has $M_\psi(\boldsymbol{\omega}) = 1$ for all $\boldsymbol{\omega} \in B_{0,\varrho^+} \backslash B_{0,\varrho^-}$.

Proof. From (20) and (28), for all $\boldsymbol{\omega} \in B_{0,\varrho^+} \backslash B_{0,\varrho^-}$ we have,

$$M_\psi(\boldsymbol{\omega}) = 2\pi \int_0^{2\pi} \int_{\varrho^-}^{\varrho^+} |\hat{\psi}(e^\tau \mathbf{R}_\theta^{-1}\boldsymbol{\omega})|^2 d\tau d\theta = 2\pi \int_0^{2\pi} \int_{\varrho^-}^{\varrho^+} |\sqrt{A(\varphi-\theta)B(e^\tau\rho)}|^2 d\tau d\theta = 1.$$

□ □

Lemma 15 can be translated into discrete framework $\mathbb{R}^2 \rtimes (\mathbb{T}_N \times \mathbb{D}_M)$, recall (21) and (22), where condition (33) is replaced respectively by,

$$\frac{1}{N} \sum_{k=0}^{N-1} |A(\varphi - \theta_k)| = 1 \text{ and } \frac{1}{M} \sum_{l=0}^{M-1} |B(e^{a_l}\rho)| = 1. \tag{34}$$

where we have made use of discrete notations introduced in (23).
If moreover $2\pi \int_0^{2\pi} \sqrt{|A(\varphi)|} d\varphi \approx 1$ and $\int_{\tau^-}^{\tau^+} |\sqrt{B(\rho)}| d\rho \approx 1$, we have a fast and simple approximation for the reconstruction:

$$\tilde{f}(\mathbf{x}) = 2\pi \int_0^{2\pi} \int_{\tau^-}^{\tau^+} (\mathcal{W}_\psi f)(\mathbf{x}, \tau, \theta) d\tau d\theta \approx \mathcal{F}^{-1}[\boldsymbol{\omega} \mapsto (\sqrt{M_\psi} * \mathcal{F}[f](\boldsymbol{\omega}))](\mathbf{x}), \text{ for a.e. } \boldsymbol{\omega} \in B_{0,\varrho^+} \backslash B_{0,\varrho^-}.$$

$$M_\psi \approx 1_{B_{0,\varrho^+} \setminus B_{0,\varrho^-}} \Rightarrow \tilde{f} \approx f \in \mathbb{L}_2^{\varrho^-,\varrho^+}(\mathbb{R}^2) \tag{35}$$

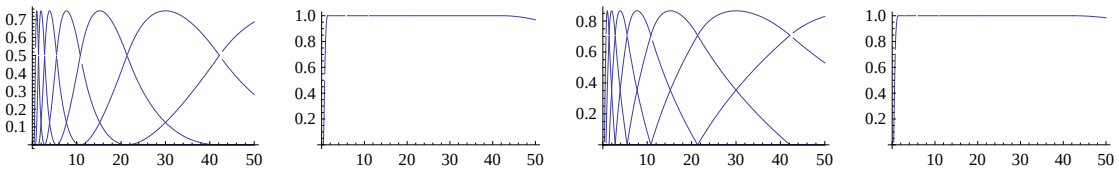

Figure 4: Plot for the B-splines in (39). Values chosen: $a^- = \varrho^- = 10^{-8}$, $a^+ = \varrho^+ = 50$, $N_s = 7$. From Left to Right: Plot of each B-spline, $B^k\left(\frac{\log[\rho]}{s_\rho} - l\right)$. The B-splines are skewed because of non linear sampling in the scale dimension; $\sum_{l=0}^{N_s-1} B^k\left(\frac{\log[\rho]}{s_\rho} - l\right) = 1$; plot of square root of the B-spline, i.e. $\sqrt{B^k\left(\frac{\log[\rho]}{s_\rho} - l\right)}$; $\sum_{l=0}^{N_s-1} \sqrt{B^k\left(\frac{\log[\rho]}{s_\rho} - l\right)} \approx 1$.

We have made use of the description of $(\mathcal{W}_\psi f)$ given in (31). We need to fulfil the requirement $M_\psi(\boldsymbol{\omega}) \approx 1$ with an appropriate choice of kernel satisfying the condition given above, to achieve this simple reconstruction.

The idea is to "*fill the cake by pieces of the cake*" in the Fourier domain. In order to avoid high frequencies in the spatial domain, these pieces must be smooth and thereby must overlap. A choice of B-spline based functions in the angular and the log-radial direction is an appropriate choice for such a wavelet kernel. This design of wavelets in the Fourier domain is similar to the framework of curvelets [21, 22]. However, our decomposition of unity in the Fourier domain is more suited for the subsequent design of left-invariant diffusions in the wavelet domain.

The k^{th} order B-spline denoted by B^k is defined as,

$$B^k(x) = (B^{k-1} * B^0)(x),\ B^0(x) = \begin{cases} 1 & if -1/2 < x < +1/2 \\ 0 & otherwise \end{cases} \tag{36}$$

with the property that B-splines add up to 1. For more details see [38].

Based on the requirements and considerations above we propose the following kernel

$$\psi(\mathbf{x}) = \mathcal{F}^{-1}_{\mathbb{R}^2}[\boldsymbol{\omega} \to \sqrt{A(\varphi)B(\rho)}](\mathbf{x}) G_{\sigma_s}(\mathbf{x}), \tag{37}$$

where G_{σ_s} is a Gaussian window that enforces spatial locality cf. requirement 5. Note that such window relates to a diffusion in the Fourier domain and does not affect the reconstruction properties (M_ψ).

$A : \mathbb{T} \to \mathbb{R}^+$, is defined by,

$$A(\varphi) = B^k\left(\frac{(\varphi \bmod 2\pi) - \pi/2}{s_\varphi}\right), \tag{38}$$

where $s_\varphi = \frac{2\pi}{N_\theta}$ (N_θ denotes the number of orientations chosen) and B^k denotes the kth order B-spline.

$B : [\varrho^-, \varrho^+] \to \mathbb{R}^+$, is defined as,

$$B(\varrho) = \sum_{l=0}^{N_s-1} B^k\left(\frac{\log[\rho]}{s_\rho} - l\right), \tag{39}$$

where $s_\rho = (\log[a^+] - \log[a^-])/N_s$, with N_s equals the number of chosen scales and a^-, a^+ are predefined scales, based on ϱ^-, ϱ^+ respectively. See Figure 4 for a plot of these B-splines. Note that,

$$\sum_{l=0}^{N_s-1} B^k\left(\frac{\log[\rho]}{s_\rho} - l\right) = 1 \text{ and } \sum_{l=0}^{N_s-1} \sqrt{B^k\left(\frac{\log[\rho]}{s_\rho} - l\right)} \approx 1.$$

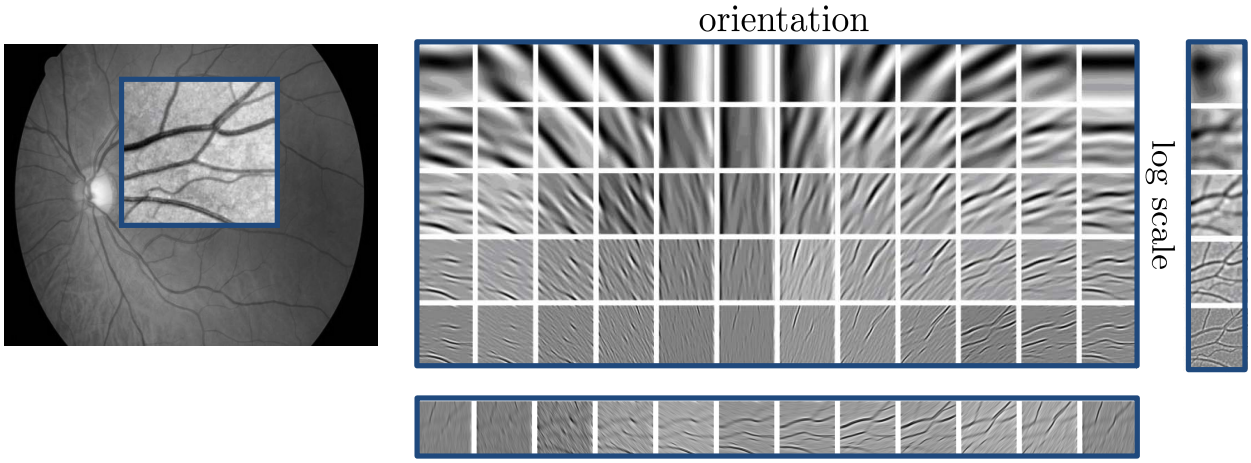

Figure 5: Scale-OS of a retinal image. As shown, Scale-OS can be used to create the Orientation Score and Gaussian-Scale Space of the image.

3 Operators on Scores

There exists exists a 1-to-1 correspondence between bounded operators $\Phi \in \mathbb{B}(\mathbb{C}_K^G)$ on orientation scores and bounded operators $\Upsilon \in \mathcal{B}(\mathbb{L}_2(\mathbb{R}^d))$:

$$\Upsilon[f] = (\mathcal{W}_\psi^* \circ \Phi \circ \mathcal{W}_\psi)[f], \ f \in \mathbb{L}_2(\mathbb{R}^d), \tag{40}$$

which allows us to relate operations on orientation scores to operations on images in a robust manner. To get a schematic view of the operations see Figure 1.
Recall from Corollary 10 that the range of the unitary wavelet transform $\mathcal{W}_\psi : \mathbb{L}_2(\mathbb{R}^2) \to \mathbb{C}_K^G$ is the space of orientation scores as a closed linear subspace of $\mathbb{H}_\psi$, which is a vector subspace of $\mathbb{L}_2(G)$. For proper wavelets we have (approximative) $\mathbb{L}_2$-norm preservation and therefore $\mathbb{L}_2(G) \cong \mathbb{H}_\psi$ (with $\mathbb{L}_2(G) = \mathbb{H}_\psi$ if $M_\psi = 1$).
In general if, $\Phi : \mathbb{L}_2(G) \to \mathbb{L}_2(G)$ is a bounded operator on $\mathbb{L}_2(G)$, then the range of restriction of this operator to the subspace $\mathbb{C}_K^G$ of orientation scores need not be contained in $\mathbb{C}_K^G$, i.e. $\Phi(U_f)$ need not be the orientation score of an image. To this end we also consider $\widetilde{\mathcal{W}}_\psi : \mathbb{L}_2(\mathbb{R}^d) \to \mathbb{L}_2(G)$ given by $\widetilde{\mathcal{W}}_\psi f = \mathcal{W}_\psi f$. It's adjoint is given by,

$$(\widetilde{\mathcal{W}}_\psi)^*(V) = \int_G \mathcal{U}_g\psi \ V(g) d\mu_G(g), \ V \in \mathbb{L}_2(G).$$

The operator $\mathbb{P}_\psi = \widetilde{\mathcal{W}}_\psi(\widetilde{\mathcal{W}}_\psi)^*$ is the orthogonal projection on the space of orientation scores $\mathbb{C}_K^G$. This projection can be used to decompose the manipulated orientation score:

$$\Phi(U_f) = \mathbb{P}_\psi(\Phi(U_f)) + (I - \mathbb{P}_\psi)(\Phi(U_f)).$$

Notice that the orthogonal complement $(\mathbb{C}_K^G)^\perp$, which equals $\mathcal{R}(I - \mathbb{P}_\psi)$, is exactly the null-space of $(\widetilde{\mathcal{W}}_\psi)^*$ as $\mathcal{N}((\widetilde{\mathcal{W}}_\psi)^*) = \mathcal{N}((\mathcal{W}_\psi)^*) = (\mathcal{R}(\mathcal{W}_\psi))^\perp = (\mathbb{C}_G^K)^\perp$ and so

$$[(\widetilde{\mathcal{W}}_\psi)^* \circ \Phi \circ \widetilde{\mathcal{W}}_\psi][f] = [(\widetilde{\mathcal{W}}_\psi)^* \circ \mathbb{P}_\psi \circ \Phi \circ \widetilde{\mathcal{W}}_\psi][f], \tag{41}$$

for all $f \in \mathbb{L}_2(\mathbb{R}^2)$ and all $\Phi \in \mathcal{B}(\mathbb{L}_2(G))$, so we see that the net operator on scores associated to $\Phi : \mathbb{L}_2(G) \to \mathbb{L}_2(G)$ is given by $\mathbb{P}_\psi \circ \Phi : \mathbb{L}_2(G) \to \mathbb{C}_K^G$.
In the reminder of this section we present design principles for Υ followed by a detailed theoretical discussion on them.

3.1 Design Principles

We now formulate a few desirable properties of Υ, and sufficient conditions for Φ that guarantee that Υ meets these requirements.

1. *Covariance with respect to rotation and translation*:

$$\Upsilon \circ \mathcal{U}_g^{SIM(2)} = \mathcal{U}_g^{SIM(2)} \circ \Upsilon, \quad \forall g = (x, y, \tau, \theta). \tag{42}$$

   This is an important requirement because the net operations on images should not be affected by rotation and translation of the original image. Typically, this is achieved by restricting one self to left-invariant operators Φ. Covariance with respect to scaling can be achieved as well, but is not an important requirement.

2. *Left invariant vector fields*: In order to achieve the Euclidean invariance mentioned above, we need to employ left invariant vector fields (/differential operators) on $SIM(2)$ as a moving frame of reference.

3. *Nonlinearity*: The requirement that Υ commute with $\mathcal{U}$ immediately rules out linear operators Φ. Recall that $\mathcal{U}$ is irreducible, and by Schur's lemma [39], any linear intertwining operator is a scalar multiple of the identity operator.

4. *Left-invariant parabolic evolutions on the Similitude group*: We consider the following two types of evolutions which include the wavelet transform as a initial condition.

   - Combine linear diffusions with monotone operations on the co-domain (i.e. scattering operators [40] in the wavelet domain)
   - Non linear adaptive diffusion

5. *Probabilistic models for contextual multi-scale feature propagation in the wavelet domain*: Instead of uncorrelated soft-thresholding of wavelet coefficients we aim for PDE flows that amplify the wavelet coefficients which are probabilistically coherent w.r.t. neighbouring coefficients. This coherence w.r.t. neighbouring coefficients is based on underlying stochastic processes (random walks) for multiple-scale contour enhancement.

In Subsections 3.2-3.5 we will elaborate on these design principles.

3.2 Covariance with respect to Rotations and Translations

Let $G = \mathbb{R}^d \rtimes T$ denote an arbitrary affine Lie-group.

Definition 16. *An operator $\Phi : \mathbb{L}_2(G) \to \mathbb{L}_2(G)$ is left invariant iff*

$$\Phi[\mathcal{L}_h f] = \mathcal{L}_h[\Phi f], \text{ for all } h \in G, \ f \in \mathbb{L}_2(\mathbb{R}^2), \tag{43}$$

where the left regular action $\mathcal{L}_g$ of $g \in G$ onto $\mathbb{L}_2(G)$ is given by

$$\mathcal{L}_g \psi(h) = \psi(g^{-1}h). \tag{44}$$

Recall the definition of Hilbert space H from (9).

Theorem 17. *Let Φ be a bounded operator on $\mathbb{C}_K^G$, $\Phi : \mathbb{C}_K^G \to \mathbb{L}_2(G)$. Then the unique corresponding operator Υ on H, which is given by $\Upsilon[f] = (\widetilde{\mathcal{W}}_\psi)^* \circ \Phi \circ \widetilde{\mathcal{W}}_\psi[f]$ is Euclidean (and scaling) invariant, i.e. $\mathcal{U}_g \Upsilon = \Upsilon \mathcal{U}_g$ for all $g \in G$ if and only if $\mathcal{P}_\psi \circ \Phi$ is left invariant, i.e. $\mathcal{L}_g(\mathbb{P}_\psi \circ \Phi) = (\mathbb{P}_\psi \circ \Phi)\mathcal{L}_g$, for all $g \in G$.*

Proof. As,

$$\widetilde{\mathcal{W}}_\psi[\mathcal{U}_g[f]](h) = (\mathcal{U}_h\psi, \mathcal{U}_g f)_{\mathbb{L}_2(\mathbb{R}^d)} = (\mathcal{U}_{g^{-1}h}\psi, f)_{\mathbb{L}_2(\mathbb{R}^d)} = \mathcal{L}_g[\widetilde{\mathcal{W}}_\psi[f]](h)$$

we conclude that,

$$\widetilde{\mathcal{W}}_\psi \mathcal{U}_g = \mathcal{L}_g \widetilde{\mathcal{W}}_\psi, \text{ for all } g \in G. \tag{45}$$

Moreover,

$$(\widetilde{\mathcal{W}}_\psi \mathcal{U}_g f, U)_{\mathbb{L}_2(G)} = (\mathcal{L}_g \widetilde{\mathcal{W}}_\psi, U)_{\mathbb{L}_2(G)} \Leftrightarrow (f, \mathcal{U}_{g^{-1}}(\widetilde{\mathcal{W}}_\psi)^* U)_{\mathbb{L}_2(G)} = (f, (\widetilde{\mathcal{W}}_\psi)^* \mathcal{L}_{g^{-1}} U)_{\mathbb{L}_2(G)}$$

for all $U \in \mathbb{L}_2(G)$, $f \in \mathbb{L}_2(\mathbb{R}^d)$, $g \in G$ and therefore we have,

$$\mathcal{U}_g(\widetilde{\mathcal{W}}_\psi)^* = \mathcal{L}_g(\widetilde{\mathcal{W}}_\psi)^*, \text{ for all } g \in G. \tag{46}$$

(Necessary condition) Assuming that $(\mathbb{P}_\psi \circ \Phi)$ is left invariant it follows from (41), (45) and (46) that

$$\begin{aligned}
\Upsilon[\mathcal{U}_g f] &= (\widetilde{\mathcal{W}}_\psi)^* \circ \Phi \circ \widetilde{\mathcal{W}}_\psi \circ \mathcal{U}_g[f] \\
&= (\widetilde{\mathcal{W}}_\psi)^* \circ (\mathbb{P}_\psi \circ \Phi) \circ \widetilde{\mathcal{W}}_\psi \circ \mathcal{U}_g[f] \\
&= (\widetilde{\mathcal{W}}_\psi)^* \circ (\mathbb{P}_\psi \circ \Phi) \circ \mathcal{L}_g \circ \widetilde{\mathcal{W}}^g_\psi[f] \\
&= (\widetilde{\mathcal{W}}_\psi)^* \circ \mathcal{L}_g \circ (\mathbb{P}_\psi \circ \Phi) \circ \widetilde{\mathcal{W}}_\psi[f] \\
&= \mathcal{U}_g \circ (\widetilde{\mathcal{W}}_\psi)^* \circ (\mathbb{P}_\psi \circ \Phi) \circ \widetilde{\mathcal{W}}_\psi[f] \\
&= \mathcal{U}_g \circ (\widetilde{\mathcal{W}}_\psi)^* \circ \Phi \circ \widetilde{\mathcal{W}}_\psi[f] = \mathcal{U}_g[\Upsilon[f]]
\end{aligned} \tag{47}$$

for all $f \in \mathbb{L}_2(\mathbb{R}^2)$ and $g \in G$. Thus we have $\Upsilon \mathcal{U}_g = \mathcal{U}_g \Upsilon$ for all $g \in G$.
(Sufficient condition) Now suppose Υ is Euclidean invariant. Then again by (45) and (46) we have that,

$$(\widetilde{\mathcal{W}}_\psi)^* \circ \Phi \circ \mathcal{L}_g \circ \widetilde{\mathcal{W}}_\psi[f] = (\widetilde{\mathcal{W}}_\psi)^* \circ \mathcal{L}_g \circ \Phi \circ \widetilde{\mathcal{W}}_\psi[f],$$

for all $f \in \mathbb{L}_2(\mathbb{R}^2)$ and $g \in G$. Since the range of $\mathcal{L}_g\big|_{\mathbb{C}_K^G}$ and the range of $(\mathbb{P}_\psi \circ \Phi)$ is contained in $\mathbb{C}_K^G$ and since $(\widetilde{\mathcal{W}}_\psi)^*\big|_{\mathbb{C}_K^G} = (\mathcal{W}_\psi)^{-1}$, we have $(\mathbb{P}_\psi \circ \Phi) \circ \mathcal{L}_g \circ \widetilde{\mathcal{W}}_\psi = \mathcal{L}_g \circ (\mathbb{P}_\psi \circ \Phi) \circ \widetilde{\mathcal{W}}_\psi$. As the range of $\widetilde{\mathcal{W}}_\psi$ equals $\mathbb{C}_K^G$, we have, $\mathcal{L}_g \circ (\mathbb{P}_\psi \circ \Phi) = (\mathbb{P}_\psi \circ \Phi) \circ \mathcal{L}_g$ for all $g \in G$. □

Practical Consequence: Now let us return to our case of interest $G = SIM(2)$. Euclidean invariance of Υ is of great practical importance, since the result of operators on scores should not be essentially different if the original image is rotated or translated. In addition in our construction scaling the image also does not affect the outcome of the operation which may not always be desirable.

3.3 Left Invariant Vector fields (differential operators) on $SIM(2)$

Left invariant differential operators are crucial in the construction of appropriate left-invariant evolutions on $G = SIM(2)$. Similar to Definition 16, the right regular action $\mathcal{R}_g$ of $g \in G$ onto $\mathbb{L}_2(G)$ is defined by

$$\mathcal{R}_g \psi(h) = \psi(hg), \ \forall g, h \in G, \ \psi \in \mathbb{L}_2(G). \tag{48}$$

A vector field (now considered as a differential operator[8]) $\mathcal{A}$ on a group G is called left-invariant if it satisfies

$$\mathcal{A}_g \phi = \mathcal{A}_e(\phi \circ L_g) = \mathcal{A}_e(h \mapsto \phi(gh)),$$

[8]Any tangent vector $X \in T(G)$ can be considered as a differential operator acting on a function $U : G \to \mathbb{R}$. So, for instance, if we are using $X_e \in T_e(G)$ in the context of differential operators, all occurrences of $\mathbf{e}_i$ will be replaced by ∂_i, which is the short-hand notation for $\frac{\partial}{\partial x_i}$. See [41] for the equivalence between these two viewpoints.

for all smooth functions $\phi \in C_c^\infty(\Omega_g)$ where Ω_g is an open set around $g \in G$ and with the left multiplication $L_g : G \to G$ as defined in the previous section. The linear space of left-invariant vector fields $\mathcal{L}(G)$ equipped with the Lie product $[\mathcal{A}, \mathcal{B}] = \mathcal{A}\mathcal{B} - \mathcal{A}\mathcal{B}$ is isomorphic to $T_e(G)$ by means of the isomorphism,

$$T_e(G) \ni A \leftrightarrow \mathcal{A} \in \mathcal{L}(G) \Leftrightarrow \mathcal{A}_g(\phi) = A(\phi \circ L_g) = A(h \mapsto \phi(gh)) = (L_g)_* A(\phi)$$

for all smooth $\phi : G \supset \Omega_g \to \mathbb{R}$.
We define an operator $d\mathcal{R} : T_e(G) \to \mathcal{L}(G)$,

$$(d\mathcal{R}(A)\phi)(g) := \lim_{t \downarrow 0} \frac{(\mathcal{R}_{\exp(tA)}\phi)(g) - \phi(g)}{t}, \ A \in T_e(G), \ \phi \in \mathbb{L}_2(G), \ g \in G, \tag{49}$$

and where $\mathcal{R}$ and exp are the right regular representation and the exponential map respectively. Using $d\mathcal{R}$ we obtain the corresponding basis for left-invariant vector fields on G:

$$\{\mathcal{A}_1, \mathcal{A}_2, \mathcal{A}_3, \mathcal{A}_4\} := \{d\mathcal{R}(A_1), d\mathcal{R}(A_2), d\mathcal{R}(A_3, d\mathcal{R}(A_4)\}, \tag{50}$$

or explicitly in coordinates

$$\{\mathcal{A}_1, \mathcal{A}_2, \mathcal{A}_3, \mathcal{A}_4\} = \{\partial_\theta, \partial_\xi, \partial_\eta, \partial_\beta\} = \{\partial_\theta, a(\cos\theta\partial_x + \sin\theta\partial_y), a(-\sin\theta\partial_x + \cos\theta\partial_y), a\partial_a\}, \tag{51}$$

where we use the short notation $\partial_a := \frac{\partial}{\partial a}$ for the partial derivatives and where,

$$\{\mathcal{A}_1\big|_e, \mathcal{A}_2\big|_e, \mathcal{A}_3\big|_e, \mathcal{A}_4\big|_e\} = \{A_1, A_2, A_3, A_4\} = \{\partial_\theta, \partial_x, \partial_y, \partial_a\}.$$

To simplify the scale related left invariant differential operator, we introduce a new variable, $\tau = \log_e a$, which leads to the following change in left invariant derivatives

$$\{\mathcal{A}_1, \mathcal{A}_2, \mathcal{A}_3, \mathcal{A}_4\} = \{\partial_\theta, e^\tau(\cos\theta\partial_x + \sin\theta\partial_y), e^\tau(-\sin\theta\partial_x + \cos\theta\partial_y), \partial_\tau\}. \tag{52}$$

The set of differential operators $\{\mathcal{A}_1, \mathcal{A}_2, \mathcal{A}_3, \mathcal{A}_4\} = \{\partial_\theta, \partial_\xi, \partial_\eta, \partial_\tau\}$ is the appropriate set of differential operators to be used in orientation scores because all $SIM(2)$-coordinate independent linear and nonlinear combinations of these operators are left invariant. Further at each scale ∂_ξ is always the spatial derivative tangent to the orientation θ and ∂_η is always orthogonal to this orientation. Figure 6 illustrates this for ∂_η versus ∂_y. It is important to note that unlike derivatives $\{\partial_x, \partial_y, \partial_a, \partial_\theta\}$ which commute, the left-invariant derivatives $\{\partial_\xi, \partial_\eta, \partial_\tau, \partial_\theta\}$ do not commute. However these operators satisfy the same commutator relations as their Lie algebra counterparts as $d\mathcal{R}$ generates a Lie-algebra isomorphism

$$[A_i, A_j] = \sum_{k=1}^{4} c_{ij}^k A_k \leftrightarrow [\mathcal{A}_i, \mathcal{A}_j] = \mathcal{A}_i\mathcal{A}_j - \mathcal{A}_j\mathcal{A}_i = \sum_{k=1}^{4} c_{ij}^k \mathcal{A}_k, \tag{53}$$

where c_{ij}^k are the structure constants.
An exponential curve is obtained by using the *exp* mapping of the Lie algebra elements, i.e an exponential curve passing through the identity element $e \in SIM(2)$ at $t = 0$ can be written as

$$\gamma_c(t) = exp\left(t \sum_{i=1}^{4} c^i \mathcal{A}_i\Big|_{g=e}\right) = exp\left(t \sum_{i=1}^{4} c^i A_i\right), \tag{54}$$

and an exponential curve passing through $g_0 \in SIM(2)$ can be obtained by left multiplication with $g_0 = (x_0, y_0, e^{\tau_0}, \theta_0)$, i.e. $g_0\gamma_c(t)$. The following theorem applies the method of characteristics (for PDEs) to transport along exponential curves. The explicit formulation is important because left-invariant convection-diffusion on $SIM(2)$ takes place only along exponential curves, see Theorem 30.

Theorem 18. *Let $A \in T_e(SIM(2))$. Then the following holds.*

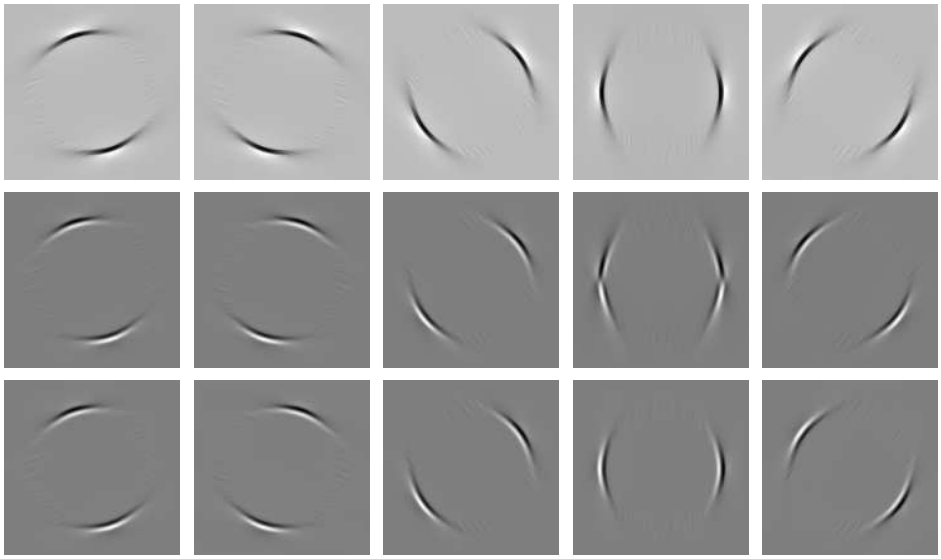

Figure 6: The difference between cartesian derivatives and left-invariant derivatives, shown on a scale-OS (at a fixed scale) of an image with a single circle. From left to right, several orientations are shown. Row 1: Scale-OS of a circle image at a fixed scale; Row 2: Cartesian derivative ∂_y; Row 3 : Left-invariant derivative ∂_η. Comparing the derivatives ∂_y and ∂_η (Column 4) we observe that ∂_η is invariant under rotation, i.e. the interpretation of ∂_η stays the same.

1. *$U \in \mathcal{D}(d\mathcal{R}(A)) \Rightarrow \mathcal{R}_{e^{tA}} U \in \mathcal{D}(d\mathcal{R}(A))$, where $\mathcal{D}(X)$ denotes the domain of operator X.*
2. *$e^{td\mathcal{R}(A)} = \mathcal{R}_{e^{tA}}$, $\forall t > 0$ where $d\mathcal{R}$ is defined in (49).*
3. *$\gamma_c(t) = g_0 \; exp\left(t \sum_{i=1}^{4} c^i A_i\right)$ are the characteristics for the following PDE,*

$$\frac{\partial W}{\partial t} = -\sum_{i=1}^{4} c^i \mathcal{A}_i W, \; W(g,0) = U. \tag{55}$$

Proof. See D for proof. □

The exponential map defined on $T_e(SIM(2))$ is surjective, and so we can define the logarithm mapping, $\log = (\exp)^{-1} : SIM(2) \to T_e(SIM(2))$. For proof see [19, Chap. 4]. For the explicit formulation of the exponential and logarithm curves in our case see C. The explicit form of the log map will be used to approximate the solution for linear evolutions on $SIM(2)$ in Section 4.1.

3.4 Quadratic forms on Left Invariant vector fields

We apply the general theory of evolutions (convection-diffusion) on Lie groups, [9], to the $SIM(2)$ group and consider the following left-invariant second-order evolution equations,

$$\begin{cases} \partial_t W(g,t) = Q^{\mathbf{D},\mathbf{a}}(\mathcal{A}_1, \mathcal{A}_2, \mathcal{A}_3, \mathcal{A}_4) W(g,t), \\ W(\cdot, t=0) = \mathcal{W}_\psi f(\cdot), \end{cases} \tag{56}$$

where $W : SIM(2) \times \mathbb{R}^+ \to \mathbb{C}$ and $Q^{\mathbf{D},\mathbf{a}}$ is the following quadratic form on $\mathcal{L}(SIM(2))$,

$$Q^{\mathbf{D},\mathbf{a}}(\mathcal{A}_1, \mathcal{A}_2, \mathcal{A}_3, \mathcal{A}_4) = \sum_{i=1}^{4} \left(-a_i \mathcal{A}_i + \sum_{j=1}^{4} D_{ij} \mathcal{A}_i \mathcal{A}_j \right), \quad a_i, D_{ij} \in \mathbb{R}, \; \mathbf{D} := [D_{ij}] \geq 0, \; \mathbf{D}^T = \mathbf{D}. \tag{57}$$

Throughout this article we restrict ourselves to the diagonal case with $a_1 = a_2 = a_4 = 0$. This is a natural choice when a_i and D_{ij} are constant, as we do not want to impose a-priori curvature and a-priori scaling drifts in our flows. However, when adapting D and a to the initial condition (i.e. wavelet transform data) such restrictions are not necessary. In fact, practical advantages can be obtained when choosing D diagonal w.r.t. optimal gauge frame, [5, 28]. Choosing $D_{ij} = D_{ii}\delta_{ij},\ i,j \in \{1,2,3,4\}$, the quadratic form becomes,

$$Q^{\mathbf{D},\mathbf{a}}(\mathcal{A}_1,\mathcal{A}_2,\mathcal{A}_3,\mathcal{A}_4) = [-a_1\partial_\theta - a_2\partial_\xi - a_3\partial_\eta - a_4\partial_\tau + D_{11}(\partial_\theta)^2 + D_{22}(\partial_\xi)^2 + D_{33}(\partial_\eta)^2 + D_{44}(\partial_\tau)^2]. \quad (58)$$

The first order part of (58) takes care of transport (convection) along the exponential curves, deduced in Section 3.3. The second order part takes care of diffusion in the $SIM(2)$ group. Also note that these evolution equations are left-invariant as they are constructed by linear combinations of left-invariant vector fields.
Hörmander in [42] gave necessary and sufficient conditions on the convection and diffusion parameters, respectively $a = (a_1, a_2, a_3, a_4)$ and $\mathbf{D} = D_{ij}$, in order to get smooth Green's functions of the left-invariant convection-diffusion equation (56) with generator (58). By these conditions the non-commutative nature of $SIM(2)$ in certain cases takes care of missing directions in the diffusion tensor. Applying the Hörmander's theorem [42] produces necessary and sufficient conditions for smooth (resolvent) Green's functions on $SIM(2)\backslash\{e\}$ on the diffusion and convection parameters $(\mathbf{D}, a)$ in the generator (58) of (56) for diagonal $\mathbf{D}$:

$$\{1,2,4\} \subset \{i|\ a_i \neq 0 \vee D_{ii} \neq 0\} \vee \{1,3,4\} \subset \{i|\ a_i \neq 0 \vee D_{ii} \neq 0\}. \quad (59)$$

A covariant derivative of a co-vector field $\mathbf{a}$ on the manifold $(SIM(2), \mathcal{G})$ is a $(0,2)$-tensor field with components $\nabla_j a_i = \mathcal{A}_j a_i - \Gamma^k_{ij} a_k$, whereas the covariant derivative of a vector field $\mathbf{v}$ on $SIM(2)$ is a $(1,1)$-tensor field with components $\nabla_{j'} v^i = \mathcal{A}_{j'} v^i + \Gamma^i_{j'k'} v^{k'}$, where we have made use of the notation $\nabla_j := D_{\mathcal{A}_j}$, when imposing the Cartan connection (tangential to the $SE(2)$-case in [28], $SE(3)$-case in [43] and the $H(2d+1)$-case in [11]) .The Christoffel symbols equal minus the structure constants of the Lie algebra $\mathcal{L}(SIM(2))$, i.e. $\Gamma^k_{ij} = -c^k_{ij}$. The Christoffel symbols are anti-symmetric as the underlying Cartan connection D has constant torsion. The left-invariant equations (56) with a diagonal diffusion tensor (58) can be rewritten in covariant derivatives as

$$\begin{cases} \partial_s W(g,s) = \sum_{i,j=1}^{4} \mathcal{A}_i((D_{ij}(W))(g,s)\mathcal{A}_j W)(g,s) = \sum_{i,j=1}^{4} \nabla_i((D_{ij}(W))(g,s)\nabla_j W)(g,s), \\ W(g,0) = \mathcal{W}_\psi f(g), \text{ for all } g \in SIM(2),\ s > 0. \end{cases} \quad (60)$$

Both convection and diffusion in the left-invariant evolution equations (56) take place along the exponential curves in $SIM(2)$ which are covariantly constant curves with respect to the Cartan connection. For proof and various details see F.

3.5 Probabilistic models for contextual feature propagation

Section 3.4 described the general form of convection-diffusion operators on the $SIM(2)$ group. For the particular case of contour enhancement i.e. diffusion on the $SIM(2)$ group, which corresponds to the choice $D_{ij} = D_{ii}\delta_{ij},\ i,j \in \{1,2,3,4\},\ D_{33} = 0$ and $\mathbf{a} = \mathbf{0}$, we have the following result.

Theorem 19. *The evolution on $SIM(2)$ given by*

$$\begin{cases} \partial_t W(g,t) = [D_{11}(\partial_\theta)^2 + D_{22}(\partial_\xi)^2 + D_{44}(\partial_\tau)^2]W(g,t), \\ W(\cdot, t=0) = \mathcal{W}_\psi f(\cdot), \end{cases} \quad (61)$$

is the forward Kolmogorov (Fokker-Planck) equation of the following stochastic process for multi-scale contour

enhancement

$$\begin{cases} \mathbf{X}(s) = \mathbf{X}(0) + \sqrt{2D_{22}}\epsilon_2 \int_0^s \big(\cos(\Theta(t))e_x + \sin(\Theta(t)e_y)e^{\mathfrak{T}(t)}d(\sqrt{t}\big) \\ \Theta(s) = \Theta(0) + \sqrt{s}\sqrt{2D_{11}}\epsilon_1 \\ \mathfrak{T}(s) = \mathfrak{T}(0) + \sqrt{s}\sqrt{2D_{44}}\epsilon_4, \end{cases} \tag{62}$$

where $e_1, e_2, e_4 \sim \mathcal{N}(0,1)$ *are the standard random variables and* $D_{11}, D_{22}, D_{44} > 0$.

In order to avoid technicalities regarding probability measures on Lie groups, see [44] for details, we only provide a short and basic explanation which covers the essential idea of the proof.
The stochastic differential equation in (62) can be considered as limiting case of the following discrete stochastic processes on $SIM(2)$:

$$\begin{cases} G_{n+1} := (\mathbf{X}_{n+1}, \Theta_{n+1}, \mathfrak{T}_{n+1}) = G_n + \sqrt{\Delta s} \sum_{i=1,2,4} \sum_{j=1,2,4} \frac{\epsilon_{i,n+1}}{\sqrt{N}} \sqrt{2D_{ii}}\ e_i\big|_{G_N}, \\ G_0 = (\mathbf{X}_0, \Theta_0, \mathfrak{T}_0), \end{cases} \tag{63}$$

where $n = 1, \cdots, N-1, N \in \mathbb{N}$ denotes the number of steps with step-size $\Delta s > 0$, $\{\epsilon_{i,n+1}\}_{i=1,2,4}$ are independent normally distributed $\epsilon_{i,n+1} \sim (0,1)$ and $e_j\big|_{G_n} \equiv \mathcal{A}_j\big|_{G_n}$, i.e.

$$e_1\big|_{G_n} = \begin{pmatrix} 0 \\ 0 \\ 0 \\ 1 \end{pmatrix},\ e_2\big|_{G_n} = \begin{pmatrix} e^{\mathfrak{T}}\cos\Theta \\ e^{\mathfrak{T}}\sin\Theta \\ 0 \\ 0 \end{pmatrix},\ e_3\big|_{G_n} = \begin{pmatrix} -e^{\mathfrak{T}}\sin\Theta \\ e^{\mathfrak{T}}\cos\Theta \\ 0 \\ 0 \end{pmatrix},\ e_4\big|_{G_n} = \begin{pmatrix} 0 \\ 0 \\ 1 \\ 0 \end{pmatrix}.$$

Note that the continuous process (62) directly arises from the discrete process (63) by recursion and taking the limit $N \to \infty$.

4 Left-invariant Diffusions on $SIM(2)$

Following our framework of stochastic left-invariant evolutions on $SIM(2)$ we will restrict ourselves to contour enhancement, where the Forward-Kolmogorov equation is essentially a hypo-elliptic[9] diffusion on the $SIM(2)$ group and therefore we recall (61)

$$\begin{cases} \partial_t W(g,t) = [D_{11}(\partial_\theta)^2 + D_{22}(\partial_\xi)^2 + D_{44}(\partial_\tau)^2]W(g,t), \\ W(\cdot, t=0) = \mathcal{W}_\psi f(\cdot). \end{cases} \tag{64}$$

In the remainder of this paper we study linear diffusion (combined with monotone operations on the co-domain) and non-linear diffusion on the $SIM(2)$ group in the context of our imaging application.

4.1 Approximate Contour Enhancement Kernels for Linear Diffusion on Scale-OS

In [26, 27], the authors derive the exact Green's function of (56) for the $SE(2)$ case. To our knowledge explicit and exact formulae for heat kernels of linear diffusion on $SIM(2)$ do not exist in the literature. However using the general theory in [45, 46] one can compute Gaussian estimates for Green's function of left-invariant diffusions on Lie groups. As a first step this involves approximating $SIM(2)$ by a parametrized class of groups $(SIM(2))_q,\ q \in [0,1]$ in between $SIM(2)$ and the nilpotent Heisenberg approximation $SIM(2)_0$. This idea of contraction has been explained in E.

[9] Eq. (64) is not elliptic as the direction ∂_η is missing, but it's called hypo-elliptic as it satisfies the Hörmander condition [42].

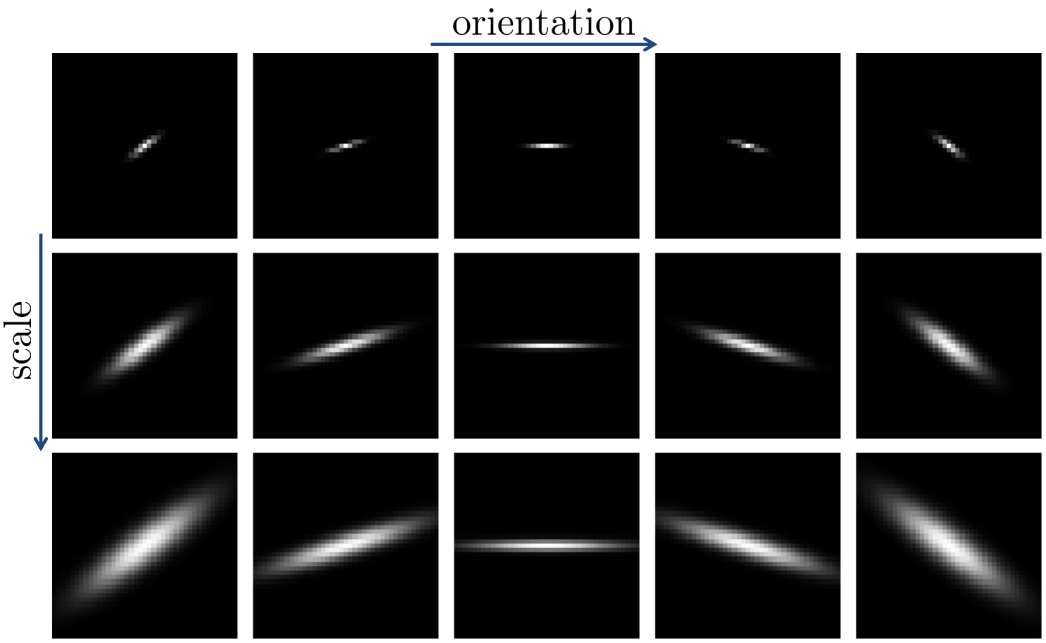

Figure 7: Plots of enhancement kernels generated on a 41×41 grid at different scales and orientations. Parameters chosen: $D_{11} = 0.05,\ D_{22} = 1,\ D_{44} = 0.01,\ t = 0.7$.

According to the general theory in [46], the heat-kernels $K_t^{q,\mathbf{D}} : (SIM(2))_q \to \mathbb{R}^+$ (i.e. kernels for contour enhancement whose convolution yields diffusion on $SIM(2))_q$) on the parametrized class of groups $(SIM(2))_q,\ q \in [0,1]$ in between $SIM(2)$ and $(SIM(2))_0$ satisfy the Gaussian estimates

$$|K_t^{q,\mathbf{D}}(g)| \leq Ct^{-\frac{5}{2}} \exp\left(\frac{-b\|g\|_q^2}{4t}\right),\ \text{with } C, b > 0 \text{ (constant)}, g \in (SIM(2))_q\ , \tag{65}$$

where the norm $\|\cdot\|_q : (SIM(2))_q \to \mathbb{R}^+$ is given by $\|g\|_q = |\log_{(SIM(2))_q}(g)|_q$. $\log_{(SIM(2))_q} : (SIM(2))_q \to T_e((SIM(2))_q)$, is the logarithmic mapping on $(SIM(2))_q$, which is computed explicitly for the case of $(SIM(2))_{q=1} = SIM(2)$ in C, and where the weighted modulus, see [46, Prop 6.1], in our special case of interest is given by,

$$\begin{aligned}\left|\sum_{i=1}^{4} c_q^i A_i^q\right|_q &= \sqrt{|c_q^1|^{2/w_1} + |c_q^2|^{2/w_2} + |c_q^3|^{2/w_3} + |c_q^4|^{2/w_4}} \\ &= \sqrt{((c_q^1)^2 + (c_q^2)^2 + (c_q^4)^2) + |c_q^3|},\end{aligned} \tag{66}$$

where recall the weightings from (81).

Remark 20. *The constants b, C in (65) can be taken into account by the transformations $t \mapsto \frac{t}{b}$, $f \mapsto Cf$ respectively.*

A sharp estimate for the front factor constant C in (65) is given by

$$C = \frac{1}{4\pi D_{11} D_{22}} \frac{1}{\sqrt{D_{44}}}. \tag{67}$$

This follows from the general theory in [46] where the choice of constant C is uniform for all groups $(SIM(2))_q,\ q \in [0,1]$. Thus to determine C we need to determine the front factor constant for the green's

function G of the following resolvent equation

$$\left((D_{11}(\mathcal{A}_1^0)^2 + D_{22}(\mathcal{A}_2^0)^2 + D_{44}(\mathcal{A}_4^0)^2)\right) G(x,y,\tau,\theta) = +\delta_e$$

where $\mathcal{A}^0$ denote the basis for $\mathcal{L}(H)$ (recall $H = (SIM(2))_{q\downarrow 0}$) and e is the identity of H. Since $\{\mathcal{A}_i^0\}_{i=1,2}$ are independent of τ the Green's function in our case is separable, i.e.

$$G(x,y,\tau,\theta) = G^{D_{11},D_{22}}_{(SE(2))_{q=0}}(x,y,\theta) \cdot G^{D_{44}}_{\mathbb{R}}(\tau)$$

where $G^{D_{11},D_{22}}_{(SE(2))_{q=0}}(x,y,\theta)$ and $G^{D_{44}}_{\mathbb{R}}(\tau)$ are Green's function for linear diffusion on $SE(2)$ and $\mathbb{R}$ respectively. The Green's function for the Heisenberg case of $SE(2)$ has been derived explicitly in [27] with the front factor $\frac{1}{4\pi D_{11}D_{22}t^2}$ and the Green's function of diffusion on $\mathbb{R}$ is $G^{D_{44}}_{\mathbb{R}}(\tau) = \frac{|\tau|}{\sqrt{tD_{44}}}$.
Using this theory we arrive at the Gaussian estimates for the case $SIM(2) = (SIM(2))_{q=1}$. Applying the definition of $c^i,\ i \in \{1,2,3,4\}$ from C we arrive at,

$$|K_t^{q=1,\mathbf{D}}(g)| \leq \frac{1}{4\pi t^{\frac{5}{2}} D_{11}D_{22}\sqrt{D_{44}}} \exp\left(\frac{-1}{4t}\left(\frac{\theta^2}{D_{11}} + \frac{(c^2)^2}{D_{22}} + \frac{\tau^2}{D_{44}} + \frac{|c^3|}{\sqrt{D_{11}D_{22}D_{44}}}\right)\right) \tag{68}$$

where,

$$c^2 = \frac{(y\theta - x\tau) + (-\theta\eta + \tau\xi)}{t\left(1 + e^{2\tau} - 2e^{\tau}cos\theta\right)},\ c^3 = \frac{-(x\theta + y\tau) + (\theta\xi + \tau\eta)}{t\left(1 + e^{2\tau} - 2e^{\tau}cos\theta\right)}.$$

A problem with these estimates is that they are not differentiable everywhere. This problem can be solved by using the estimate

$$|a| + |b| \geq \sqrt{a^2 + b^2} \geq \frac{1}{\sqrt{2}}(|a| + |b|),$$

which holds for all $a, b \in \mathbb{R}$, to the exponents of our Gaussian estimates. Thus we estimate the weighted modulus by the equivalent (for all $q > 0$) weighted modulus $|\cdot|_q : T_e((SIM(2))_q) \to \mathbb{R}^+$ by $\left|\sum_{i=1}^4 c_q^i A_i^q\right|_q := \sqrt[4]{((c_q^1)^2 + (c_q^2)^2 + (c_q^4)^2)^2 + |c_q^3|^2}$, yielding the Gaussian estimate,

$$|K_t^{q=1,\mathbf{D}}(g)| \leq \frac{1}{4\pi t^{\frac{5}{2}} D_{11}D_{22}\sqrt{D_{44}}} \exp\left(\frac{-1}{4t}\left(\left[\frac{\theta^2}{D_{11}} + \frac{(c^2)^2}{D_{22}} + \frac{\tau^2}{D_{44}}\right]^2 + \frac{|c^3|^2}{D_{11}D_{22}D_{44}}\right)\right). \tag{69}$$

Figure 7 shows the typical structure of these enhancement kernels.

Remark 21. *When cascading group convolutions and transformations in the co-domain of the scores one can generalize the scattering operators by Mallat on $\mathbb{R}^n$, see [40], to left-invariant scattering operators on affine Lie groups such as $SIM(2)$ which would provide us with stability under local deformations.*

In practice, medical images exhibit complicated structures which require local adaptivity per group location via gauge frames. This brings us to non-linear diffusions that we will solve numerically in the next section.

4.2 Nonlinear Left Invariant Diffusions on $SIM(2)$

Adaptive nonlinear diffusion on the $2D$ Euclidean motion group $SE(2)$ called coherence enhancing diffusion on orientation scores (CED-OS) was introduced in [5, 27]. We wish apply this adaptive $SE(2)$ diffusion to each scale in our scale-OS, which is possible because at a fixed scale the scale-OS is a function on the $SE(2)$ group. In this section we present a brief outline of the CED-OS algorithm and then apply it to our case of interest.

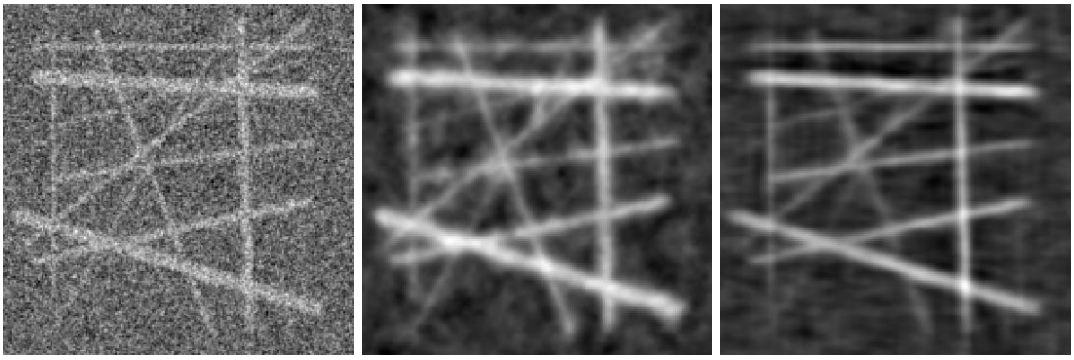

(a) Noisy input image (b) $SE(2)$ Linear Diffusion (c) $SIM(2)$ Linear Diffusion

Figure 8: Comparison of enhancement via linear diffusion using Gaussian estimates for heat kernels on $SE(2)$ and $SIM(2)$. Left:Original image, Center: Enhancement via Linear diffusion on $SE(2)$ group using Gaussian estimates in [27], Right: Enhancement via Linear diffusion on $SIM(2)$ group using estimate in (69). Parameters- OS: $N_\theta = 20, N_s = 5$; $SE(2)$ estimate: $D_{11} = 0.05,\ D_{22} = 1,\ t = 3$;$SIM(2)$ estimate: $D_{11} = 0.05,\ D_{22} = 1,\ D_{44} = 0.01,\ t = 0.7$.

4.2.1 CED-OS - Brief Outline

CED-OS involves the following two steps:

- *Curvature Estimation.* Curvature estimation of a spatial curve is based on the optimal exponential curve fit at each point. We find the best exponential curve fit (and the corresponding curvature) to the data $(x, y, \theta) \mapsto |(\mathcal{W}_\psi f)(x, y, \theta)|$ by using the exponential map,

$$t \mapsto \exp\left(t(c^1_* A_1 + c^2_* A_2 + c^3_* A_3)\right) \text{ with } (c^1_*)^2 + \beta^2 (c^2_*)^2 + \beta^2 (c^3_*)^2 = 1,$$

  via the techniques explained in [5, 28] and summarized in G.

- *Adaptive curvatures based diusion scheme using gauge coordinates.* The best exponential curve fit mentioned above is parametrized by $\mathbf{c}_* = (c^1_*, c^2_*, c^3_*) \in \mathbb{R}^3$ which provides us the curvature κ (and deviation from horizontality d_H if we do not impose $c^3_* = 0$). In fact it furnishes a whole set of gauge frames $\{\partial_a, \partial_b, \partial_c\}$ as can be seen in Figure 9. The gauge frames in spherical coordinates read

$$\begin{aligned} \partial_a &= -\cos\alpha \cos d_H \partial_\xi - \cos\alpha \sin d_H \partial_\eta + \beta \sin\alpha \partial_\theta, \\ \partial_b &= \sin\alpha \cos d_H \partial_\xi + \sin\alpha \sin d_H \partial_\eta + \beta \cos\alpha \partial_\theta, \\ \partial_a &= -\sin d_H \partial_\xi + \cos d_H \partial_\eta. \end{aligned} \tag{70}$$

  The resulting nonlinear evolution equations on orientation scores is

$$\begin{cases} \partial_t U(g,t) = \begin{pmatrix} \beta\partial_\theta & \partial_\xi & \partial_\eta \end{pmatrix} M^T_{\alpha,d_H} \begin{pmatrix} D_{aa} & 0 & 0 \\ 0 & D_{bb} & 0 \\ 0 & 0 & D_{cc} \end{pmatrix} M_{\alpha,d_H} \begin{pmatrix} \beta\partial_\theta \\ \partial_\xi \\ \partial_\eta \end{pmatrix} U(g,t),\ t > 0, \\ U(g, t=0) = \mathcal{W}_\psi[f](g) \text{ for all } g \in SE(2), \end{cases} \tag{71}$$

  where we use the shorthand notation $D_{ii} = (D_{ii}(U))(g,t)$, for $i = a, b, c$. The matrix

$$M_{\alpha,d_H} = \begin{pmatrix} \sin\alpha & -\cos\alpha\cos d_H & -\cos\alpha \sin d_H \\ \cos\alpha & \cos d_H \sin\alpha & \sin\alpha \sin d_H \\ 0 & -\sin d_H & \cos d_H \end{pmatrix}$$

  is the rotation matrix in $SO(2)$ that maps the left-invariant vector fields $\{\beta\partial_\theta, \partial_\xi, \partial_\eta\}$ onto the gauge frames $\{\partial_a, \partial_b, \partial_c\}$.

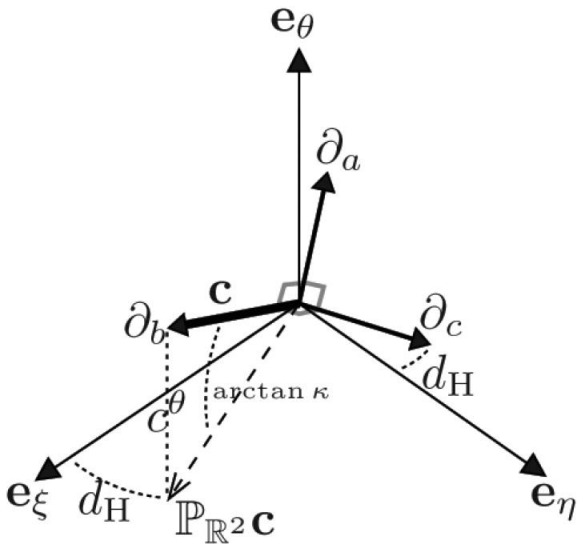

Figure 9: Illustration of curvature κ and deviation from horizontality d_H and the gauge frame (70). Note that $e_\theta \leftrightarrow \partial_\theta,\ e_\xi \leftrightarrow \partial_\xi,\ e_\eta \leftrightarrow \partial_\eta$.

Figure 10 depicts the dependence of the corresponding local linear diffusion kernel on curvature and orientation strengths. Eq.(71) is implemented by a Euler forward finite difference scheme involving the parameters $(\widetilde{\rho}, \rho_s, c, \beta)$,

$$U_{n+1} = \Delta t(QU_n) + U_n,$$

where $U_n = U(\cdot,\cdot,t_n)$ with discrete time steps and the generator is given by,

$$(QU)(\cdot,\cdot,t) = \begin{pmatrix}\beta\partial_\theta^D & \partial_\xi^D & \partial_\eta^D\end{pmatrix} M_{\alpha,d_H}^T \left(G_{\rho_s,\rho_s,\rho_s\beta^2} * \begin{pmatrix} D_{aa}(U(\cdot,\cdot,t)) & 0 & 0 \\ 0 & D_{bb}(U(\cdot,\cdot,t)) & 0 \\ 0 & 0 & D_{cc}(U(\cdot,\cdot,t)) \end{pmatrix} \right) M_{\alpha,d_H} \begin{pmatrix}\beta\partial_\theta^D \\ \partial_\xi^D \\ \partial_\eta^D\end{pmatrix},$$

where $G_{\rho_s,\rho_s,\rho_s\beta^2}(x,y,\theta)$ denotes a Gaussian kernel, which is isotropic on each spatial plane with spatial scale $\rho_s = \frac{1}{2}\sigma_s^2$ and anisotropic with scale $\rho_s\beta^2$ in orientation. Here ∂_j^D denotes the left-invariant finite difference operator in the j^{th} direction implemented via B-spline interpolation [5]. Further $D_{bb} = 0$, $(D_{aa}U)(\cdot,\cdot,t) = (D_{cc}U)(\cdot,\cdot,t) = e^{\frac{-(s(|U|)(\cdot,\cdot,t))^2}{c}},\ c > 0$, with the orientation confidence $s(U(\cdot,\cdot,t)) = (\partial_a^2 + \partial_b^2)U(\cdot,\cdot,t)$. The derivatives ∂_a, ∂_b are Gaussian derivatives, computed with scales $(\widetilde{\rho}, \widetilde{\rho}, \widetilde{\rho}\beta^2)$, orthogonal to locally optimal direction with c being the eigenvector of the Hessian matrix corresponding to best exponential curve fit where we enforce horizontality by setting $d_H = 0$ (see Figure 10).

4.2.2 CED-OS on Scale-OS (CED-SOS)

For an image $f \in \mathbb{L}^2(\mathbb{R}^2)$ the corresponding scale-OS $\mathcal{W}_\psi(f) \in \mathbb{C}_K^{SIM(2)} \subset \mathbb{L}^2(SIM(2))$ and for any fixed $a \in (0,\infty)$, $\mathcal{W}_\psi(f)(\cdot,\cdot,a,\cdot) \in \mathbb{L}_2(SE(2))$. Let $\Phi_t : \mathbb{L}_2(SE(2)) \to \mathbb{L}_2(SE(2))$ denote nonlinear adaptive diffusion (CED-OS) on the $SE(2)$ group which is the solution operator of (71) at stopping time t. We propose the operator Λ on scale-OS defined as

$$(\Lambda[(\mathcal{W}_\psi f])(x,y,a_i,\theta) = \sum_{i=1}^m (\Phi_{t_{a_i}}[\mathcal{W}_\psi f(\cdot,\cdot,a_i,\cdot)])(x,y,\theta), \tag{72}$$

where $g \in \mathbb{R}^2 \times [0,2\pi) \times [a^-,a^+]$ and $\{a_i\}_{i=1}^m$ is the discretization of $[a^-,a^+]$. Recall the defintion of $0 < a^- < a^+ < \infty$ from Section 2.4. Here we make the specific choice of t_{a_i} with $t_{a_i} \leq t_{a_k}$ where

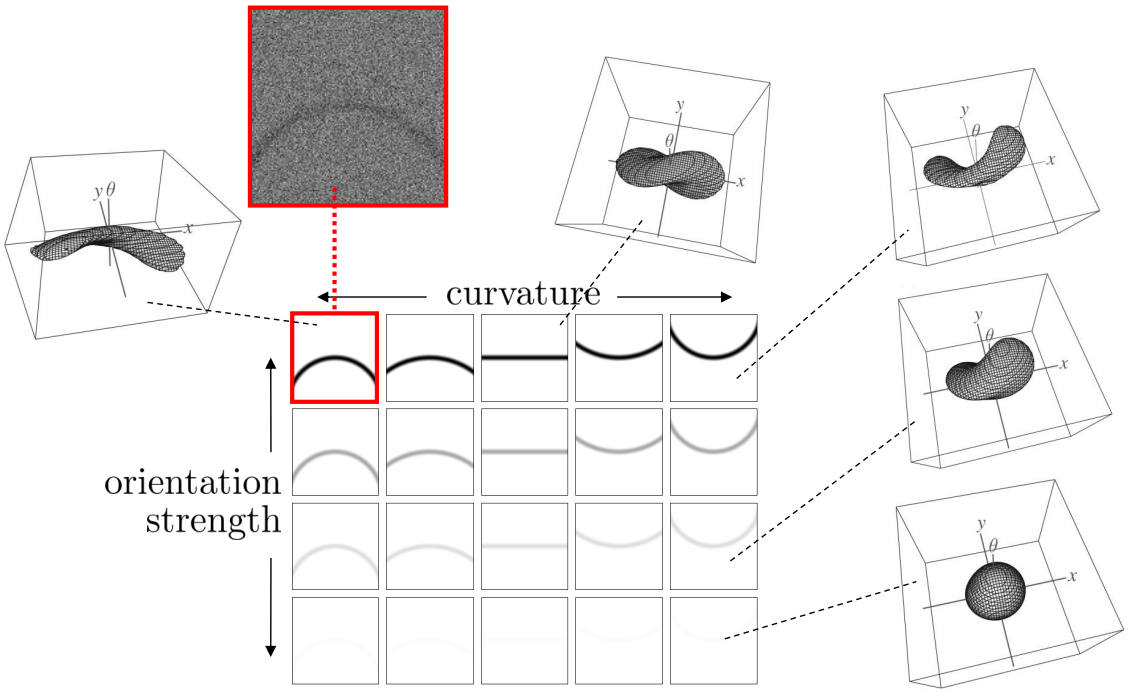

Figure 10: Illustration of heat kernels $K_t^D : SE(2) \to \mathbb{R}^+$ on $SE(2)$ corresponding to varying curvature and orientation strengths. Note that as orientation strength decreases the kernels become more isotropic (which is required for noise reduction). Furthermore, as curvature increases the diffusion kernels in $SE(2)$ bend accordingly.

$1 \leq i < k \leq m$. The idea here is that on lower scales we have to diffuse more as noise is typically dominant at lower scales and therefore lower scales need higher diffusion time.

5 Results

Parameters are used for creating the scale orientation score: No. of scales = 4, No. of orientations = 20. The parameters that we used for CED are (see[4]): $\sigma = 0.5$, $\rho = 4$, $C = 1$ and $\alpha = 0.001$. The non-linear diffusion parameters for CED-OS and CED-SOS for each scale are: $\rho_s = 12$, $\widetilde{\rho} = 1.5$, $\beta = 0.058$ and $c = 0.08$. All the experiments in this section use these parameters and the varying end times are indicated below the images. We have enforced horizontality in the experiments involving CED-OS, see [5] for more details.
Figure 11 compares the effect of CED, CED-OS and CED-SOS on an artificial image containing additive superimposition of two images with concentric circles of varying widths. The new proposed method yields visually better results compared to both CED and CED-OS.
Figure 12 shows the results on a microscopy image of collagen fibres. These kind of images are acquired in tissue engineering research where often the goal is to create artificial heart valves, [47].
Figure 13 shows the results on an image from the Brodatz texture dataset. The top row of Figure 14 shows the loss of small-scale data in CED-OS compared to CED-SOS. The bottom row compares the result of a basic tracking algorithm on these enhanced images. Clearly tracking on CED-SOS outperforms tracking on CED-OS.
Although CED-SOS is clearly advantageous for handling multi-scale complex structures and crossings, CED-OS has the advantage that it is considerable faster as it's implementation consumes far less memory.

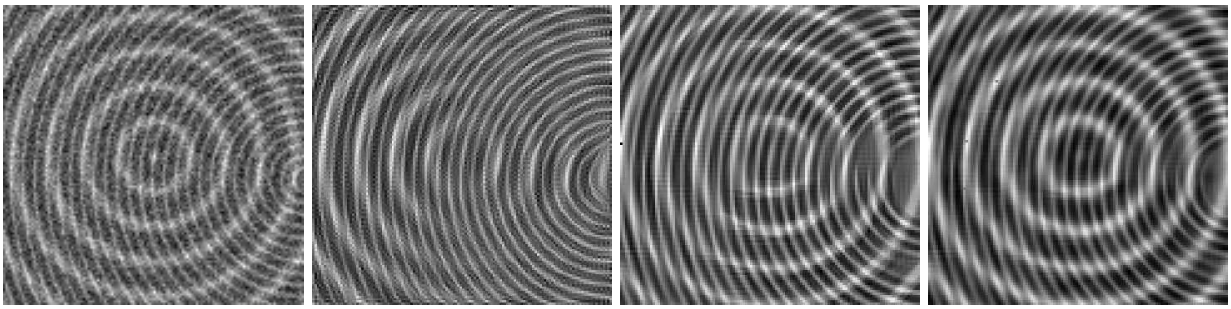

(a) Noisy image (b) CED $t = 15$ (c) CED-OS $t = 6$ (d) CED-SOS, $t_i = 0, 2, 6, 12$

Figure 11: Comparison of CED, CED-OS and our proposed method CED-SOS. In CED-SOS multi-scale crossing stuctures are better preserved. Observe that CED-OS and CED-SOS deal appropriately with crossings, unlike CED

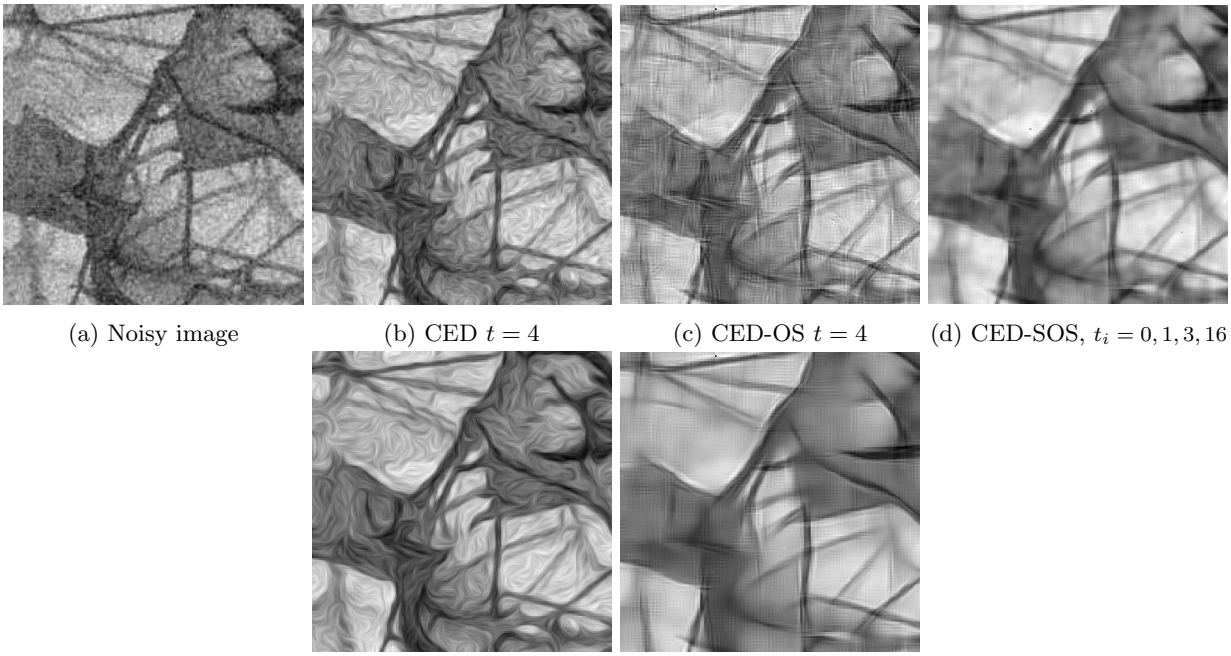

(a) Noisy image (b) CED $t = 4$ (c) CED-OS $t = 4$ (d) CED-SOS, $t_i = 0, 1, 3, 16$

(e) CED $t = 10$ (f) CED-OS $t = 10$

Figure 12: Results of CED, CED-OS and CED-SOS on a microscopy image of a Collagen tissue. CED-OS exhibits artefacts for small end time, see (c), which vanish if the algorithm is allowed to run longer at the cost of small-scale information, see (f). Therefore best visual results are obtained with CED-SOS.

6 Conclusions

There are two different tasks achieved in this article.

1. Designing an invertible score on $SIM(2)$, which also allows for accurate and efficient implementation of subsequent enhancement by contextual flows.

2. Construction of contextual flows in the wavelet domain for the enhancement of elongated multi-scale crossing/bifurcating structures, via left-invariant PDEs on $SIM(2)$.

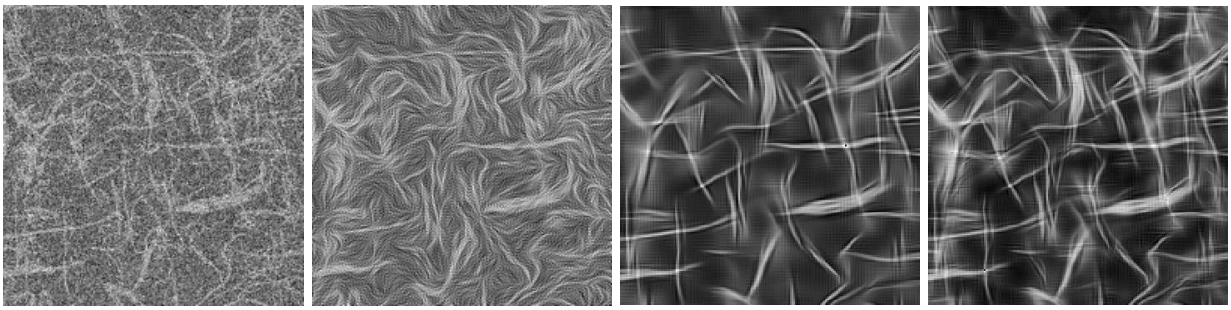

(a) Noisy image (b) CED $t = 6$ (c) CED-OS $t = 7$ (d) CED-SOS, $t_i = 0, 1, 6, 10$

Figure 13: Results of enhancement via of CED, CED-OS and CED-OS on Scale-OS on a Brodatz image.

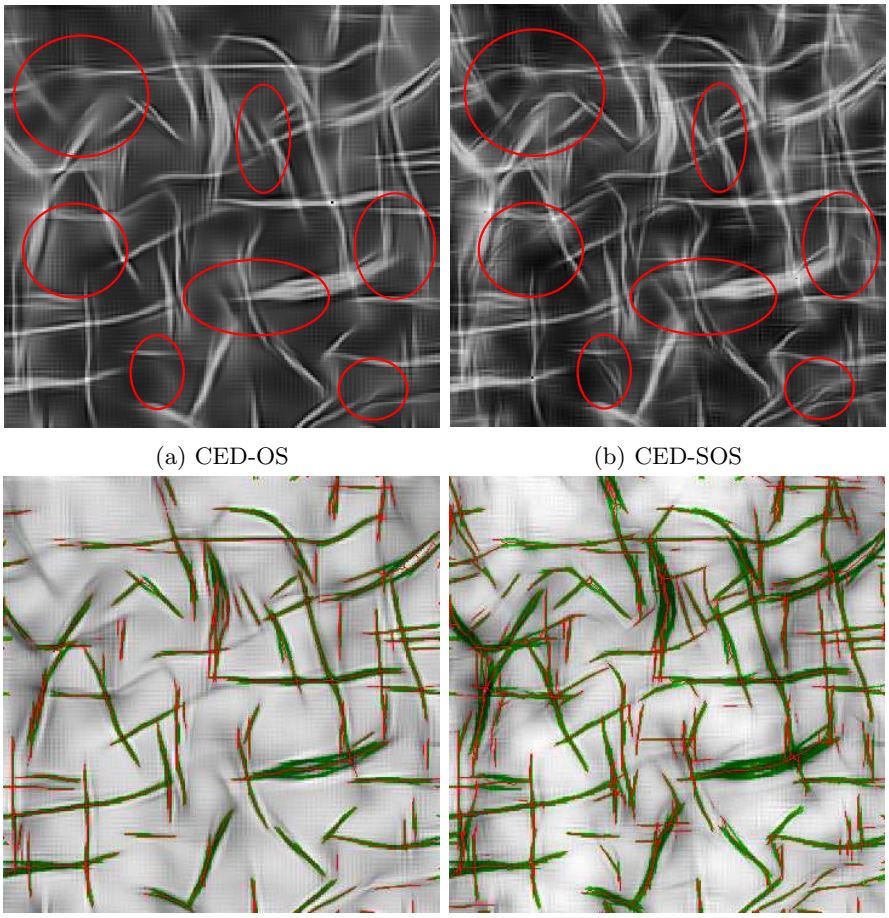

(a) CED-OS (b) CED-SOS

(c) Vessel tracking on CED-OS (d) Vessel tracking on CED-SOS

Figure 14: Top: Comparison of CED-OS and CED-SOS. Regions circled show loss of small-scale information in CED compared CED-SOS. Bottom: Results of a simple vessel tracking method on the images enhanced by CED-OS and CED-SOS. As expected tracking on CED-SOS enhanced images give better results.

Regarding the first task we have presented a generalized unitarity result for algebraic affine Lie groups. This result is then used to design a multi-scale orientation score appropriate for subsequent left-invariant flows.

For the second task we have shown that only left-invariant flows on multi-scale orientation scores (defined on $SIM(2)$) robustly relate to Euclidean invariant operations on images. Furthermore we have provided a differential-geometric and probabilistic interpretation of left-invariant PDEs on $SIM(2)$ which provides a strong intuitive rationale for the choice of left-invariant PDEs and involved diffusion parameters.
We have also derived analytic approximations of Green's function of linear diffusion on $SIM(2)$. Finally, we have presented crossing multiple-scale (curvature adaptive) flows via non-linear left-invariant diffusions on invertible scores. Our preliminary results indicate that including the notion of scale in the framework of invertible orientation scores indeed has advantages over existing PDE techniques (CED, CED-OS).
An interesting next step would be to include scale interactions in numerical implementation of non-linear diffusion on $SIM(2)$. Extending the framework of Scattering operators (Mallat [40]) to Lie groups would also be an interesting theoretical problem for future work.

Acknowledgements The authors wish to thank Erik Bekkers (Technische Universiteit Eindhoven) for fruitful discussions, ideas regarding numerical implementation of scale orientation score and the tracking algorithm to create Figure 14.

A Proof of Lemma 5

Proof. Let $f \in \langle V_\psi \rangle^\perp$. Thus

$$\forall_{\mathbf{b}\in\mathbb{R}^{\mathbf{d}}} \forall_{t\in T} (\mathcal{U}_{\mathbf{b},t}\psi, f)_{\mathbb{L}_2(\mathbb{R}^d)} = 0. \tag{73}$$

We know that,

$$(\mathcal{U}_{\mathbf{b},t}\psi, f)_{\mathbb{L}_2(\mathbb{R}^d)} = (\mathcal{F}\mathcal{R}_t\mathcal{T}\psi, \mathcal{F}f)_{\mathbb{L}_2(\mathbb{R}^d)} = (\mathcal{F}^{-1}[\overline{\mathcal{F}\mathcal{R}_t\psi}\mathcal{F}f])(\mathbf{b}).$$

Thus Equation(73) implies

$$\begin{aligned}
&\forall_{\mathbf{b}\in\mathbb{R}^{\mathbf{d}}} \forall_{t\in T} \left((\mathbf{b},t) \mapsto \mathcal{F}^{-1}[\overline{\mathcal{F}\mathcal{R}_t\psi}\mathcal{F}f])(\mathbf{b}) \right) = 0 \\
\Rightarrow \quad &\left((\boldsymbol{\omega},t) \mapsto \overline{\mathcal{F}\mathcal{R}_t\psi}(\boldsymbol{\omega})\mathcal{F}f(\boldsymbol{\omega}) \right) = 0 \ \ a.e.\ on\ \mathbb{R}^d \rtimes T \\
\Rightarrow \quad &\left((\boldsymbol{\omega},t) \mapsto |\mathcal{F}\mathcal{R}_t\psi(\boldsymbol{\omega})\mathcal{F}f(\boldsymbol{\omega})|^2 \right) = 0 \ \ a.e.\ on\ \mathbb{R}^d \rtimes T.
\end{aligned}$$

Therefore,

$$M_\psi(\boldsymbol{\omega})|(\mathcal{F}f)(\boldsymbol{\omega})| = (2\pi)^{d/2} \int_T \left| \frac{\mathcal{F}\mathcal{R}_t\psi(\boldsymbol{\omega})\mathcal{F}f(\boldsymbol{\omega})}{\sqrt{det\tau(t)}} \right|^2 d\mu_T(t) = 0 \ \ a.e.\ on\ \mathbb{R}^d.$$

Since $M_\psi \neq 0$ *a.e.* as ψ is an admissible wavelet, this implies that $|\mathcal{F}f|^2 = 0$ which implies $f = 0$. □ □

B Proof of Theorem 7

Proof. By Theorem 2, every $\Phi \in \mathbb{C}_K^G$ has a $\mathcal{W}_\psi$ pre-image $f \in \mathbb{L}_2(\mathbb{R}^d)$, i.e. $f = (\mathcal{W}_\psi)^{-1}[\Phi]$ with

$$\|\Phi\|^2_{\mathbb{C}_K^G} = (\Phi,\Phi)_{\mathbb{C}_K^G} = (f,f)_{\mathbb{L}_2(\mathbb{R}^d)} = \|f\|^2_{\mathbb{L}_2(\mathbb{R}^d)}.$$

We need to show that $\|\Phi\|^2_{\mathbb{C}_K^G} = \|\Phi\|^2_{M_\psi} := (\Phi,\Phi)^{\frac{1}{2}}_{M_\psi}$, where we recall (12) for the definition of the M_ψ-inner product. We have,

$$\int_{\mathbb{R}^d} |f(y)|^2\, dy = \int_{\mathbb{R}^d} |\hat{f}(\omega)|^2 d\omega = \int_{\overline{\Omega}} |\hat{f}(\omega)|^2 \frac{M_\psi(\omega)}{M_\psi(\omega)} d\omega = \int_{\Omega} |\hat{f}(\omega)|^2 \frac{M_\psi(\omega)}{M_\psi(\omega)} d\omega. \tag{74}$$

The second equality follows from from (9). Recall that T is assumed to be a linear algebraic Lie group and therefore it has locally closed (dual) orbits. This leads to $\Omega_c = \Omega_{cr}$ in [34, Ch 5] and since Ω_{cr} is open, [34, Prop 5.7], we have that $\mu(\overline{\Omega}\backslash\Omega) = 0$, where μ is the usual Lebesgue measure on $\mathbb{R}^d$, giving us the final equality in (74). We can further write (74) as,

$$\begin{aligned}\int\limits_{\mathbb{R}^d} |f(y)|^2\, dy &= \int\limits_{\Omega} |\hat{f}(\omega)|^2 \frac{1}{M_\psi(\omega)} \int\limits_T \frac{|(\mathcal{F}\mathcal{R}_t\psi)(\omega)|^2}{det(\tau(t))} d\mu_T(t) d\omega = \int\limits_{\Omega} \left\{ \int\limits_T \frac{\overline{\hat{f}(\omega)\,(\mathcal{F}\mathcal{R}_t\psi(\omega))}\hat{f}(\omega)\,(\mathcal{F}\mathcal{R}_t\psi(\omega))}{det(\tau(t))} \right\} \frac{d\omega}{M_\psi(\omega)} \\ &= \int\limits_{\Omega} \int\limits_T \overline{(\mathcal{F}\Phi(\cdot,t))\,(\omega)}\,(\mathcal{F}\Phi(\cdot,t))\,(\omega) d\mu_T(t) \frac{d\omega}{M_\psi(\omega)} = \int\limits_{\Omega} \left(\int\limits_T |\mathcal{F}\Phi(\cdot,t)(\omega)|^2\, d\mu_T(t) \right) M_\psi^{-1}(\omega) d\omega.\end{aligned}$$

As a result $\Phi \in \mathbb{H}_\psi \otimes \mathbb{L}_2(T; \frac{d\mu_T(t)}{det(\tau(t))})$ and we have,

$$(f,f)_{\mathbb{L}_2(\mathbb{R}^d)} = (\mathcal{W}_\psi f, \mathcal{W}_\psi f)_{\mathbb{C}_K^G} = \int\limits_T \left(M_\psi^{-\frac{1}{2}} \mathcal{F}\Phi(\cdot,t), M_\psi^{-\frac{1}{2}} \mathcal{F}\Phi(\cdot,t) \right) d\mu_T(t),$$

from which the result follows. □ □

C Explicit formulation of exponential and logarithm curves

The exponential curves $g_0\gamma_c(t) = (x(t), y(t), \tau(t), \theta(t))$ passing through $g_0 = \{x_0, y_0, e^{\tau_0}, \theta_0\}$ at $t = 0$ is,

$$\begin{aligned} x(t) &= \frac{1}{c_1^2 + c_4^2}[e^{\tau_0} c_1 \left(\left(-\sin[\theta_0] + e^{tc_4} \sin[tc_1 + \theta_0] \right) c_2 + \left(-\cos[\theta_0] + e^{tc_4} \cos[tc_1 + \theta_0] \right) c_3 \right) + c_1^2 x_0 + \\ &\quad c_4 \left(e^{\tau_0} \left(-\cos[\theta_0] + e^{tc_4} \cos[tc_1 + \theta_0] \right) c_2 + e^{\tau_0} \left(\sin[\theta_0] - e^{tc_4} \sin[tc_1 + \theta_0] \right) c_3 + c_4 x_0 \right)] \\ y(t) &= \frac{1}{c_1^2 + c_4^2}[e^{\tau_0} c_1 \left(\left(\cos[\theta_0] - e^{tc_4} \cos[tc_1 + \theta_0] \right) c_2 + \left(-\sin[\theta_0] + e^{tc_4} \sin[tc_1 + \theta_0] \right) c_3 \right) + c_1^2 y_0 + \\ &\quad c_4 \left(e^{\tau_0} \left(-\sin[\theta_0] + e^{tc_4} \sin[tc_1 + \theta_0] \right) c_2 + e^{\tau_0} \left(-\cos[\theta_0] + e^{tc_4} \cos[tc_1 + \theta_0] \right) c_3 + c_4 y_0 \right)] \\ \tau(t) &= tc_4 + \tau_0 \\ \theta(t) &= tc_1 + \theta_0. \end{aligned} \tag{75}$$

To explicitly determine the log map, we solve for $\{c^1, c^2, c^3, c^4\}$ from the equality, $g = \exp\left(t \sum\limits_{i=1}^{4} c^i A_i \right)$, where $g \in SIM(2)$ and c^i's are as defined earlier. This is achieved by substituting $g_0 = e$, i.e. $x_0 = y_0 = \theta_0 = \tau_0 = 0$, in (75) yielding,

$$\begin{aligned} c^1 &= \theta/t \\ c^2 &= \frac{y\theta - x\tau - e^\tau(y\theta - x\tau)\cos\theta + e^\tau(x\theta + y\tau)\sin\theta}{t\,(1 + e^{2\tau} - 2e^\tau \cos\theta)} \\ c^3 &= \frac{-x\theta - y\tau + e^\tau(x\theta + y\tau)\cos\theta + e^\tau(y\theta - x\tau)\sin\theta}{t\,(1 + e^{2\tau} - 2e^\tau \cos\theta)} \\ c^4 &= \tau/t, \end{aligned} \tag{76}$$

where recall that $g = (x, y, e^\tau, \theta) \in SIM(2)$. The formulae in (76) can be written in a simplified form,

$$\begin{aligned} c^1 &= \theta/t \\ c^2 &= \frac{(y\theta - x\tau) + (-\theta\eta + \tau\xi)}{t\,(1 + e^{2\tau} - 2e^\tau \cos\theta)} \\ c^3 &= \frac{-(x\theta + y\tau) + (\theta\xi + \tau\eta)}{t\,(1 + e^{2\tau} - 2e^\tau \cos\theta)} \\ c^4 &= \tau/t, \end{aligned} \tag{77}$$

where we have made use of the definition of ξ and η,

$$\xi = e^{\tau}(x\cos\theta + y\sin\theta),\ \eta = e^{\tau}(-x\sin\theta + y\cos\theta).$$

D Proof of Theorem 18

Proof. We first note that, $U \in \mathcal{D}(d\mathcal{R}(A)) \Rightarrow (d\mathcal{R}(A)U) \in H$, where $H = \mathbb{L}_2(SIM(2))$. Then, $\mathcal{R}_{e^{tA}}U \in \mathcal{D}(d\mathcal{R}(A))$ follows as $[d\mathcal{R}(A)\mathcal{R}_{e^{tA}}](U) = [\mathcal{R}_{e^{tA}}d\mathcal{R}(A)](U),$ for all $U \in \mathcal{D}(d\mathcal{R}(A))$.

$$\begin{aligned}
[d\mathcal{R}(A)\mathcal{R}_{e^{tA}}](U)(g) &= \left[\lim_{h\to 0}\frac{\mathcal{R}_{e^{hA}} - I}{h}\right](\mathcal{R}_{e^{tA}}U)(g) \\
&= \lim_{h\to 0}\frac{\mathcal{R}_{e^{hA}}\mathcal{R}_{e^{tA}}(U(g)) - \mathcal{R}_{e^{tA}}(U(g))}{h} \\
&= \lim_{h\to 0}\frac{\mathcal{R}_{e^{tA}}\mathcal{R}_{e^{hA}}(U(g)) - \mathcal{R}_{e^{tA}}(U(g))}{h} \\
&= [\mathcal{R}_{e^{tA}}d\mathcal{R}(A)](U)(g),
\end{aligned}$$

where we have used $\mathcal{R}_h(U(g)) = U(gh)$ and $e^{tA}e^{hA} = e^{(t+h)A} = e^{hA}e^{tA}$. This proves (1). We need to prove that $e^{td\mathcal{R}(A)}U = \mathcal{R}_{e^{tA}}U$, where[10] $U \in \mathcal{D}(d\mathcal{R}(A)),$ for all $A \in T_e(G),$ for all $t > 0$. By definition $e^{td\mathcal{R}(A)}U$ is the (strong) solution for $\frac{\partial W}{\partial t}(\cdot,t) = d\mathcal{R}(A)W(\cdot,t)$ with $W(g,0) = U$. Now $\frac{\partial(\mathcal{R}_{e^{tA}}U)}{\partial t} = d\mathcal{R}(A)(\mathcal{R}_{e^{tA}}U)$, follows from,

$$\begin{aligned}
\frac{\partial(\mathcal{R}_{e^{tA}}U)}{\partial t} &= \lim_{h\to 0}\frac{\mathcal{R}_{e^{(t+h)A}}U - \mathcal{R}_{e^{tA}}U}{h} = \lim_{h\to 0}\frac{\mathcal{R}_{e^{hA}}\mathcal{R}_{e^{tA}}U - \mathcal{R}_{e^{tA}}U}{h} \\
&= \lim_{h\to 0}\left[\left(\frac{\mathcal{R}_{e^{hA}} - I}{h}\right)\mathcal{R}_{e^{tA}}U\right] = d\mathcal{R}(A)(\mathcal{R}_{e^{tA}}U). \qquad (78)
\end{aligned}$$

Note that the limit used above is defined on the space $H = \mathbb{L}_2(SIM(2))$.

Let $d\mathcal{R}(A) = \mathcal{A} = \sum_{i=1}^{4} c^i\mathcal{A}_i$. Then the solution for (55) is, $W(\cdot,t) = e^{-td\mathcal{R}(A)}U = \mathcal{R}_{e^{-tA}}U$, where the second equality follows from (2). Thus we have,

$$W(g,t) = U(ge^{-tA})\ \ \forall g \in SIM(2),\ \forall t > 0 \Rightarrow W(g_0e^{tA},t) = U(g_0)\ \ \forall t > 0. \qquad (79)$$

From which the result follows. □ □

E Approximation of $SIM(2)$ by a Nilpotent Group via Contraction

Following the general framework by ter Elst and Robinson [46], which involves semigroups on Lie groups generated by subcoercive operators, we consider a particular case by setting the Hilbert space $H = \mathbb{L}_2(SIM(2))$, the group $G = SIM(2)$ and the right-regular representation $\mathcal{R}$. Furthermore we consider the algebraic basis $\{\mathcal{A}_1 = \partial_\theta, \mathcal{A}_2 = \partial_\xi, \mathcal{A}_4 = \partial_\tau\}$ leading to the following filtration of the Lie algebra

$$\mathfrak{g}_1 := \text{span}\{\mathcal{A}_1,\mathcal{A}_2,\mathcal{A}_4\} \subset \mathfrak{g}_2 = [\mathfrak{g}_1,\mathfrak{g}_1] = \text{span}\{\mathcal{A}_1,\mathcal{A}_2,\mathcal{A}_3,\mathcal{A}_4\} = \mathcal{L}(SIM(2)). \qquad (80)$$

Based on this filtration we assign the following weights to the generators:

$$w_1 = w_2 = w_4 = 1 \text{ and } w_3 = 2. \qquad (81)$$

[10] $\mathcal{D}(A)$ denotes the domain of the operator A.

For e.g. $w_2 = 1$ since $\mathcal{A}_2$ occurs first in $\mathfrak{g}_1$, while $w(3) = 2$ since $\mathcal{A}_3$ occurs in $\mathfrak{g}_2$ and not $\mathfrak{g}_1$. Based on these weights we define the following dilations on the Lie algebra $T_e(SIM(2))$ (recall $A_i = \mathcal{A}_i|_e$),

$$\gamma_q\left(\sum_{i=1}^{4} c^i A_i\right) = \sum_{i=1}^{4} q^{w_i} c^i A_i, \ \forall c^i \in \mathbb{R},$$
$$\tilde{\gamma}_q(x, y, \tau, \theta) = \left(\frac{x}{q^{w_2}}, \frac{y}{q^{w_3}}, \frac{\tau}{q^{w_4}}, e^{i\frac{\theta}{q^{w_1}}}\right),$$

with the weights w_i defined in (81), and for $0 < q \leq 1$ we define the Lie product $[A, B]_q = \gamma_q^{-1}[\gamma_q(A), \gamma_q(B)]$. Let $(SIM(2))_t$ be the simply connected Lie group generated by the Lie algebra[11] $(T_e(SIM(2)), [\cdot, \cdot]_q)$. The group products on these intermediate groups $(SIM(2))_{q\in(0,1]}$ are given by,

$$(x, y, \tau, \theta) \cdot_q (x', y', \tau', \theta') = (x + e^{\tau q}[\cos(q\theta)x' - q\sin(q\theta)y'], y + e^{\tau q}[\frac{\sin(q\theta)}{q}x' + \cos(q\theta)y'], \tau + \tau', \theta + \theta'). \quad (82)$$

The dilation on the Lie algebra coincides with the pushforward of the dilation on the group $\gamma_q = (\tilde{\gamma}_q)_*$ and therefore the left-invariant vector fields on $(SIM(2))_t$ are given by

$$\mathcal{A}_i^q|_g = (\tilde{\gamma}_q^{-1} \circ L_g \circ \tilde{\gamma}_q)_* A_i,$$

for all $q \in (0, 1]$ which leads to,

$$\begin{aligned}\mathcal{A}_i^q|_g \phi &= (\tilde{\gamma}_q^{-1} \circ L_g)_*(\tilde{\gamma}_q)_* A_i \phi = (\tilde{\gamma}_q^{-1} \circ L_g)_*(\gamma_q)(A_i)\phi = t^{w_i}(\tilde{\gamma}_q^{-1} \circ L_g)_*(A_i)\phi \\ &= q^{w_i}(\tilde{\gamma}_q^{-1})_* \mathcal{A}_i|_g \phi = q^{w_i} \mathcal{A}_i|_{\tilde{\gamma}_q^{-1} g}(\phi \circ \tilde{\gamma}_q),\end{aligned}$$

for all smooth complex valued functions ϕ defined on a open neighbourhood around $g \in SIM(2)$. So for all $g = (x, y, \tau, \theta) \in SIM(3)$ we have,

$$\begin{aligned}\mathcal{A}_1^t|_g &= q(\frac{1}{q}\partial_\theta) = \partial_\theta \\ \mathcal{A}_2^q|_g &= q\left[e^{\tau q}\left(\frac{\cos(q\theta)}{q}\partial_x + \frac{\sin(q\theta)}{q^2}\partial_y\right)\right] = e^{\tau q}\left(\cos(q\theta)\partial_x + \frac{\sin(q\theta)}{q}\partial_y\right) \\ \mathcal{A}_3^q|_g &= q^2\left[e^{\tau q}\left(-\frac{\sin(q\theta)}{q}\partial_x + \frac{\cos(q\theta)}{q^2}\partial_y\right)\right] = e^{\tau q}\left(-q\sin(q\theta)\partial_x + \cos(q\theta)\partial_y\right) \\ \mathcal{A}_4^q|_g &= \partial_\tau.\end{aligned} \quad (83)$$

For example,

$$\begin{aligned}\mathcal{A}_3^q|_g &= (\tilde{\gamma}_q^{-1} \circ L_g \circ \tilde{\gamma}_q)_* A_3 = (\tilde{\gamma}_q^{-1} \circ L_g)_*(\tilde{\gamma}_q)_* A_3 = (\tilde{\gamma}_q^{-1} \circ L_g)_*(q^2\partial_y) \\ &= q^2(\tilde{\gamma}_q^{-1})_*(\partial_\eta) = q^2 e^{\tau q}(\tilde{\gamma}_q^{-1})_*(-\sin(q\theta)\partial_x + \cos(q\theta)\partial_y) \\ &= q^2 e^{\tau q}(-\sin(q\theta)\gamma_q^{-1}(\partial_x) + \cos(q\theta)\gamma_q^{-1}(\partial_y)) = q^2 e^{\tau q}(\frac{-\sin(q\theta)}{q}\partial_x + \frac{\cos(q\theta)}{q^2}\partial_y).\end{aligned}$$

Further, $[A_i, A_j]_q = \gamma_q^{-1}[\gamma_q(A_i), \gamma_q(A_j)] = \gamma_q^{-1} q^{w_i + w_j}[A_i, A_j] = \sum_{k=1}^{4} q^{w_i + w_j - w_k} c_{ij}^k A_k$ and therefore

$$[A_1, A_2]_q = A_3, \quad [A_1, A_3]_q = -q^2 A_2, \quad [A_4, A_2]_q = qA_2, \quad [A_4, A_3]_q = qA_3. \quad (84)$$

Analogously to the case $q = 1$, $(SIM(2))_{q=1} = SIM(2)$, there exists an isomorphism of the Lie algebra at the unity element $T_e((SIM(2))_q)$ and the left-invariant vector fields on the group $\mathcal{L}((SIM(2))_q)$:

$$(A_i \leftrightarrow \mathcal{A}_i^q \text{ and } A_j \leftrightarrow \mathcal{A}_j^q) \Rightarrow [A_i, A_j]_q \leftrightarrow [\mathcal{A}_i^q, \mathcal{A}_j^q]. \quad (85)$$

[11] Note that $(SIM(2))_q = exp_q(T_e(SIM(2)))$.

It can be verified that the left invariant vector fields $\mathcal{A}_i^q$ satisfy the same commutation relations as (84). In the case $H \equiv \lim_{q\downarrow 0} (SIM(2))_q$ the left-invariant vector fields are given by

$$\mathcal{A}_1^0 = \partial_\theta,\ \mathcal{A}_2^0 = \partial_x + \theta\partial_y,\ \mathcal{A}_3^0 = \partial_y,\ \mathcal{A}_4^0 = \partial_\tau. \tag{86}$$

So, the homogeneous nilpotent contraction Lie group equals

$$H_3 = \lim_{q\downarrow 0} (SIM(2))_q \text{ and } SIM(2) = (SIM(2))_{q=1}/(\{0\}\times\{0\}\times\{0\}\times 2\pi\mathbb{Z}), \tag{87}$$

with the Lie algebra $\mathcal{L}(H) = \text{span}\{\partial_\theta, \partial_x + \theta\partial_y, \partial_y, \partial_\tau\}$ and $\mathcal{L}(SIM(2)) = \text{span}\{\partial_\theta, \partial_\xi, \partial_\eta, \partial_\tau\}$.

F Differential-geometric interpretation of Left-invariant Evolutions

In order to keep track of orthogonality and parallel transport in such diffusions we need an invariant first fundamental form $\mathcal{G}$ on $SIM(2)$, rather than the trivial, bi-invariant (i.e. left and right invariant), first fundamental form on $(\mathbb{R}^4, T(\mathbb{R}^4))$, where each tangent space $T_{\mathbf{x}(\mathbb{R}^4)}$ is identified with $T_0(\mathbb{R}^4)$ by standard parallel transport on $\mathbb{R}^4$, i.e. $\mathcal{G}_{\mathbb{R}^4}(\mathbf{x},\mathbf{y}) = \mathbf{x}\cdot\mathbf{y} = x^1y^1 + x^2y^2 + x^3y^3 + x^4y^4$.
Recall Theorem 17 which essentially states that operators Φ on scale-OS should be left-invariant (i.e. $\mathcal{L}_g \circ \Phi = \Phi \circ \mathcal{L}_g$) and not right-invariant in order to ensure that the effective operator Υ_ψ on the image is a Euclidean invariant operator. This suggests that the first fundamental form required for our diffusions on $SIM(2)$ should be left-invariant. The following theorem characterizes the formulation of a left-invariant first fundamental form w.r.t the $SIM(2)$ group.

Theorem 22. *The only real valued left-invariant (symmetric, positive, semidefinite) first fundamental form $\mathcal{G} : SIM(2)\times T(SIM(2))\times T(SIM(2)\to\mathbb{C}$ on $SIM(2)$ are given by,*

$$\mathcal{G} = \sum_{i=1}^4\sum_{j=1}^4 g_{ij}\ \omega^i\otimes\omega^j,\ g_{ij}\in\mathbb{R}. \tag{88}$$

where the dual basis $\{\omega^1,\omega^2,\omega^3,\omega^4\} \subset (\mathcal{L}(SIM(2)))^*$ of the dual space $(\mathcal{L}(SIM(2)))^*$ of the vector space $\mathcal{L}(SIM(2))$ of left-invariant vector fields spanned by

$$\{\mathcal{A}_1,\mathcal{A}_2,\mathcal{A}_3,\mathcal{A}_4\} = \{\partial_\theta, e^\tau(\cos\theta\partial_x + \sin\theta\partial_y), e^\tau(-\sin\theta\partial_x + \cos\theta\partial_y), \partial_\tau\}, \tag{89}$$

obtained by applying the operator $d\mathcal{R} : T_e(G)\to\mathcal{L}(G)$, defined as

$$(d\mathcal{R}(A)\phi)(g) = \lim_{t\downarrow 0}\frac{(\mathcal{R}_{exp(tA)}\phi)(g) - \phi(g)}{t},\ A\in T_e(G), \phi\in\mathbb{L}_2(G), g\in G, \tag{90}$$

to the standard basis in the Lie algebra

$$\{A_1,A_2,A_3,A_4\} = \{\partial_\theta,\partial_x,\partial_y,\partial_a\} \subset T_e(SIM(2)), \tag{91}$$

is given by

$$\{\omega^1,\omega^2,\omega^3,\omega^4\} = \{d\theta, \frac{1}{e^\tau}(\cos\theta dx + \sin\theta dy), \frac{1}{e^\tau}(-\sin\theta dx + \cos\theta dy), d\tau\}. \tag{92}$$

Proof. Recall that $d\mathcal{R}$ yields the fundamental isomorphism between the Lie algebra $T_e(SIM(2))$ and $\mathcal{L}(SIM(2))$. The dual basis (92) satisfy $\langle\mathcal{A}^i,\mathcal{A}_j\rangle = \delta^i_j$. A first fundamental form $\mathcal{G} : SIM(2)\times T(SIM(2))\times T(SIM(2)\to\mathbb{C}$ on $SIM(2)$ by definition is left invariant if for all $h,g\in SIM(2)$, for all $X,Y\in T(SIM(2))$: $\mathcal{G}_h(X_h,Y_h) =$

$\mathcal{G}_{gh}((L_g)_*X_h,(L_g)_*Y_h)$. The dual tangent space $(T_g(SIM(2))^*$, $g\in SIM(2)$ is spanned by $\{\omega^1|_g,\omega^2|_g,\omega^3|_g,\omega^4\}|_g$. Thus for all $g\in SIM(2)$ there exist numbers $g_{ij}\in\mathbb{R},\ i,j\in\{1,2,3,4\}$ such that

$$\mathcal{G}_g=\sum_{i=1}^{4}\sum_{j=1}^{4}g_{ij}(g)\ \omega^i\big|_g\otimes\omega^j\big|_g. \tag{93}$$

$\mathcal{G}$ is left-invariant iff $\mathcal{G}_g(\mathcal{A}_i|_g,\mathcal{A}_j|_g)=\mathcal{G}_e((L_{g^{-1}})_*\mathcal{A}_i|_g,(L_{g^{-1}})_*\mathcal{A}_j|_g)=\mathcal{G}_e(A_i,A_j),\ \forall i,j\in\{1,2,3,4\}\ \forall g\in SIM(2)$ which implies that $\forall i,j\in\{1,2,3,4\},\ g_{ij}(g)=g_{ij}$. □ □

We consider the Maurer-Cartan form on $SIM(2)$ (discussed in the remainder of the subsection) and impose the following left-invariant, first fundamental form $\mathcal{G}_\beta:SIM(2)\times T(SIM(2))\times T(SIM(2))\to\mathcal{C}$ on $SIM(2)$,

$$\mathcal{G}=\sum_{i=1}^{4}\sum_{j=1}^{4}g_{ij}\ \omega^i\otimes\omega^j=\alpha^2\omega^1\otimes\omega^1+\beta^2\omega^2\otimes\omega^2+\beta^2\omega^3\otimes\omega^3+\sigma^2\omega^4\otimes\omega^4. \tag{94}$$

Here σ tunes the cost of changing scale, β the cost of moving spatially and α the cost of moving angularly. By homogeneity we set $\alpha=1$, as it is only $\frac{\beta}{\alpha}$, $\frac{\sigma}{\alpha}$ that matter. In order to understand the meaning of the next two theorems we need some definitions from differential geometry. See [48] for more details on these concepts.

Definition 23. *Let M be a smooth manifold and G be a Lie group. A principle fiber bundle $P_G:=(P,M,\pi,R)$ above a manifold M with structure group G is a tuple (P,M,π,R) such that P is a smooth manifold (called the total space of the principle bundle), $\pi:P\to M$ is a smooth projection map with $\pi(P)=M$ and $\pi(u\cdot a)=\pi(a),\ \forall u\in P,\ a\in G$, R a smooth right action $R_gp=p\cdot g,\ p\in P,\ g,h\in G$. Finally it should satisfy the "local triviality" condition: For each $p\in M$ there is a neighbourhood U of p and a diffeomorphism $t:\pi^{-1}(U)\to U\times G$ of the form $t(u)=(\pi(u),\phi(u))$ where ϕ satisfies $\phi(u\cdot a)=\phi(u)a$ where the latter product is in G.*

Definition 24. *A principle fiber bundle $P_G:=(P,M,\pi,R)$ is commonly equipped with a Cartan-Ehresmann connection form ω. This by definition is a Lie algebra $T_e(G)$-valued 1-form $\omega:P\times T(P)\to T_e(G)$ on P such that*

$$\begin{aligned}&\omega(d\mathcal{R}(A))=A\ \text{for all}\ A\in T_e(G)\\&\omega((R_h)_*\mathcal{A})=Ad(h^{-1})\omega(\mathcal{A})\ \text{for all vector fields}\ \mathcal{A}\ \text{in}\ G.\end{aligned} \tag{95}$$

It is also common practice to relate principle fiber bundles to vector bundles. Here one uses an external representation $\rho:G\to F$ into a finite-dimensional vector space F of the structure group to put an appropriate vector space structure on the fibers $\{\pi^{-1}(m)|\ m\in M\}$ in the principle fiber bundles.

Definition 25. *Let P be a principle fiber bundle with finite dimensional structure group G. Let $\rho:G\to F$ be a representation in a finite-dimensional vector space F. Then the associated vector bundle is denoted by $P\times_\rho F$ and equals the orbit space under the right action*

$$(P\times F)\times G\to P\times F\ \text{given by}\ ((u,X),g)\mapsto(ug,\rho(g)X),$$

for all $g\in G,\ X\in F$ and $u\in P$.

Remark 26. *$GL(T_e(SIM(2)))$ denotes the collection of linear operators on the Lie algebra $T_e(SIM(2))$. Note that each linear operator $\overline{Q}\in GL(T_e(SIM(2)))$ on $T_e(SIM(2))$ is 1-to-1 related to bilinear form Q on $(T_e(SIM(2)))^*\times T_e(SIM(2))$ by means of*

$$\langle B,\overline{Q}A\rangle=Q(B,A),\ \text{for all}\ B\in(T_e(SIM(2)))^*,\ A\in T_e(SIM(2))\ \text{and}\ \overline{Q}=\sum_{i=1}^{4}Q(\omega^i|_e,\cdot)A_i.$$

So a basis for $GL(T_e(SIM(2)))$ is given by $\{\overline{\omega^i|_e\otimes A_j|}\ i,j\in\{1,2,3,4\}\}$. For the simplicity of notation we omit the overline and write $\omega^i|_e\otimes A_j$ as it is clear from context whether we mean the bilinear form or the linear mapping.

Theorem 27. *The Maurer-Cartan form ω on $SIM(2)$ can be formulated as*

$$\omega_g(X_g) = \sum_{i=1}^{4} \langle \omega^i|_g, X_g \rangle A_i, \;\; X_g \in T_g(SIM(2)), \tag{96}$$

where $\{\omega^i\}_{i=1}^4$ is given by (92) and $A_i = \mathcal{A}_i|_e$; recall (89). It is a Cartan-Ehresmann connection form on the principle fiber bundle $P = (SIM(2), e, SIM(2), \mathcal{L}(SIM(2)))$, where $\pi(g) = e$, $R_g u = ug$, $u, g \in SIM(2)$. Let Ad denote the adjoint action of $SIM(2)$ on its own Lie algebra $T_e(SIM(2))$, i.e. $Ad(g) = (R_{g^{-1}} L_g)_*$, i.e. the push-forward of conjugation. Then the adjoint representation of $SIM(2)$ on the vector space $\mathcal{L}(SIM(2))$ of left-invariant vector-fields is given by

$$\widetilde{Ad}(g) = d\mathcal{R} \circ Ad(g) \circ \omega. \tag{97}$$

The adjoint representation gives rise to the associated vector bundle $SIM(2) \times_{\widetilde{Ad}} \mathcal{L}(SIM(2))$. The corresponding connecting form on this vector bundle is given by

$$\tilde{\omega} = \mathcal{A}_2 \otimes \omega^3 \wedge \omega^1 + \mathcal{A}_3 \otimes \omega^1 \wedge \omega^2 + \mathcal{A}_2 \otimes \omega^4 \wedge \omega^2 + \mathcal{A}_3 \otimes \omega^4 \wedge \omega^3. \tag{98}$$

Then $\tilde{\omega}$ yields the following 4×4 matrix-valued 1-form:

$$\tilde{\omega}_j^k(\cdot) := -\tilde{\omega}(\omega^k, \cdot, \mathcal{A}_j), \;\; k, j \in \{1, 2, 3, 4\} \tag{99}$$

on the frame bundle, where the sections are moving frames[12]*. Let $\{\mu_k\}_{k=1}^4$ denote the sections in the tangent bundle $E := (SIM(2), T(SIM(2)))$ which coincides with the left-invariant vector fields $\{\mathcal{A}_k\}_{k=1}^4$. Then the matrix-valued 1-form (89) yields the Cartan connection* [13] *D on the tangent bundle $(SIM(2), T(SIM(2)))$ given by the covariant derivatives*

$$\begin{aligned} D_{X|_{\gamma(t)}}(\mu(\gamma(t))) &:= D(\mu(\gamma(t)))(X|_{\gamma(t)}) \\ &= \sum_{k=1}^{4} \dot{a}^k \mu_k(\gamma(t)) + \sum_{k=1}^{4} a^k(\gamma(t)) \sum_{k=1}^{4} \tilde{\omega}_k^j(X|_{\gamma(t)}) \mu_j(\gamma(t)) \\ &= \sum_{k=1}^{4} \dot{a}^k \mu_k(\gamma(t)) + \sum_{k=1}^{4} \dot{\gamma^i}(t) a^k(\gamma(t)) \Gamma_{ik}^j \mu_j(\gamma(t)), \end{aligned} \tag{100}$$

with $\dot{a}^k = \dot{\gamma}^i(t)(\mathcal{A}_i|_{\gamma(t)} a^k)$, for all tangent vectors $X|_{\gamma(t)} = \dot{\gamma}^i(t)\mathcal{A}_i|_{\gamma(t)}$ along a curve $t \mapsto \gamma(t) \in SIM(2)$ and all sections $\mu(\gamma(t)) = \sum_{k=1}^{4} a^k(\gamma(t))\mu_k(\gamma(t))$. The Christoffel symbols in (100) are constant $\Gamma_{ik}^j = -c_{ik}^j$, with c_{ik}^j the structure constants of the Lie algebra $T_e(SIM(2))$.

Proof. As in Theorem 22, we set $\{A_1, A_2, A_3, A_4\} = \{\partial_\theta, \partial_x, \partial_y, \partial_a\}$ as a basis for the Lie algebra $T_e(SIM(2))$ and $\{\mathcal{A}_1, \mathcal{A}_2, \mathcal{A}_3, \mathcal{A}_4\} = \{d\mathcal{R}(A_1), d\mathcal{R}(A_2), d\mathcal{R}(A_3), d\mathcal{R}(A_4)\} = \{\partial_\theta, \partial_\xi, \partial_\eta, \partial_\tau\}$ as the basis for the space $\mathcal{L}(SIM(2))$ of left-invariant vector fields with corresponding dual basis $\{\omega^1, \omega^2, \omega^3, \omega^4\} \subset (\mathcal{L}(SIM(2)))^*$. The Maurer-Cartan form $\omega : (SIM(2), T(SIM(2))) \to T_e(SIM(2))$ is defined as

$$\omega_g(Y_g) = (L_{g^{-1}})_* Y_g, \tag{101}$$

where $(L_{g^{-1}})_*$ denotes the push- forward of the inverse left multiplication $h \mapsto L_g h = g^{-1}h$ i.e. $\omega_g(Y_g)\phi = Y_g(\phi \circ L_{g^{-1}})$ for all $\phi : \Omega_e \to \mathbb{R}$ smooth and defined on some open local set Ω_e around the unity e. Recall

[12] See [48, Ch.8] for more details on frame bundles and moving frames.

[13] Following the definitions in [48], formally this is not a Cartan connection but a Koszul connection, see [48, Ch.6] , corresponding to a Cartan connection, i.e. a associated differential operator corresponding to a Cartan connection. We avoid these technicalities and use "Cartan connection" (a Koszul connection in [48]) and "Cartan-Ehresmann connection form" (Ehresmann connection in [48]).

that the left-invariant vector fields $\{\mathcal{A}_i\}_{i=1}^4$ satisfy $\mathcal{A}_i|_g = (L_g)_* A_i$ and therefore the dual elements (the corresponding co-vector fields) are obtained by the pull-back from $T_e(SIM(2))$, i.e. $\omega^i|_g = (L_{g^{-1}})_* \omega^i|_e$ since $\langle (L_g^{-1})_* \omega^i|_e, (L_g)_* A_j \rangle = \langle \omega^i|_e, A_j \rangle = \delta^i_j$. Now for any $X_g \in T_g(SIM(2))$, direct computation yields (96),

$$\begin{aligned}\omega_g(X_g) = (L_{g^{-1}})_* X_g &= \sum_{i=1}^4 \langle \omega^i|_e, (L_{g^{-1}})_* X_g \rangle A_i \\ &= \sum_{i=1}^4 \langle (L_g)_* \omega^i|_e, X_g \rangle A_i = \sum_{i=1}^4 \langle \omega^i, X_g \rangle A_i.\end{aligned}$$

Now we show that the Maurer-Cartan form indeed forms a Cartan-Ehresmann connection form, recall Definition 24, on the principle fiber bundle, $P = (SIM(2), e, SIM(2), \mathcal{L}(SIM(2))$. Now recall from Theorem 22 that the left invariant vector fields are obtained from the operator $d\mathcal{R}$, i.e. $\mathcal{A}_i = d\mathcal{R}(A_i)$. The Maurer-Cartan form does the reverse in the sense that it connects each tangent space $T_g(SIM(2))$ to $T_e(SIM(2))$. To this end note that

$$\lim_{h \downarrow 0} \frac{\phi(g \cdot e^{hA_i}) - \phi(g)}{h} =: (d\mathcal{R}(A_i))_g \phi = (\mathcal{A}_i)_g \phi = (L_g)_* A_i \phi = A_i(\phi \circ L_g) \in \mathbb{R}$$

for all $g \in SIM(2)$ and all smooth $\phi : \Omega_g \to \mathbb{R}$. Therefore we have

$$\forall i \in \{1,2,3,4\} : \ \omega \circ d\mathcal{R}(A_i) = \omega(\mathcal{A}_i) = A_i \Leftrightarrow \omega \circ d\mathcal{R} = I.$$

The second requirement in Definition24 follows from the following computation,

$$\omega_{gh}((R_h)_* Y_g) = (L_{h^{-1}} \circ L_{g^{-1}})_* ((R_h)_* Y_g) = (L_{h^{-1}})_* \circ (L_{g^{-1}})_* \circ (R_h)_* Y_g = Ad(h^{-1}) \omega_g Y_g.$$

To show that equality (97) holds we note that the left multiplication L_g and the right multiplication R_g commute and this leads to

$$(R_{g^{-1}} L_g)_* = (L_g R_{g^{-1}})_* = (L_g)_* (R_{g^{-1}})_* = (L_g)_* (R_{g^{-1}} L_g)_* (L_g^{-1})_*,$$

which implies that $\widetilde{Ad}(g) = d\mathcal{R} \circ Ad(g) \circ \omega$. The adjoint representation $Ad : SIM(2) \to GL(T_e(SIM(2)))$ coincides with the derivative of the conjugate automorphism $h \mapsto conj(g)(h) = ghg^{-1}$ evaluated at e, i.e. $Ad(g) = D_e conj(g) = (R_{g^{-1}} L_g)_*$. Recall Definition 25 of an associated vector bundle and set

$$P = SIM(2), \ M = e, \ G = SIM(2), \ F = \mathcal{L}(SIM(2)), \ \rho = \widetilde{Ad}, \ \pi(g) = e, \ R_g u = ug, \tag{102}$$

where $\mathcal{L}(SIM(2))$ denotes the Lie algebra of left invariant vector fields on $SIM(2)$ and $\widetilde{Ad}$ the adjoint representation of $SIM(2)$ into $GL(\mathcal{L}(SIM(2))$ given by

$$\widetilde{Ad}(g) X = (R_g^{-1} L_g)_* X, \ X \in \mathcal{L}(SIM(2)), \ g \in SIM(2).$$

A connection ω on a principle fiber bundle P is 1-to-1 related to a connection $\tilde{\omega}$ on the vector bundle $P \times_\rho F$ by means of

$$\omega = \sum_j A_j \otimes dx^j \leftrightarrow \tilde{\omega} = \sum_j \rho_*(A_j) \otimes dx^j,$$

where $\{dx^j\}$ are dual forms on F, see [49] for more details on this bijection. In our case we have $F = \mathcal{L}(SIM(2))$ and the corresponding dual forms $\{\omega^j\}_{j=1}^4$. Note that we applied the convention mentioned in the remark. So in our case (102) the push-forward ρ_* of $\rho = \widetilde{Ad}$ equals

$$\begin{aligned}(\widetilde{Ad})_* &= (d\mathcal{R} \circ Ad_*)(A_j) = (d\mathcal{R} \circ ad \circ \omega)(\mathcal{A}_j) \\ &= \widetilde{ad}(\mathcal{A}_j) = [\cdot, \mathcal{A}_j]_{\mathcal{L}(SIM(2))} = \sum_{i,j,k=1}^4 c_{ij}^k \mathcal{A}_k \otimes \omega^i.\end{aligned}$$

Thereby the connection form on the vector bundle $SIM(2) \times_{\widetilde{Ad}} \mathcal{L}(SIM(2))$ is given by

$$\tilde{\omega} = \sum_{j=1}^{4} \widetilde{ad}(\mathcal{A}_j) \otimes \omega^i = \sum_{i,j,k=1}^{4} c_{ij}^k \mathcal{A}_k \otimes \omega^i \otimes \omega^j \tag{103}$$

where c_{ij}^k are the structure constants of the Lie group $SIM(2)$, so $\widetilde{ad}(\mathcal{A}_j)(\mathcal{A}_i) = [\mathcal{A}_i, \mathcal{A}_j] = \sum_{i,j,k=1}^{4} c_{ij}^k \mathcal{A}_k$. Using the nonzero structure constants $c_{12}^3 = -c_{21}^3 = -c_{13}^2 = c_{31}^2 = -c_{34}^3 = c_{43}^3 = c_{42}^2 = -c_{24}^2 = 1$ and by using the definition anti-symmetric products $da \wedge db = da \otimes db - db \otimes da$ in (103) we arrive at (98).
From $\tilde{\omega}$ defined in (103) we can construct the 16-connection 1-form $\{\tilde{\omega}_j^k(\cdot)\}_{k,j=1}^4$ via (99) which together form a 4×4 matrix-valued 1-form on the frame bundle where the sections are moving frames.
Let $\{\mu_k\}_{k=1}^4$ denote the sections in $(SIM(2), T(SIM(2)))$ which coincide respectively with the left-invariant vector fields $\{\mathcal{A}_k\}_{k=1}^4$. Then the Cartan connection D on (the vector bundle $SIM(2) \times_{\widetilde{Ad}} \mathcal{L}(SIM(2))$ is isomorphic to) the tangent bundle $(SIM(2), T(SIM(2)))$ equals

$$D := d + \overline{\omega} \text{ with } \overline{\omega}(\mu_k)(\cdot) := \sum_{j=1}^{4} \tilde{\omega}_k^j(\cdot)\mu_j, \tag{104}$$

or more precisely the covariant derivatives are given by

$$\begin{aligned} D_{X|_{\gamma(t)}}(\mu(\gamma(t))) &:= (D\mu(\gamma(t)))(X|_{\gamma(t)}) \\ &= \sum_{k=1}^{4} \dot{a}^k \mu_k(\gamma(t)) + \sum_{k=1}^{4} a^k(\gamma(t)) \sum_{k=1}^{4} \tilde{\omega}_k^j(X|_{\gamma(t)})\mu_j(\gamma(t)) \\ &= \sum_{k=1}^{4} \dot{a}^k \mu_k(\gamma(t)) + \sum_{k=1}^{4} \dot{\gamma^i}(t) a^k(\gamma(t)) \Gamma_{ik}^j \mu_j(\gamma(t)), \end{aligned}$$

with $\dot{a}^k = \dot{\gamma}^i(t)(\mathcal{A}_i|_{\gamma(t)} a^k)(\gamma(t))$, for all curves $\gamma : \mathbb{R} \to SIM(2)$ and tangent vectors $X|_{\gamma(t)} = \sum_{i=1}^{4} \dot{\gamma}^i(t) \mathcal{A}_i|_{\gamma(t)} \in T_{\gamma(t)}(SIM(2))$ and all sections

$$\mu(\gamma(t)) = \sum_{k=1}^{4} a^k(\gamma(t)) \mu_k(\gamma(t))$$

and where the Christoffel symbols Γ_{ij}^k are constant

$$\Gamma_{ij}^k = \tilde{\omega}_j^k(\mathcal{A}_i) = -\tilde{\omega}(\omega^k, \mathcal{A}_i, \mathcal{A}_j) = -c_{ij}^k = c_{ji}^k.$$

□ □

As seen in the theorem above, we define the notion of covariant derivatives independent of the metric $\mathcal{G}$ on $SIM(2)$, which is the underlying principle behind the Cartan connection. Although in principle these two entities need not be related, in Lemma 29 we show that the connection induced above is metric compatible.

Definition 28. *Let $(M, \mathcal{G})$ be a Riemannian manifold (or pseudo-Riemannian manifold) where M and $\mathcal{G}$ denote the manifold and the metric defined on it respectively. Let ∇ denote a connection on $(M, \mathcal{G})$. Then ∇ is called metric compatible with respect to $\mathcal{G}$ if*

$$\nabla_Z \mathcal{G}(X, Y) = \mathcal{G}(\nabla_Z X, Y) + \mathcal{G}(X, \nabla_Z Y), \tag{105}$$

for all $X,\ Y,\ Z \in T(M)$.

Lemma 29. *The Cartan connection D on $(SIM(2), T(SIM(2)))$ is metric compatible with respect to $\mathcal{G}_\beta : SIM(2) \times T(SIM(2)) \times T(SIM(2)) \to \mathcal{C}$ on $SIM(2)$ defined in (94).*

Proof. We first note that $D_{\mathcal{A}_i}\mathcal{G}(\mathcal{A}_j,\mathcal{A}_k)=0,\ i\in\{1,2,3,4\}$ as the covariant derivative of a scalar field is the same as partial derivative. Here $\{\mathcal{A}_i\}_{i=1}^4$ denote the basis of the left invariant vector fields $\mathcal{L}(SIM(2))$. The following brief computation

$$\mathcal{G}(D_{\mathcal{A}_i}\mathcal{A}_j,\mathcal{A}_k)+\mathcal{G}(\mathcal{A}_j,D_{\mathcal{A}_i}\mathcal{A}_k)=\mathcal{G}(c_{ij}^l\mathcal{A}_l,\mathcal{A}_k)+\mathcal{G}(\mathcal{A}_j,c_{ik}^m\mathcal{A}_m)=-c_{ij}^k-c_{ik}^j, \tag{106}$$

where we have used the fact that $\Gamma_{ij}^k=c_{ji}^k$ along with non-zero structure constants $c_{12}^3=-c_{21}^3=-c_{13}^2=c_{31}^2=-c_{34}^3=c_{43}^3=c_{42}^2=-c_{24}^2=1$, leads to the result. □ □

The next theorem relates the previous results on Cartan connections and covariant derivatives to the non-linear diffusion schemes on $SIM(2)$.

Theorem 30. *covariant derivative of a co-vector field* **a** *on the manifold* $(SIM(2),\mathcal{G})$ *is a* $(0,2)$*-tensor field with components* $\nabla_j a_i=\mathcal{A}_j a_i-\Gamma_{ij}^k a_k$*, whereas the covariant derivative of a vector field* **v** *on* $SIM(2)$ *is a* $(1,1)$*-tensor field with components*[14] $\nabla_{j'}v^i=\mathcal{A}_{j'}v^i+\Gamma_{j'k'}^i v^{k'}$*. The Christoffel symbols equal minus the structure constants of the Lie algebra* $\mathcal{L}(SIM(2))$*, i.e.* $\Gamma_{ij}^k=-c_{ij}^k$*. The Christoffel symbols are anti-symmetric as the underlying Cartan connection* D *has constant torsion. The left-invariant equations* (56) *with a diagonal diffusion tensor* (58) *can be rewritten in covariant derivatives as*

$$\begin{cases}\partial_s W(g,s)=\sum\limits_{i,j=1}^4\mathcal{A}_i((D_{ij}(W))(g,s)\mathcal{A}_jW)(g,s)=\sum\limits_{i,j=1}^4\nabla_i((D_{ij}(W))(g,s)\nabla_jW)(g,s),\\ W(g,0)=\mathcal{W}_\psi f(g),\ \textit{for all } g\in SIM(2),\ s>0.\end{cases} \tag{107}$$

Both convection and diffusion in the left-invariant evolution equations (56) *take place along the exponential curves in* $SIM(2)$ *which are covariantly constant curves with respect to the Cartan connection.*

Proof. The first part of the proof follows from Theorem 27. The torsion tensor $T(X,Y)=D_XY-D_YX-[X,Y]$ is constant follows from a simple computation

$$T(\mathcal{A}_i,\mathcal{A}_j)=D_{\mathcal{A}_i}\mathcal{A}_j-D_{\mathcal{A}_j}\mathcal{A}_i-[\mathcal{A}_i,\mathcal{A}_j]=\sum_{k=1}^4(\Gamma_{ij}^k\mathcal{A}_k-\Gamma_{ji}^k\mathcal{A}_k-c_{ij}^k\mathcal{A}_k)=-3\sum_{k=1}^4c_{ij}^k\mathcal{A}_k.$$

The covariant constant curves[15] γ are by definition given by $D_{\dot\gamma}\dot\gamma=0$ on the tangent bundle $(SIM(2),T(SIM(2)))$

$$D_{\dot\gamma}\dot\gamma=D_{\dot\gamma^i\mathcal{A}_i|_{\gamma(t)}}\dot\gamma^i\mathcal{A}_i|_{\gamma(t)}=\ddot\gamma^i\mathcal{A}_i|_{\gamma(t)}+\dot\gamma^i\dot\gamma^k\Gamma_{ik}^j\mathcal{A}_j=\ddot\gamma^i\mathcal{A}_i|_{\gamma(t)}=0, \tag{108}$$

where we have made use of the Einstein's summation convention and applied automatic summation over double indices and where $\Gamma_{ij}^k=-\Gamma_{ji}^k=c_{ji}^k=-c_{ij}^k$. Note that the tangent vectors to these auto-parallel curves have constant coefficients with respect to $\{\mathcal{A}_1,\mathcal{A}_2,\mathcal{A}_3,\mathcal{A}_4\}$ as $\forall t>0,\ \dot\gamma^i(t)=\langle\omega^i|_{\gamma(t)},\dot\gamma(t)\rangle=|_{\gamma(0)},\dot\gamma(0)\rangle=c^i\in\mathbb{R},\ i\in\{1,2,3,4\}$. For smooth $U:SIM(2)\to\mathbb{C}$ one has

$$\begin{aligned}\frac{d}{dt}U(\gamma(t))&=\lim_{h\to0}\frac{U(\gamma(t+h)-U(\gamma(t)))}{h}=(d\mathcal{R}(\sum_{i=1}^4c^iA^i)U)(\gamma(t))\\&=\sum_{i=1}^4c^i(d\mathcal{R}(A_i)U)(\gamma(t))=\sum_{i=1}^4c^i\mathcal{A}_iU|_{\gamma(t)},\end{aligned} \tag{109}$$

where $\gamma(t)=g_0e^{t\sum_{i=1}^4c^iA^i}$. Therefore these curves $\gamma(t)$ coincide with the exponential curves in $SIM(2)$, see (75). As mentioned earlier the connection D is a Koszul connection which has the property that $\nabla_i(U\mathcal{A}_j)\phi=\nabla_i(U\nabla_j)\phi=U\nabla_i\nabla_j\phi+(\nabla_iU)\nabla_j\phi$ for all $U\in C^1(SIM(2))$ and all smooth $\phi\in C^\infty(SIM(2))$. Set $U=D_{ij}(W)(\cdot,s)$ and $\phi=W(\cdot,s)$ for all $s>0$, use $D_{ij}=D_{ji}$ and $\Gamma_{ij}^k=-\gamma_{ji}^k$, take the sum over both indices i,j and (107) follows. □ □

[14] We have made use of the notation $\nabla_j:=D_{\mathcal{A}_j}$, when imposing the Cartan connection.

[15] Also called "auto-parallel" curves.

Remark 31. *Though the connection D is $\mathcal{G}$ compatible (Lemma 29) , we have shown in the previous theorem that our connection is not torsion free, i.e. the torsion tensor $T(X,Y) \neq 0$ for all $X, Y \in T(SIM(2))$. As a result minimum distance curves in the group $SIM(2)$ are curves minimizing the induced Riemannian metric and do not coincide with "straight curves" (auto-parallel curves) in the group $SIM(2)$. The auto-parallel curves are the exponential curves. A full analysis of the shortest distance curves in $SIM(2)$ is beyond the scope of this article.*

G Curvature estimation via best Exponential Curve fit

Curvature estimation of a spatial curve using $SE(2)$-OS is based on the optimal exponential curve fit at each point. In [5, 28] the authors suggest two methods for such best exponential curve fit. Below is a brief summary.

- Compute the curvature of the projection $\mathbf{x}(s(t)) = \mathbb{P}_{\mathbb{R}^2}(g_0 \exp(t \sum_{i=1}^3 c_*^i A_i))$ of the optimal exponential curve in $SE(2)$ on the ground plane from an eigenvector $\mathbf{c}_* = (c_*^\theta, c_*^\xi, c_*^\eta)$. This eigenvector of $(\tilde{H}_\beta |U|)^T (\tilde{H}_\beta |U|)$, with a 3×3 Hessian

$$\tilde{H}_\beta |U| = \begin{pmatrix} \beta^2 \partial_\theta \partial_\theta |U| & \beta \partial_\xi \partial_\theta |U| & \beta \partial_\eta \partial_\theta |U| \\ \partial_\theta \partial_\xi |U| & \partial_\xi \partial_\xi |U| & \partial_\eta \partial_\xi |U| \\ \partial_\theta \partial_\eta |U| & \partial_\xi \partial_\eta |U| & \partial_\eta \partial_\eta |U| \end{pmatrix}, \tag{110}$$

  corresponds to the smallest eigenvalue. The curvature estimation is given by,

$$\kappa_{est} = \|\ddot{x}(s)\| sgn(\ddot{x}(s) \cdot \mathbf{e}_\eta) = \frac{c_*^\theta sign(c_*^\xi)}{\sqrt{(c_*^\xi)^2 + (c_*^\xi)^2}}.$$

  Note that unlike the $SIM(2)$ case curvature is constant in this case.

- In this method the choice of optimal exponential curve is restricted to horizontal exponential curves, which are curves in the $(SE(2), \omega^3)$ sub-Riemannian manifold. The idea is to diffuse along horizontal curves because typically the mass of a $SE(2)$-OS is concentrated around a horizontal curve [5] and therefore this is a fast curvature estimation method.

  Compute the curvature of the projection $\mathbf{x}(s(t)) = \mathbb{P}_{\mathbb{R}^2}(g_0 \exp(t \sum_{i=1}^3 c_*^i A_i))$ of the optimal exponential curve in $SE(2)$ on the ground plane from the eigenvector $\mathbf{c}_* = (c_*^\theta, c_*^\eta)$. This eigenvector of $(\tilde{H}_\beta^{hor} |U|)^T (\tilde{H}_\beta^{hor} |U|)$, with a 3×2 horizontal Hessian

$$\tilde{H}_\beta^{hor} |U| = \begin{pmatrix} \beta^2 \partial_\theta \partial_\theta |U| & \beta \partial_\xi \partial_\theta |U| \\ \partial_\theta \partial_\xi |U| & \partial_\xi \partial_\xi |U| \\ \partial_\theta \partial_\eta |U| & \partial_\xi \partial_\eta |U| \end{pmatrix}, \tag{111}$$

  corresponds to the smallest eigenvalue. The curvature estimation given by,

$$\kappa_{est}^{hor} = \|\ddot{x}(s)\| sgn(\ddot{x}(s) \cdot \mathbf{e}_\eta) = \frac{c_*^\theta}{c_*^\xi}.$$

  For numerical experiments on these curvature estimates on orientation scores of noisy images, see [5].

References

[1] T. Lindeberg. *Scale-Space Theory in Computer Vision.* Kluwer international series in engineering and computer science: Robotics: Vision, manipulation and sensors. Springer, 1993.

[2] H. Romeny. *Geometry-Driven Diffusion in Computer Vision.* Computational Imaging and Vision. Springer, 1994.

[3] P. Perona and J. Malik. Scale-space and edge detection using anisotropic diffusion. *Pattern Analysis and Machine Intelligence, IEEE Transactions on*, 12(7):629 –639, jul 1990.

[4] Joachim Weickert. Coherence-enhancing diffusion filtering. *International Journal of Computer Vision*, 31(2-3):111–127, 1999.

[5] E. Franken and R. Duits. Crossing-preserving coherence-enhancing diffusion oninvertible orientation scores. *International Journal of Computer Vision*, 85:253–278, 2009.

[6] H. Scharr and K. Krajsek. A short introduction to diffusion-like methods. In *Mathematical methods for signal and image analysis and representation*, Computational imaging and vision, chapter 1. Springer London, 2012.

[7] R. Duits, M. Felsberg, G. Granlund, and B. Romeny. Image analysis and reconstruction using a wavelet transform constructed from a reducible representation of the euclidean motion group. *Int. J. Comput. Vision*, 72(1):79–102, April 2007.

[8] J. Weickert and H. Scharr. A scheme for coherence-enhancing diffusion filtering with optimized rotation invariance. *Journal of Visual Communication and Image Representation*, 13(12):103 – 118, 2002.

[9] R. Duits and B. Burgeth. Scale spaces on lie groups. In *Proceedings of the 1st international conference on Scale space and variational methods in computer vision*, SSVM'07, pages 300–312, Berlin, Heidelberg, 2007. Springer-Verlag.

[10] Giovanna Citti and Alessandro Sarti. A cortical based model of perceptual completion in the roto-translation space. *Journal of Mathematical Imaging and Vision*, 24(3):307–326, 2006.

[11] Remco Duits, Hartmut Führ, Bart Janssen, Mark Bruurmijn, Luc Florack, and Hans van Assen. Evolution equations on gabor transforms and their applications. *Applied and Computational Harmonic Analysis*, 2012.

[12] R. Duits. *Perceptual Organization in Image Analysis.* PhD thesis, Technische Universiteit Eindhoven, 2005.

[13] Gregory C. DeAngelis, Izumi Ohzawa, and Ralph D. Freeman. Receptive-field dynamics in the central visual pathways. *Trends in Neurosciences*, 18(10):451 – 458, 1995.

[14] R.A. Young. The gaussian derivative model for spatial vision: I. retinal mechanisms. *Spatial Vision*, 2(4):273–293, 1987.

[15] M.S. Landy and J.A. Movshon. *Computational models of visual processing.* Bradford book. Mit Press, 1991.

[16] W. Bosking, Y. Zhang, B. Schofield, and D. Fitzpatrick. Orientation selectivity and the arrangement of horizontal connections in tree shrew striate cortex. *The Journal of Neuroscience*, 17(6):2112–2127, 1997.

[17] J.P. Antoine and R. Murenzi. Two-dimensional directional wavelets and the scale-angle representation. *Signal Processing*, 52(3):259 – 281, 1996.

[18] J.P. Antoine, R. Murenzi, and P. Vandergheynsta. Directional wavelets revisited: Cauchy wavelets and symmetry detection in patterns. *Applied and Computational Harmonic Analysis*, 6(3):314 – 345, 1999.

[19] J.P. Antoine, R. Murenzi, P. Vandergheynst, and S.T. Ali. *Two-dimensional wavelets and their relatives.* Cambridge University Press, 2004.

[20] D.L. Donoho and E.J. Candès. Ridgelets: a key to higher-dimensional intermittency? *Royal Society of London Philosophical Transactions Series A*, 357:2495, September 1999.

[21] D. Donoho and E. Candès. Continuous curvelet transform: I. resolution of the wavefront set. *Applied and Computational Harmonic Analysis*, 19(2):162 – 197, 2005.

[22] D.L. Donoho and E.J. Candès. Continuous curvelet transform: II. discretization and frames. *Applied and Computational Harmonic Analysis*, 19(2):198 – 222, 2005.

[23] S.T. Ali. A general theorem on square-integrability: Vector coherent states. *J. Math. Phys.*, 39(8):3954–3964, 1998.

[24] David H Hubel. Evolution of ideas on the primary visual cortex, 1955-1978: A biased historical account. *Physiology or Medicine Literature Peace Economic Sciences, Nobel Prize Lectures*, page 24, 1993.

[25] StiliyanN. Kalitzin, BartM.TerHaar Romeny, and MaxA. Viergever. Invertible apertured orientation filters in image analysis. *International Journal of Computer Vision*, 31(2-3):145–158, 1999.

[26] R. Duits and M.V. Almsick. The explicit solutions of linear left-invariant second order stochastic evolution equations on the 2D euclidean motion group. *Quarterly of Applied Mathematics*, 66:27–67, 2008.

[27] R. Duits and E. Franken. Left-invariant parabolic evolutions on $SE(2)$ and contour enhancement via invertible orientation scores part I: Linear left-invariant diffusion equations on $SE(2)$. *Quarterly of Applied Mathematics*, 68:255–292, 2010.

[28] R. Duits and E. Franken. Left-invariant parabolic evolutions on $SE(2)$ and contour enhancement via invertible orientation scores part II: Nonlinear left-invariant diffusions on invertible orientation scores. *Quarterly of Applied Mathematics*, 68:293–331, 2010.

[29] A. Grossmann, J. Morlet, and T. Paul. Transforms associated to square integrable group representations. I. General results. *J. Math. Phys.*, 26(10):2473–2479, 1985.

[30] A.K. Louis, P. Maab, and A. Rieder. *Wavelets Theory and Applications*. John Wiley and Sons, 1997.

[31] N. Aronszajn. Theory of reproducing kernels. *Trans. Amer. Math. Soc*, 68:337–404, 1950.

[32] M. Duits. A functional hilbert space approach to frame transforms and wavelet transforms. Master's thesis, Technische Universiteit Eindhoven, 2004.

[33] F.J.L. Martens. *Spaces of analytic functions on inductive/projective limits of Hilbert Spaces*. PhD thesis, Technische Universiteit Eindhoven, 1988.

[34] H. Führ. *Abstract Harmonic Analysis of Continuous Wavelet Transforms*. Number 1863 in Lecture Notes in Mathematics. Springer, 2005.

[35] J.P. Serre. *A Course in Arithmetic*. Graduate Texts in Mathematics. Springer, 1973.

[36] I.N. Bankman. *Handbook of Medical Image Processing and Analysis*. Academic Press Series in Biomedical Engineering. Elsevier/Academic Press, 2008.

[37] J. Zhang and H.K. Huang. Automatic background recognition and removal (abrr) in computed radiography images. *Medical Imaging, IEEE Transactions on*, 16(6):762 –771, dec. 1997.

[38] M. Unser. Splines: A perfect fit for signal/image processing. *IEEE Signal Processing Magazine*, 16:22–38, 1999.

[39] J. Dieudonné. *Treatise on Analysis*. Number v. 5 in Pure and applied mathematics. Academic Press, 1977.

[40] Stéphane Mallat. Group invariant scattering. *Communications on Pure and Applied Mathematics*, 65(10):1331–1398, 2012.

[41] T. Aubin. *A course in differential geometry*. Graduate studies in mathematics. American Mathematical Society, 2001.

[42] L. Hörmander. Hypoellptic second order differential equations. *Acta Mathematica*, 119:147–171, 1967.

[43] R. Duits and E. Franken. Left-invariant diffusions on the space of positions and orientations and their application to crossing-preserving smoothing of hardi images. *Int. J. Comput. Vision*, 92(3):231–264, May 2011.

[44] E. Hsu. *Stochastic analysis on manifolds*. Contemporary Mathematics. AMERICAN MATHEMATICAL SOCIETY, 2002.

[45] A. Nagel, F. Ricci, and E. M. Stein. Fundamental solutions and harmonic analysis on nilpotent groups. *Bulletin of American Mathematical Society*, 23:139–144, 1990.

[46] A.F.M ter Elst and D.W. Robinson. Weighted subcoercive operators on lie groups. *Journal of Functional Analysis*, 157(1):88 – 163, 1998.

[47] M. Rubbens, A. Mol, R. Boerboom, R. Bank, F. Baaijens, and C. Bouten. Intermittent straining accelerates the development of tissue properties in engineered heart valve tissue. *TISSUE ENGINEERING: Part A*, 15 (5), 2009.

[48] M. Spivak. *A Comprehensive Introduction to Differential Geometry, Vol-II, 3rd ed.* Publish or Perish Inc., 1970.

[49] H.G.J. Pijls. The yang-mills equations. In *Mathematical structures in field theories, ed. E.M. de Jager and H.G.J. Pijls, pp.119-182*, 1984.

PREVIOUS PUBLICATIONS IN THIS SERIES:

Number	Author(s)	Title	Month
13-13	M.H. Duong	Finite-time blow-up and variational approximation scheme for a Wigner-Fokker-Planck equation with a nonlocal perturbation	May '13
13-14	T. Aiki A. Muntean	Large-time behavior of a two-scale semilinear reaction-diffusion system for concrete sulfatation	May '13
13-15	R. Pulch E.J.W. ter Maten F. Augustin	Sensitivity analysis and model order reduction for random linear dynamical systems	June '13
13-16	B.S. van Lith C. Storm A. Muntean	A multiscale model for self-assembly with secondary nucleation-like properties	June '13
13-17	U. Sharma R. Duits	Left-invariant evolutions of wavelet transforms on the similitude group	June '13

Ontwerp: de Tantes,
Tobias Baanders, CWI